National Library of Canada
Canadian Theses Service
Ottawa, Canada
K1A 0N4

Bibliothèque nationale du Canada
Services des thèses canadiennes

CANADIAN THESES

THÈSES CANADIENNES

NOTICE

The quality of this microfiche is heavily dependent upon the quality of the original thesis submitted for microfilming. Every effort has been made to ensure the highest quality of reproduction possible.

If pages are missing, contact the university which granted the degree.

Some pages may have indistinct print especially if the original pages were typed with a poor typewriter ribbon or if the university sent us an inferior photocopy.

Previously copyrighted materials (journal articles, published tests, etc.) are not filmed.

Reproduction in full or in part of this film is governed by the Canadian Copyright Act, R.S.C. 1970, c. C-30. Please read the authorization forms which accompany this thesis.

AVIS

La qualité de cette microfiche dépend grandement de la qualité de la thèse soumise au microfilmage. Nous avons tout fait pour assurer une qualité supérieure de reproduction.

S'il manque des pages, veuillez communiquer avec l'université qui a conféré le grade.

La qualité d'impression de certaines pages peut laisser à désirer, surtout si les pages originales ont été dactylographiées à l'aide d'un ruban usé ou si l'université nous a fait parvenir une photocopie de qualité inférieure.

Les documents qui font déjà l'objet d'un droit d'auteur (articles de revue, examens publiés, etc.) ne sont pas microfilmés.

La reproduction, même partielle, de ce microfilm est soumise à la Loi canadienne sur le droit d'auteur, SRC 1970, c. C-30. Veuillez prendre connaissance des formules d'autorisation qui accompagnent cette thèse.

THIS DISSERTATION
HAS BEEN MICROFILMED
EXACTLY AS RECEIVED

LA THÈSE A ÉTÉ
MICROFILMÉE TELLE QUE
NOUS L'AVONS REÇUE

NL 339 (r. 86/01)

Canada

National Library of Canada
Bibliothèque nationale du Canada

191

Ottawa, Canada
K1A 0N4

TC –

IS 0-315-23385-0

CANADIAN THESES ON MICROFICHE SERVICE – SERVICE DES THÈSES CANADIENNES SUR MICROFICHE

PERMISION TO MICROFILM – AUTORISATION DE MICROFILMER

• Please print or type – Écrire en lettres moulées ou dactylographier

AUTHOR – AUTEUR

Full Name of Author – Nom complet de l'auteur

TIMOTHY · PETER HILBICH

Date of Birth – Date de naissance
24 September 1960

Canadian Citizen – Citoyen canadien
☑ Yes / Oui ☐ No / Non

Country of Birth – Lieu de naissance
Canada

Permanent Address – Résidence fixe
5411 17 Avenue
Edmonton, Alberta
T6L 3T4

THESIS – THÈSE

Title of Thesis – Titre de la thèse

A Finite Element Model For Mode Classification of Crankshafts

Degree for which thesis was presented
Grade pour lequel cette thèse fut présentée
M. Sc. (Mech. Eng.)

Year this degree conferred
Année d'obtention de ce grade
1985

University – Université
U. of Alberta

Name of Supervisor – Nom du directeur de thèse
Dr. A. Craggs

AUTHORIZATION – AUTORISATION

Permission is hereby granted to the NATIONAL LIBRARY OF CANADA to **microfilm** this thesis and to **lend** or **sell copies of the film.**

The author reserves other publication rights, and neither the thesis nor extensive extracts from it may be printed or otherwise reproduced without the author's written permission.

L'autorisation est, par la présente, accordée à la BIBLIOTHÈQUE NATIONALE DU CANADA de **microfilmer** cette thèse et de **prêter** ou de **vendre des exemplaires du film.**

L'auteur se réserve les autres droits de publication; ni la thèse ni de longs extraits de celle-ci ne doivent être imprimés ou autrement reproduits sans l'autorisation écrite de l'auteur.

ATTACH FORM TO THESIS – VEUILLEZ JOINDRE CE FORMULAIRE À LA THÈSE

Signature
Jim Hilbich

Date
October 15, 1985

NL-91 (r. 84/03)

Canada

THE UNIVERSITY OF ALBERTA

A FINITE ELEMENT MODEL FOR MODE CLASSIFICATION OF CRANKSHAFTS

by

© TIMOTHY PETER HILBICH

A THESIS

SUBMITTED TO THE FACULTY OF GRADUATE STUDIES AND RESEARCH

IN PARTIAL FULFILMENT OF THE REQUIREMENTS FOR THE DEGREE

OF MASTER OF SCIENCE

DEPARTMENT OF MECHANICAL ENGINEERING

EDMONTON, ALBERTA

FALL, 1985

THE UNIVERSITY OF ALBERTA

RELEASE FORM

NAME OF AUTHOR TIMOTHY PETER HILBICH

TITLE OF THESIS A FINITE ELEMENT MODEL FOR MODE CLASSIFICATION OF CRANKSHAFTS

DEGREE FOR WHICH THESIS WAS PRESENTED MASTER OF SCIENCE

YEAR THIS DEGREE GRANTED FALL, 1985

Permission is hereby granted to THE UNIVERSITY OF ALBERTA LIBRARY to reproduce single copies of this thesis and to lend or sell such copies for private, scholarly or scientific research purposes only.

The author reserves other publication rights, and neither the thesis nor extensive extracts from it may be printed or otherwise reproduced without the author's written permission.

(SIGNED) Tim. Hilbich.....

PERMANENT ADDRESS:

5411 17 AVENUE

EDMONTON, ALBERTA

T6L 1T4

DATED 11 October 1985

THE UNIVERSITY OF ALBERTA

FACULTY OF GRADUATE STUDIES AND RESEARCH

The undersigned certify that they have read, and recommend to the Faculty of Graduate Studies and Research, for acceptance, a thesis entitled A FINITE ELEMENT MODEL FOR MODE CLASSIFICATION OF CRANKSHAFTS submitted by TIMOTHY PETER HILBICH in partial fulfilment of the requirements for the degree of MASTER OF SCIENCE.

A. Craggs

Supervisor

Gary L. Faulkner

K. W. Dormer

Date 11 Oct 1985.

Dedicated to my parents

Abstract

The crankshaft in a reciprocating engine is a complex structural member capable of responding to fluctuating forces in a variety of vibrational modes. It is therefore valuable to understand and predict the dynamic behavior of this engine component. This study on the dynamic characteristics of crankshafts has a three-fold thrust.

Firstly, the literature was searched for relevant information in the areas of mode classification, stress and noise, as each relates to crankshaft dynamics.

Secondly, a numerical model was formulated from beam and shaft type finite elements with the aim of producing an economical method of predicting crankshaft natural frequencies and mode shapes. This was basically an attempt to bypass the expensive, complex, finite element models that are also in use. Tests performed for purposes of verification revealed that computed frequencies had a widely varying range of correlation with test results. Mode shape predictions were generally better and more consistent. Suggestions have been made as to areas of deficiency in the model and to means of improving the results through model modifications.

Finally, knowing the capabilities and limitations of the numerical model, mode classification and frequency spectrum analysis for coplanar crankshafts was carried out. This was done both for free-free constraints and for constraints simulating the actual conditions in an engine.

Acknowledgements

The Author would like to thank Dr. A. Craggs for the research opportunity and for funding he made available from his National Research Council grant (NRC A7431). Appreciation is also extended to the machinists and technicians at the Department of Mechanical Engineering who generously offered their services for tasks involving specimen preparation, instrumentation and testing. Finally, a thank you to fellow graduate students who provided support by their encouragement and dedicated examples.

Table of Contents

Chapter — Page

1. INTRODUCTION 1

   1.1 Context of the Problem 1

   1.2 Objectives and Thesis Outline 4

2. LITERATURE REVIEW AND HISTORICAL METHODS 7

   2.1 Crankshaft Mode Analysis 8

   2.2 Strength and Stress Analysis 11

   2.3 Engine Noise 14

   2.4 Holzer Method for Torsional Natural Frequency 19

3. MODEL FORMULATION 28

   3.1 Finite Elements and the Energy Approach 28

   3.2 Element Description 31

   3.3 Transformations and Assembly 38

   3.4 Constraints and Solution 48

   3.5 Modelling Deficiencies 52

   3.6 Example Crankshaft Models 56

4. VERIFICATION OF THE COMPUTER MODEL 65

   4.1 Axial Compression Test 65

   4.2 Resonance Testing 66

      4.2.1 Boundary Conditions and Test Methods 66

      4.2.2 Determination of Modal Parameters and Accuracy 69

      4.2.3 Test Results 74

   4.3 Comparisons of Computed and Experimental Results 87

5. MODE CLASSIFICATION 93

5.1 Free - Free Constraints 93

5.2 Simple Bearing Constraints 96

6. APPLICATION AND CONCLUSIONS 107

6.1 Application: Dynamic Response Prediction 107

6.2 Conclusions and Recommendations 113

BIBLIOGRAPHY 118

APPENDIX A - Energy Formulations for Sub-elements 125

APPENDIX B - Computer Program Input, Output and Codes 129

List of Tables

Table		Page
2.1	Mass and Stiffness Properties of the Equivalent System for ATX5	20
2.2	Holzer Tabulation for ATX5 in Free Constraint	25
2.3	Holzer Tabulation for ATX5 in Fixed - End Constraint	27
5.1	Mode Classifications for Coplanar Crankshafts in Free Constraint	94
5.2	Mode Classifications for Coplanar Crankshafts in Simple Bearing Constraints	103

List of Figures

Figure		Page
2.1	Actual ATX5 Crankshaft	20
2.2	Equivalent System for ATX5	20
2.3	"Derived Figures" Method for Counterweight Inertias	22
3.1	Sub-elements Used in Composite Element	32
3.2	Composite Finite Element	32
3.3	Plate Bending	37
3.4	Web Curvature for In-Plane Bending	37
3.5	Coordinate Transformation of Elements	39
3.6	Edge Node Transformation	46
3.7	Potential Incompatabilities at Web Joints	54
3.8	Finite Element Model for Crankshaft ATX5	57
3.9	Finite Element Model for Crankshaft DT3	59
3.10	Finite Element Model for Single Cylinder Engine Crankshaft (SL2)	60
3.11	The Effects of Shear Deformation and Rotary Inertia on the Natural Frequencies of Crankshaft ATX5	63
4.1	Crankshaft DT3 Under Compressive Static Load	67
4.2	Apparatus for Resonance Testing in Free Constraint Mode	70
4.3	Measured Frequency Response for Crankshaft ATX5 in Free Constraint	75
4.4	Measured Frequency Response for Crankshaft DT3 in Free Constraint	76
4.5	Measured Frequency Response for Crankshaft SL2 in Free Constraint	77
4.6	Experimental and Computed Modes for ATX5 Crankshaft in Free-Free Constraint	78

Figure Page

4.7 Experimental and Computed Modes for DT3 Crankshaft in Free-Free Constraint 81

4.8 Experimental and Computed Modes for SL2 Crankshaft in Free-Free Constraint 84

4.9 Crankpin-Journal Overlap Geometry 88

5.1 Natural Modes of Crankshaft ATX5 in Simple Bearing Constraint 97

5.2 Natural Modes of Crankshaft DT3 in Simple Bearing Constraints 99

5.3 Natural Modes of Crankshaft SL2 in Simple Bearing Constraints 101

6.1 Critical Speed Analysis for Lowest Torsional Mode of Crankshaft ATX5 110

B.1 Geometry for "A" Type Crankthrow 133

B.2 Geometry for "D" Type Crankthrow 134

B.3 Geometry for "E" Type Shafting 135

B.4 Geometry for Annular Disc Mass 135

1. INTRODUCTION

1.1 Context of the Problem

The internal combustion (I.C.) engine is a mechanical system that is highly susceptible to vibrations. Whether in the design process or in the troubleshooting stage, the necessity for a vibrations analysis has stimulated research into ways of predicting the response to fluctuating loads and subsequently to reduce this response. In a general sense, the analysis can be broken up into three main areas. Firstly, there are the forces that cause the vibrations. Secondly, there is a mechanical system having mass, stiffness and damping upon which the forces are acting. Thirdly, as a result of particular forces acting upon a given system a unique dynamic response may be observed. After briefly detailing these areas for the reciprocating, I.C. engine and their relation to the crankshaft in particular, the scope and objective of this work will be given.

The important forces acting on a crankshaft in an I.C. engine include those due to combustion gas pressure, inertia loads of the reciprocating parts and any unbalanced rotating inertia loads. These forces, which are periodic in nature and thus may cause troublesome vibrations, are transmitted to both the static and moving parts of the engine as well as to any systems or structures connected to the engine. The total force which acts on a crankshaft is very complex. The

combustion force alone may be described as a broadband excitation (i.e. a summation of harmonic forces having a large frequency range). Hawkins & Southall [32]' plot the combustion pressure in a frequency spectrum over a range of 100 to 10,000 Hz for five different speeds of a running engine. The amplitudes of the pressure (or force) harmonics also vary significantly throughout the frequency spectrum. The amplitude is a maximum at the low end of the frequency scale and decreases to a minimum at 4 to 5 kHz. A local maximum pressure occurs near 6500 Hz.

The components of the engine each have unique material and geometric characteristics that determine their respective mass, stiffness and damping properties. The scope of this study is limited to the crucial component of the engine which transforms the reciprocating motion of the pistons to useful rotary motion. In actuality the crankshaft is an integral part of the driveline system but here it is studied separately as a "branch" system. Wilson ([77], pp.75-82) shows that because of the relatively high stiffness of a crankshaft it may be considered separately from the rest of the driveline, at least for determining its torsional natural frequency.

Once the vibration transmission characteristics of the crankshaft are known, they may be mathematically combined with results of similar analyses applied to the connecting rods, block and all other engine components. With this type

---

'Numbers in square brackets refer to literature listed in the Bibliography.

of synthesis, a complete engine model useful for noise and vibration predictions has been attained. Ewins [23] states that this sub-structuring approach is the most efficient way of handling complex systems. He goes on to give two methods for combining the sub-structures and analyzing the resulting assembled system. In an operating engine, where all components are assembled, factors such as bearing clearance and oil films further affect the system properties, especially the stiffness and damping.

Of ultimate interest are the resulting effects of the forces acting upon this complex mechanical system. Hawkins & Southall [32] give an indication of the extent of these effects when they state:

> "Examination of any engine vibration spectrum shows that there is both a high modal density and significant response up to 10 kHz."
>
> (p. 2127)

It is most likely that the primary concern regarding fluctuating forces in an engine lies in the area of fatigue stressing. This is of crucial interest in components such as the crankshaft, which contains numerous geometric discontinuities (oil holes and fillets for example) and hence stress raisers.

Furthermore, forces transmitted to engine mounts may cause undue vibrations of other vehicle members. This may ultimately result in a rougher ride for occupants or in excitation of the acoustical resonances of the interior

passenger enclosure (see Buma [13]).

Vibration response may also be observed as direct engine noise. The largest percentage of vibration due to the combustion explosion is transferred through the crankshaft, main bearings and to the outer surfaces of the engine where the vibrations are emanated as noise (see Hayashi, et al. [33]). Therefore, resonances of the crankshaft will have an influence on the noise emitted by the engine.

The framework, or context, for the problem of crankshaft vibrations which has been discussed above may be summarized by the following statement. Knowledge of the dynamic characteristics of the crankshaft is crucial when considering how combustion, inertia and unbalance forces in an I.C. engine cause fatigue stressing of the system components, vehicle vibrations and noise emanation from engine surfaces.

1.2 Objectives and Thesis Outline

The work presented in this thesis may be seen as fulfillment of four major objectives. These goals, and a chapter by chapter outline, will be given in this section.

The first objective was to search the literature for both historic and current work done on crankshaft vibrations. Chapter 2 presents summaries and notes on a number of papers and books concerned with the subject.

The second aim was to develop a numerical model of the crankshaft that could be used to compute some of its modal

parameters. The modal parameters for each mode of a structural system are the natural frequency, mode shape and damping factor. The problem to be solved may be classified as an undamped, unforced vibration and thus only natural frequencies and mode shapes are calculated. If the dynamic response to a given excitation is desired, damping factors obtained by means of experiment will also be needed. Chapter 3 presents the formulation of the model and concludes with a presentation of three example crankshaft models and their results.

The third objective was to verify the model by means of experiment. Chapter 4 describes the tests that were conducted and gives discussion on the comparison between measured and computed results.

Having developed and tested the numerical model, a fourth objective could then be fulfilled. That is, to analyze and classify modes of a crankshaft. Chapter 5 contains a discussion of the modes of the example crankshafts for two cases of constraint - free and simple bearings.

The first section of Chapter 6 contains a brief investigation into a potential application of the model in predicting dynamic response of the crankshaft due to engine forces. Clarification will be made as to what additional information must necessarily be included with the finite element structural model and the natural mode solution. The final section contains a summary on each of the four project

objectives in terms of conclusions on the findings and recommendations for further research work. This is followed by a number of additional suggestions for applications of the model.

2. LITERATURE REVIEW AND HISTORICAL METHODS

Historically, the problem of vibration in reciprocating engine propelled systems surfaced before the turn of this century. Some of the problems and developments since then are documented by authors such as Bradbury [8] and Wilson [76]. Vibration analysis was at that time made for shaft systems as a whole and in the case of torsional vibrations attention was primarily given to the one-node mode of engine-shaft systems.

In the first two decades of this century design of the crankshaft was based on trial and error, experience of the designer, success of previous designs and only the most basic calculations. Crankshafts were designed for the expected loads and for mass balancing aspects. Resonances due to modes of the crankshaft itself was a subject that was not seriously studied until after World War I, when engines began to have more cylinders and higher turning speeds making them more susceptible to the problem. In a 1922 paper Timoshenko [70] noted,

> "The time has passed when engine design comprises merely the application of statics... The problem is no longer one of statics but concerns the dynamics of an elastic system."

As with most technology the reciprocating engine was also advancing in its development and thus new problems arose.

Included in the literature regarding crankshaft analysis are areas such as: studies of the various modes of

crankshaft vibration, stress and strength analysis and finally, investigations into noises due to vibrating engine components. After reviewing some of the work done in these areas the method used historically for calculating the torsional natural frequency will be presented.

2.1 Crankshaft Mode Analysis

It was in the early 1920's that the study of torsional vibrations of the crankshaft began to receive much attention. Papers by Fox [27], Lewis [46] and Lack & Jahnke [45] showed that the emphasis at that time was to identify, measure, predict and reduce the resonant vibrations at critical speeds due to the torsional crankshaft mode. The subject has a long standing history as a 1938 book by Bradbury [9] and a 1959 paper by Braund [11] would indicate. These later two references differ from the earlier ones in that emphasis was placed on describing the excitation torques as a summation of unique harmonics that could be determined from Fourier analysis of the engine torque curve.

A 1936 article by Lürenbaum [48] exposed the occurrence of other modes of crankshaft vibration such as flexural and longitudinal or axial and that these modes may react on each other. An interesting example was given where the torsional resonance of the crankshaft of an aero engine coincided with a flexural resonance of the propeller. Wilson [79] discussed three classifications of crankshaft vibration modes: bending, axial and torsional. He also stressed the potential

problem of modes being coupled resulting in even larger dynamic magnification. Poole [56] concentrated his efforts on the axial mode of vibration and presented the results of numerous vibration tests designed specifically to excite this mode. A simple formula, based on results of static axial stiffness tests, was presented for the fundamental frequency of axial vibration of a crankshaft.

Throughout the years prediction of the frequencies and mode shapes of vibrating crankshafts have been made through the use of numerical models. One of the earliest models for torsional resonance involved reducing the crankshaft to an equivalent uniform shaft supporting inertia discs. As mentioned previously this method will be presented in detail in the last section of this chapter. The Myklestad method [50] is a technique whereby masses are lumped to a point and joined by massless beams. Hodgetts [35,36] developed a computer model, based on this method, that provides frequencies and mode shapes of the crankshaft. The position of the mass center of each lumped mass relative to the beam ends and gyroscopic moments induced by the rotating crankshaft are also taken into account. The model is useful for determining the effect of changes in design parameters (dimensions, material properties) on the coupled whirling, torsional and axial vibrations.

Finite element models have also found their way into vibration analysis of crankshafts. Bickley & McCallion [7] presented a model that uses 3-D, eight noded elements to

represent crankshaft geometry. Although they maintained that their model is good for static analysis (load-deflection relationships) and dynamic analysis (natural frequencies and mode shapes) only results of the axial and bending stiffness of single crankthrows were presented.

Nagamatsu & Nagaike [51,52] formulated their model of the crankshaft by representing the web with tetrahedral elements while expressing the characteristics of the straight shaft parts by transfer matrices. The finite element mesh composing the web is reduced to a sub-structure having only 12 degrees of freedom. The finite element nodes lying on the surfaces adjoining to the journal and crankpin are referenced to single nodes on the crankshaft and crankpin axes respectively. These two nodes are in the plane of the adjoining surfaces and have six degrees of freedom each.

Bagci & Falconer [3] presented a finite element model that uses one-dimensional line elements. The flexural beam elements are based on Euler beam theory and mass matrices may be of the lumped or consistent variety. An added feature of their model allows one to choose whether or not to include the effect of mass or inertia at certain degrees of freedom where only the stiffness is an influential parameter. By using a technique similar to Guyan reduction [30] the size of the problem (degrees of freedom) may be decreased and computing time and costs are cut down.

A very recent publication by Kabele [40] presented a comprehensive model of torsional vibration response. The model, which is based on Newtonian vector mechanics, considers not only the firing and inertia forces but material damping and friction as well.

2.2 Strength and Stress Analysis

Under this general heading literature was found mainly in the following two categories: evaluation and measurement of crankshaft stiffness and, secondly, measurement of strain, and hence the stress, in crankshafts.

One of the first people to seriously try and come up with relations for the torsional rigidity of crankshafts was S. Timoshenko. In a 1922 paper [70] he presented a formula for torsional rigidity of a single throw crankshaft for three cases of bearing constraint: no constraint at the journals, partial constraint and full constraint. A subsequent paper [69] considered the torsion and bending of multi-throw crankshafts.

A large number of expressions for the torsional rigidity of crankshafts have been formulated by various authors. The British Internal Combustion Engine Research Association (BICERA) [53] have compiled a number of these and, in addition, developed their own unique method for calculating crankthrow torsional rigidity. A series of curves, obtained from experimental tests, are employed to give an equivalent length of web. The curves give correction

factors for such things as fillet radii, web chamfers and bored webs. This method is one of the most comprehensive and is a recommended procedure for most crankshafts. Fessler & Sood [24] performed torsion tests on single and double throw models made of epoxy resin and stated:

> "The BICERA experimental method of predicting deformation due to torsion has been shown to be reliable."

Poole [56], mentioned previously in connection with axial modes of vibration, investigated the axial stiffness of a crankshaft. Axial tension and compression tests were performed on a wide variety of crankshafts and the deflections thus obtained were compared to values from elementary beam theory equations. It may be noted here that the comparisons were generally better for crankshafts with "double throws" (two crankpins between main bearings) and where there was less overlap between crankpins and journals.

The need for a vibrations analysis is of great importance in the determination of maximum stresses that occur in a crankshaft. Howarth ([38], p.92) and also Kamath, et al. [41], stated that the dynamic magnification of torsional oscillations may be as high as 25 for a crankshaft at resonance. This increase in amplitude over and above the twist directly caused by the instantaneous torque naturally gives rise to large dynamic stresses. Dorey [20] published a lengthy paper dealing with the major causes of crankshaft failures in marine engines. Much of the work was based on

investigations into actual cases of failure. During the 1950's, Belgaumkar & Ahuja [6] perfomed a survey on engine builders, users and dealers in India and found a significant number of failures attributable to bending vibrations of the crankshaft.

Measurement and prediction of stress levels, especially in areas such as journal fillets where stress concentrations exist, is of great importance in crankshaft design. Dynamic stresses in these locations due to bending, torsional or axial vibrations are potential causes for fatigue failures. A number of papers were found which reported results of experiments that entailed the use of strain gages placed in the fillet radii at the bearing-web interface.

Butler & Ørbeck [14] performed such measurements on static, cantilevered crankshafts where the bending was due to the dead weight of the material. In this way stress distribution around the fillet radius was determined and stress concentration factors were ascertained. As papers by Roeder & Doane [58] and Foulds & D'Olier [26] show, dynamic strains may also be measured in a running engine so that actual stress conditions may be known.

The whirling or "bowing" of a rotating crankshaft due to radial forces on the crankpin will cause tensile or compressive stresses in the fillet radii. Brown & Mischke [12] did significant work in this area by investigating the effect of bearing clearance and flywheel mass on the magnitude of whirl. Although these two variables would be

expected to have substantial influence on whirl, and thus on fillet stresses, no such dependence was found.

Shaw & Richter [59] developed a generation routine for a finite element model of a crankshaft that uses isoparametric solid elements. They claimed that their model is useful as a stress analysis tool in the design process. It seems that their method is only for a static bending or torsion analysis. Their model may prove to be useful in dynamic analysis if deflections identical to those obtained from a simpler, dynamic response model of a complete crankshaft were imposed on their detailed quarter throw model. Thus, peak dynamic stresses in fillets and other stress concentration regions could be accurately predicted.

2.3 Engine Noise

Recently, the attention in engine design has shifted from such aspects as mass balancing and dynamic stress analysis to the realm of noise that originates within the engine. Investigations related to this area, discovered in the literature, include: identification of distinct noise patterns, determination of transfer paths through which the vibrations causing the noise travel, and studies on the vibration of engine surfaces that actually emanate the noise.

Starkman & Sytz [62] discussed two types of noise in their experimental analysis of a V-8 engine. "Rumble" was associated with transient bending vibrations of the

crankshaft caused by high rates of pressure rise in the cylinder combustion process. "Thud" is a similar sounding noise but is to be associated with torsional vibrations of the crankshaft caused by an advanced spark setting. Andrews and Anderton [2] described crank rumble as a noise consisting of a highly modulated waveform having a bandwidth of about 100 Hz and in the frequency range of 300 to 500 Hz. Noise, vibration and cylinder pressure measurements were made as part of their experimental analysis.

Another noise, termed "roughness", is similar to rumble in that it results from high rates of pressure rise in the combustion chamber. With rumble the pressure rise is due to multiple ignition centers and the noise can therefore be erratic. High rates of pressure rise causing roughness comes from having a combustion chamber designed for fast burning, and thus, the noise will always be present. Andon & Marks [1] investigated roughness noise and found that this rather unacceptable sound may be reduced by lowering the pressure rise rate, modifying structural stiffness or more importantly, by reducing cylinder to cylinder variations in pressure rise rate.

Priede, et al. [57] described a number of experimental tests useful for gathering information on the vibration transfer paths within the engine. Mention was made of static pressurizing of the combustion chamber, use of hydraulic rams, banger rigs that simulate the combustion explosion and hydraulic shakers for the piston slap test and main bearing

impact test. Hayashi, et al. [33] also simulated the combustion explosion and then measured vibration levels throughout the engine. They found that of the vibrations caused by combustion, 70% - 80% pass through the path consisting of the piston, connecting rod, crankshaft and main bearings before they reach the outer surfaces of the engine to be radiated as audible sound. By considering only the forces due to combustion, DeJong & Parsons [19] developed a model that predicts the noise levels emitted by an engine block due to vibrations passing through either the piston-crank-block path or the head-block path. The vibration characteristics (mobility transfer functions) of each component in the path is initially determined by means of experiment before the results are analytically combined to form a complete model. In spite of major assumptions specified in the paper, the model compared well with noise and vibration signals measured on a running engine and taken over a wide frequency range (0 to 5000 Hz).

Ochiai & Nakano [54] revealed an interesting correlation between crankshaft torsional vibration and noise emitted by engine surfaces, the crankcase in particular. In a torsional oscillation of the crankshaft the crankpin as well as the rotating part of the connecting rod mass experience alternating tangential and centrifugal acceleration. It was shown that lateral inertia forces, induced by these accelerations, act on the main bearings and subsequently result in noise. Furthermore, an n-th order

torsional vibration (i.e. n oscillations per revolution of the crankshaft) induces lateral forces of order n-1, n and n+1. In a later work on this same phenomenon, Kubozuka, et al. [44], did a detailed study on the interaction between the crankshaft torsional resonance and resonances of the block in a torsional or lateral bending mode. They concluded that block vibrations are largely influenced by how close the frequency of the induced inertia forces are to the block resonance and by the amplitude of the torsional oscillations.

Hodgetts & McDonald [34] claimed that their theoretical and experimental work shows that crankshaft resonances can significantly increase the forces transmitted to main bearings and to engine mounts. They proposed that their program could be useful for implementing design changes in a crankshaft so that force transmission be kept to an acceptable level.

By using pressure, strain, force and displacement transducers, Ishihama, et al. [39] did detailed experimental work with regards to noise generation on a fast burn, four cylinder engine. Their work concentrated on bearing load distribution and journal bearing displacements during firing. In this case the bending of the crankshaft and subsequent loading of the bulkheads rather than torsional oscillations of the crankshaft was linked to various engine block modes that caused noise emission. A most interesting conclusion set forward was that suppression of bearing cap

vibration through the use of a "bearing beam" reduced skirt vibration and noise. Another impressive experimental and numerical analysis of engine block vibrations was done by Ford, et al. [25] for the purpose of obtaining a model useful for noise reduction design. The lower block skirt and oil pan were found to be the major contributors to noise. Block vibrations were classified as bending, torsional, crankcase bulging, panel and bulkhead modes. A rather complex finite element model of an entire engine block was formulated and Guyan reduction [30] used to reduce the dynamic degrees of freedom. Through resonance test results the authors demonstrated the validity of the model and claimed it had been used in the design of a new block. Along the same lines, an article by Brandeis & Graison [10] also presented experimental and finite element analyses of engine block vibrations. Two proposals for reduction of block and bearing vibrations were investigated. First, a "bed plate" was installed on the lower flange of the crankcase skirt which considerably stiffened the block and inner bulkheads and raised the frequencies of the various modes or eliminated them entirely. However, this also added a large extra mass to the engine. The other solution was to treat each bearing bulkhead separately by adding stiffening members at the optimum locations. The second method was emphasized as the more desirable route to follow in any attempt to reduce noise.

In addition to the references mentioned above, a nine page bibliograghy given by Wilson [77] may be consulted for work done in the area of vibrating shafts, reciprocating engine shafts in particular.

2.4 Holzer Method for Torsional Natural Frequency

Holzer has been cited as the originator of a method for determining the natural torsional frequency of a shaft system.[2] In order to perform the necessary calculations an equivalent shaft must be created. The equivalent shaft is made by separating the mass and stiffness properties of the material in its original form into a series of rigid inertia discs attached to a uniform shaft having no mass or inertia associated with it. The maximum number of modes that can be extracted for a shaft in either free-free or fixed end constraint is equal to the number of shaft segments between discs. In this case, a fixed end may be considered as a disc having infinite inertia. For each mode, a frequency, the relative amplitudes of twist for each disc, and the torque in the shaft between each of the discs is calculated.

As an example, in Figure 2.1 is shown a crankshaft from a four cylinder engine (hereafter known as ATX5) and its equivalent disc-shaft system (Figure 2.2). Also shown is the manner in which the crankshaft was subdivided. Namely, each crankthrow was lumped into a disc having an inertia about the crankshaft axis equal to that of the original

---

[2] W.T. Thomson [67] refers to: H. Holzer, Die Berechnung der Drehschwingungen (Berlin: Springer-Verlag, 1921)

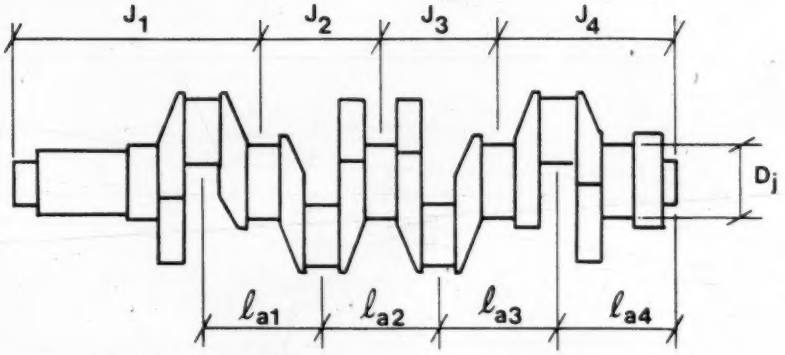

Figure 2.1 Actual ATX5 Crankshaft

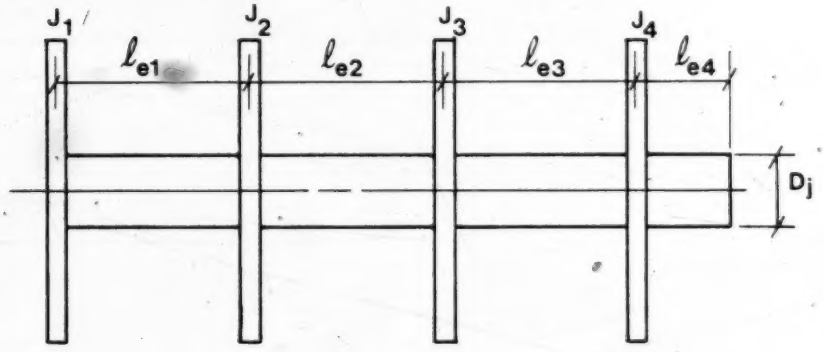

Figure 2.2 Equivalent System for ATX5

Section Number	Disc Inertia ($lb.s^2.in$)	Shaft Rigidity ($in \cdot lb/rad$)
1	2.910×10^{-2}	3.422×10^{6}
2	2.769×10^{-2}	3.422×10^{6}
3	2.655×10^{-2}	3.422×10^{6}
4	3.292×10^{-2}	5.348×10^{6}

Table 2.1 Mass and Stiffness Properties of the Equivalent System for ATX5

crankthrow. This part of the calculation is done by further subdividing each crankthrow into journal, web, crankpin and counterweight parts. The inertia of each piece about the crankshaft centerline axis is then calculated. For cylindrical or rectangular pieces this is a simple procedure but counterweights can often have very irregular geometries making an accurate calculation a difficulty. The "derived figures" method, explained in the BICERA handbook [53], was employed in this case. A counterweight contour and areas of derived figures are shown as an example in Figure 2.3. The moments of inertia about the y and z axis may be calculated from the respective radius of gyration terms. For counterweights having a relatively thin thickness these two inertia terms may be summed to obtain the moment of inertia about the x axis.

The discs are situated on the shaft such that the torsional rigidity between two discs is the same as the torsional rigidity between the crankpin centers of the corresponding crankthrows. The BICERA method of determining equivalent torsional rigidity of a crankthrow was applied. For the equivalent length of shaft that represents the web, correction terms for web width, unequal diameter of journal and crankpin, fillet radius and web chamfer were included. The actual length between the centers of journals one and two (i.e. crankthrow one) is 3.665 inches and the equivalent length is 5.296 inches.

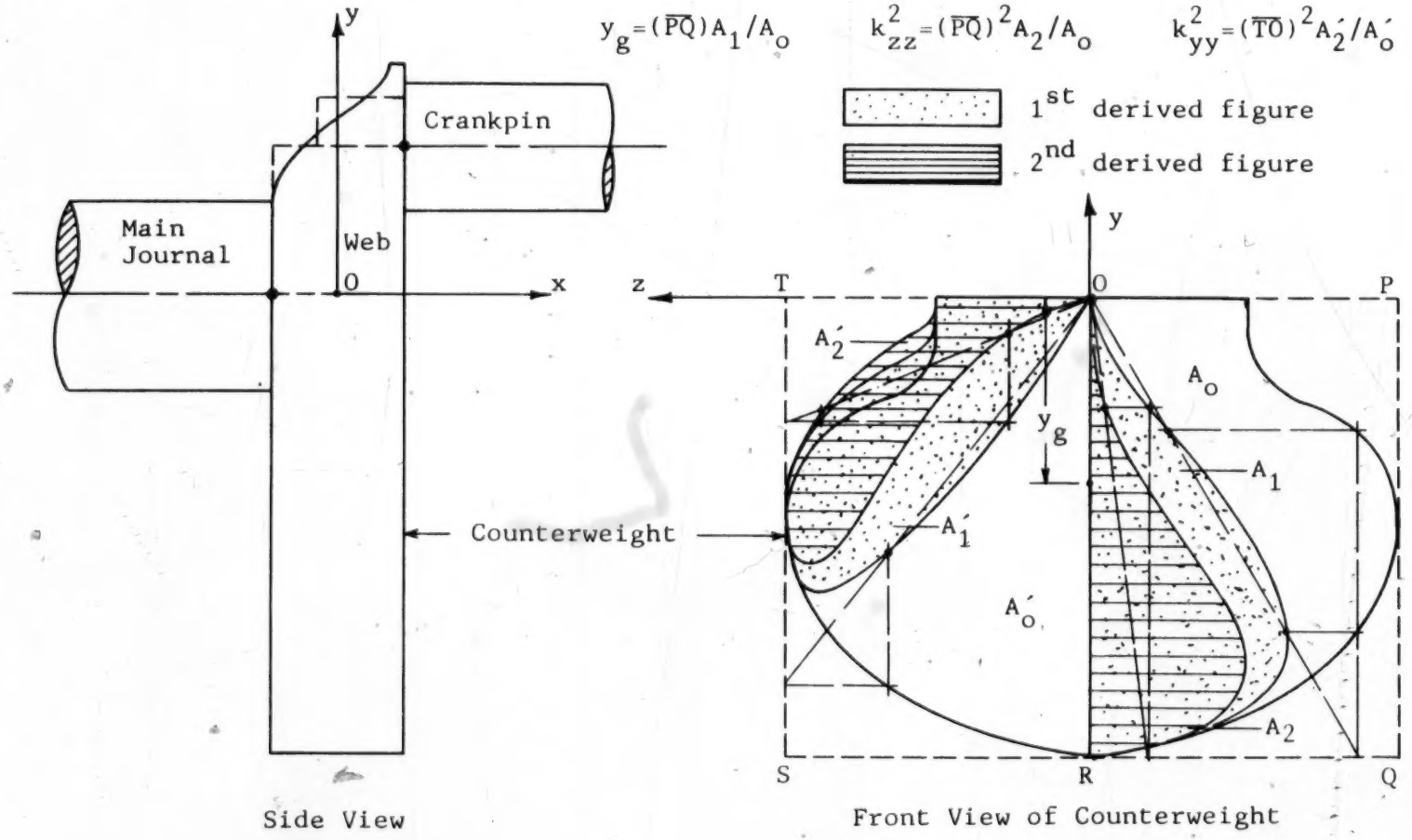

Figure 2.3 "Derived Figures" Method for Counterweight Inertias

Table 2.1 above lists the values of inertias and shaft rigidities for the example equivalent shaft system. A "section" refers to a part of the shaft system that includes an inertia disc and the shafting immediately to the right of the disc. In the Holzer method one proceeds from one end to the other (from left to right in the present case) in calculating twists and torques. The following calculation procedure is used to determine frequency, mode shape and shaft torque.

Disc one is the reference disc and always has a twist amplitude of one unit (θ_1=1.0 rad). The maximum inertia torque, T_1, of disc one may then be calculated if a frequency, ω, is assumed.

$$T_1 = J_1 \cdot \omega^2 \cdot \theta_1 \qquad (2.1)$$

This torque acts on the shaft between discs one and two, which has a torsional rigidity of K_1, and twists it by an amount of $\Delta\theta$ calculated as,

$$\Delta\theta = \theta_1 - \theta_2 = T_1/K_1 \qquad (2.2)$$

Thus θ_2, the twist amplitude of disc two, may be calculated and similar calculations are performed for disc two as was initially done for disc one. The torque acting on any section of shafting includes the inertia torques of all the discs to the left of that section. For the shaft in free-free constraint the calculation is repeated by choosing ω in a trial and error manner until the inertia torques for

all the discs have a sum of zero. Table 2.2 shows the results of a Holzer tabulation for the fundamental mode of the example crankshaft system.

In Section 1.1, mention was made of considering the crankshaft as a branch of the entire powertrain system. It has been shown (see Braund [11] for instance) that for the fundamental torsional mode of the crankshaft the node lies close to the flywheel. Thus, a close aproximation can be made in the numerical model of this branch system by rigidly constraining the flywheel end of the crankshaft. For this case the effect of bearing restraint should also be taken into account. The BICERA handbook presents a formula for a "stiffening ratio" based on a graph originally given by H. Constant[3]. The calculated equivalent length of a crankthrow is divided by this ratio; however, for ATX5 the ratio equaled unity resulting in no change to the system. The inertia of the front end pulley, timing-belt gear, connecting rods and pistons will also have an influence on the torsional natural frequency. The pulley and gear inertias were determined by torsional pendulum tests and their total value, 0.01141 $lb \cdot s^2 \cdot in$, added to the inertia of disc one. If one assumes, as is commonly done (see Wilson [77], Ch.10), that the revolving mass of the connecting rod and one half the mass of the reciprocating parts for each cylinder act at the crank radius then the inertia effect per

---

[3]The handbook gives the reference as: H. Constant, 'On the stiffness of crankshafts', Rep. Memor. Aero. Res. Comm., Lond., no.1201(E29), October 1928.

Frequency (rad/s)	Section 1		Section 2		Section 3		Section 4	
	Disc Deflection (rad)	Shaft Torque (in·lb)	Disc Deflection (rad)	Shaft Torque (in·lb)	Disc Deflection (rad)	Shaft Torque (in·lb)	Disc Deflection (rad)	Shaft Torque* (in·lb)
8080.0	1.0000	1.90×10^6	0.4448	2.70×10^6	-0.3454	2.11×10^6	-0.9606	4.06×10^4
8170.0	1.0000	1.94×10^6	0.4323	2.74×10^6	-0.3689	2.09×10^6	-0.9790	-6.34×10^4
8115.5	1.0000	1.92×10^6	0.4399	2.72×10^6	-0.3547	2.10×10^6	-0.9680	-39.

f = 1291.6 Hz

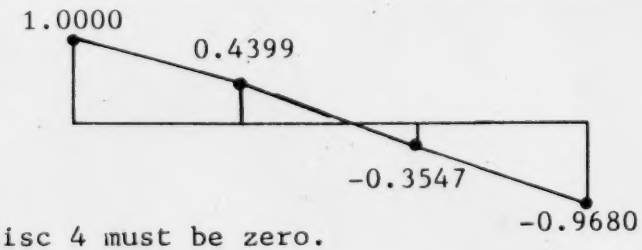

Mode Shape

* Shaft torque to the right of disc 4 must be zero.

Table 2.2 Holzer Tabulation for Torsional Vibration of Crankshaft ATX5 in Free-Free Constraint

crankthrow is,

$$J = (Mrev + 0.5 \cdot Mrec) \cdot CR^2 \qquad (2.3)$$

Mrev = 64% of the connecting rod mass. For ATX5, Mrev = 0.002507 $lb \cdot s^2/in$

Mrec = piston mass and 36% of the connecting rod mass. For ATX5, Mrec = 0.004639 $lb \cdot s^2/in$

CR = crank radius. For ATX5, CR = 1.5 inches.

Thus, an inertia of 0.01086 $lb \cdot s^2 \cdot in$ is added to each of the four inertia discs. The calculations proceed as before except that a twist amplitude of zero is sought for the fixed end rather than a summation to zero for all inertia torques. Table 2.3 shows the tabulation for this important case of crankshaft vibrations.

Frequency (rad/s)	Section 1		Section 2		Section 3		Section 4		End
	Disc Deflection (rad)	Shaft Torque (in·lb)	Disc Deflection (rad)	Shaft Torque (in·lb)	Disc Deflection (rad)	Shaft Torque (in·lb)	Disc Deflection (rad)	Shaft Torque (in·lb)	Twist* (rad)
3250.0	1.0000	5.4×10^5	0.8414	8.9×10^5	0.5828	1.1×10^6	0.2568	1.2×10^6	0.026
3350.0	1.0000	5.8×10^5	0.8315	9.4×10^5	0.5579	1.2×10^6	0.2159	1.3×10^6	-.023
3303.4	1.0000	5.6×10^5	0.8362	9.1×10^5	0.5696	1.1×10^6	0.2350	1.3×10^6	-.00005

f = 525.8 Hz

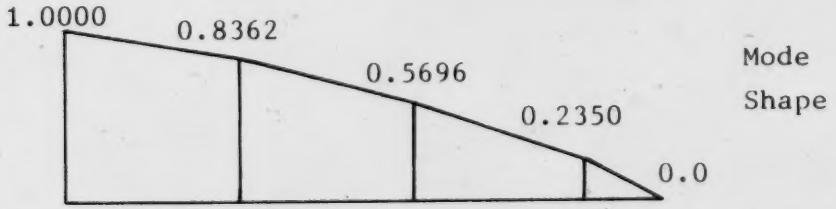

* The fixed end should have zero twist

Table 2.3 Holzer Tabulation for Torsional Vibration of Crankshaft ATX5 in Fixed End Constraint

3. MODEL FORMULATION

3.1 Finite Elements and the Energy Approach

Considering crankshaft geometry, it is not hard to see that application of the exact, analytical equations is prohibitive, if not impossible. Mathematically, the problem would be treated by writing the governing differential equations for each segment, formulating equilibrium and compatibility equations, applying appropriate boundary conditions and then solving for natural frequencies and mode shapes. It is the complex geometrical form of a crankshaft which necessitates the use of a numerical approach. In this project a finite element method is used which replaces the continuous system, having an infinite number of degrees of freedom, with a discretized model having a finite number of degrees of freedom.

The type of element used is the one dimensional (1-D) or "line" finite element that represents the basic geometry of a crankshaft as a series of cylindrical or rectangular elemental blocks. The reference to one dimension has to do with the mathematical description of the element and not its actual physical geometry. Bickley & McCallion [7] decided against the one dimensional element because of foreseeable difficulties in modelling the web by a simple beam. They surmised that correction factors, determined empirically or by detailed theoretical analysis would be necessary. A positive consequence of using this type of element is that

an entire crankshaft may be modelled with a small number of elements (24 elements for a typical four throw crankshaft).

When considering the crankshaft in terms of stress analysis it is desirable to use solid, 3-D elements as Shaw & Richter [59] do since a very fine mesh is necessary to predict stress levels accurately in areas such as journal fillets. They use 581 isoparametric elements for a quarter of a crankthrow indicating that modelling of an entire crankshaft would be an explosively large computer problem. However, in this thesis the concern is primarily with the modes of vibration rather than stress levels directly. The hypothesis is that modes of a crankshaft may be computed with sufficient accuracy using line elements. In addition, the proposed solution allows for convenient graphical presentation of the mode shape by plotting only the centerline deformation.

The energy method is a convenient way of formulating the dynamic equations of motion for free, undamped vibration. The potential or strain energy as well as the kinetic or motion energy for an individual element is first mathematically formulated in terms of specially chosen nodal degrees of freedom. The equation of motion for the element is obtained from Lagrange's equation:

$$\frac{d}{dt}\left[\frac{\partial L}{\partial \dot{p}_i}\right] - \frac{\partial L}{\partial p_i} = 0 \qquad (3.1)$$

where L is the Lagrangian defined as,

$$L = K.E. - P.E. \qquad (3.2)$$

K.E. = Kinetic Energy of the vibrating element

P.E. = Potential Energy of the vibrating element

and the variable p_i is any one of the element degrees of freedom. Thus, if there are "m" degrees of freedom for an element there will be m simultaneous equations to solve. If the kinetic and potential energy expressions are now substituted in equation 3.2, and equation 3.2 into equation 3.1, the following matrix equation of motion for an element results.

$$[ME] \cdot \{\ddot{p}\} + [KE] \cdot \{p\} = \{0\} \qquad (3.3)$$

[KE] Element stiffness matrix

[ME] Element mass matrix

Further operations are necessary before the entire system or global equations of motion may be obtained. First, transformation procedures must be applied to the nodal coordinates since the elements each have a unique postion and orientation in the system model. The equations of motion for each element in terms of transformed nodal coordinates are then combined in an assembly operation to form the global equations of motion. Finally, the resulting global matrix equation of motion is constrained to account for boundary conditions. The equations of motion are then ready to be solved for the natural frequencies and mode shapes of the system.

3.2 Element Description

Each element has two end nodes and six degrees of freedom per node. Included at each node are three translational and three rotational freedoms and thus, deformation may be three dimensional with the result that no category of mode is exempt or restricted. The basic element is actually a superposition of four sub-elements. Figure 3.1 shows the four sub-elements and in Figure 3.2 is shown how they are combined into one composite element. The nodal variables are ordered in the most convenient way for the sake of the transformation procedure to be outlined in the next section. Variables p_1, p_2 and p_3 are the translational freedoms in the x, y and z directions respectively, for node 1. Variables p_4, p_5 and p_6 are element end face rotations, about the x, y and z axis respectively, also for node 1. This pattern is repeated at node 2 for the freedoms p_7 to p_{12}. In the following discussion, reference should be made to Appendix A for the analytical expressions of the potential and kinetic energy of each of the vibrating sub-elements.

For the axial extension element the nodal variable is the displacement parallel to the length axis. A linear displacement function is prescribed for this element. The stiffness matrix may be obtained directly from the strain or potential energy expression.

For the mass matrix, rather than lumping half of the mass of the element to each node a consistent mass matrix

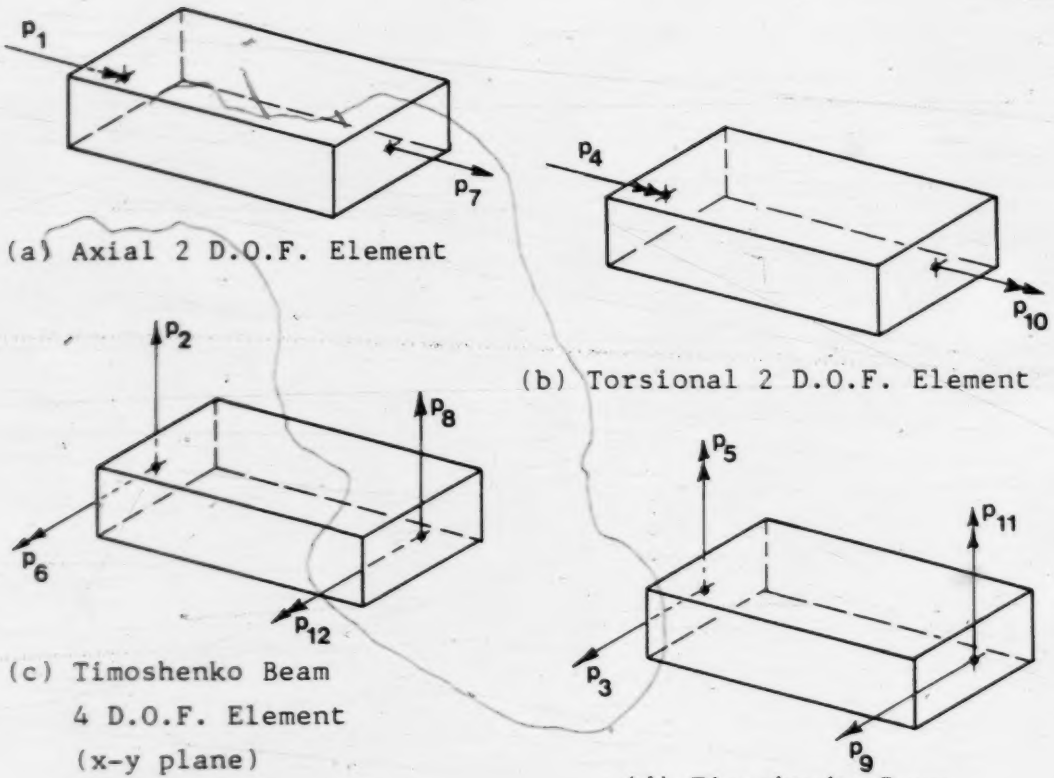

(a) Axial 2 D.O.F. Element

(b) Torsional 2 D.O.F. Element

(c) Timoshenko Beam
4 D.O.F. Element
(x-y plane)

(d) Timoshenko Beam
4 D.O.F. Element
(x-z plane)

Figure 3.1 Sub-elements Used in Composite Element

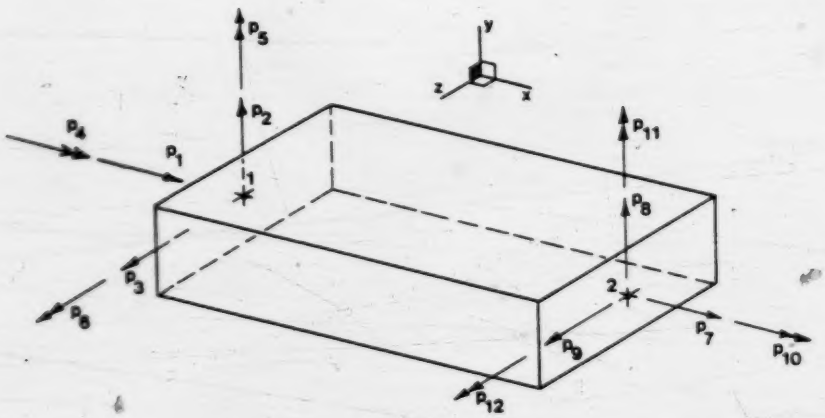

Figure 3.2 Composite Finite Element

may be found from the kinetic energy expression.

The torsional element is similar to the axial element in many respects. The nodal variable in this case is the twist about the longitudinal axis.

It should be noted here that using the conventional polar second moment of area in the torsional rigidity expression is not valid for rectangular cross-sections. Flexibility that is introduced due to warping of the cross-sectional planes is not accounted for if the simple expression is used. By using the method based on Prandtl's membrane analogy a more accurate expression for the polar second moment of area is obtained.

$$J_{xx} = k_1 \cdot b \cdot t^3 \qquad (3.4)$$

J_{xx} = polar second moment of area for rectangular cross-section.

b = width

t = thickness

k_1 = factor a function of aspect ratio

The expression requires the use of a numerical factor, k_1, which is a function of the width to thickness ratio, b/t, where b should be greater than t. Timoshenko & Goodier ([68], p.312) tabulate this factor and Stickler ([63], p.32) gives a formula to the same effect, which is especially convenient when considering the computer code.

$$\frac{1}{k_1} = 3.00 + \frac{1.39}{(b/t)} + \frac{2.70}{(b/t)^2} \qquad (3.5)$$

Although this altered expression is used for torsional rigidity in the stiffness matrix, the inertia matrix for this element contains the basic second moment of area term,

$$J_{xx} = b \cdot t \cdot (b^2 + t^2)/12 \qquad (3.6)$$

Two types of elements are in common use for accommodating the flexure in the two planes of bending. The Bernoulli-Euler beam element is based on the elementary strength of materials assumptions for a beam in flexure. That is, deflection is due only to the bending moment, cross-sections always remain plane and the strain is assumed to vary linearly across the depth of the beam. The second type of flexural element is the Timoshenko beam [71] element where the effect of transverse shearing force and rotary inertia of the beam segments on the deflections and slopes is included. These effects become more important as the radius of gyration to length ratio increases. A crankshaft finite element model is composed of some very short beam segments and thus, inclusion of these two effects in the beam finite elements is expected to increase the accuracy of the model. A quantitative evaluation of the effects of shear deformation and rotary inertia on the frequencies of an actual crankshaft will be made in Section 3.6.

The Timoshenko beam elements for the two planes of bending are derived in papers by Davis, et al. [18] and Thomas, et al. [66]. These elements assume a cubic variation in transverse displacement and a constant shear slope for

the length of the element. Nodal variables are total transverse displacement and bending or face slope. The stiffness and mass matrices may again be derived from the potential and kinetic energy expressions respectively.

All of the previously defined sub-elements are uncoupled. That is, they act independent of each other and the final deformation of an element is the linear superposition of the deformations due to each sub-element. However, as Yang & Sun [80] describe, the independent freedoms of an element may be coupled to unlike freedoms of other elements in the assembled system. This is basically due to the coordinate transformations involved.

From the elasticity solution for bending of a beam it is apparent that bending in the plane perpendicular to the lengthwise direction also occurs. Timoshenko & Goodier ([68], section 103) show how this anticlastic curvature, or Poisson effect, may also apply to plates. The result of their derivation for plates is given by the following moment-curvature relations (see also Figure 3.3):

$$M_1 = \frac{E \cdot h^3}{12(1-\nu^2)} \left[\frac{\partial^2 w}{\partial y^2} + \nu \cdot \frac{\partial^2 w}{\partial x^2} \right] \tag{3.7}$$

$$M_2 = \frac{E \cdot h^3}{12(1-\nu^2)} \left[\frac{\partial^2 w}{\partial x^2} + \nu \cdot \frac{\partial^2 w}{\partial y^2} \right] \tag{3.8}$$

w = deflection in the z direction

h = plate thickness

ν = Poisson's ratio for the plate material

E = Young's modulus for the plate material

The webs or cheeks of a crankthrow may also be described as plates rather than beams since in many cases they have small depth to width ratios. When the web is subjected to bending about the width axis it will be assumed that, as far as the "plate beam" is concerned, the deformation is purely cylindrical with no bending due to the Poisson effect (see Figure 3.4). This assumption seems to be a valid one since Fessler & Sood ([24], p.571) found no anticlastic curvature in their tests on single and double throw crankshafts. Mathematically, the curvature $\partial^2 w/\partial x^2$ in equations 3.7 and 3.8 is set to zero, assuming in this case that the y axis is the longitudinal one and the x axis is the width axis. M_2 is the internal moment necessary to keep the deformation cylindrical. M_1 for the web reduces to $EI(\partial^2 w/\partial y^2)/(1-\nu^2)$ which differs from the beam moment-curvature relation, $M=EI(\partial^2 w/\partial y^2)$, by only the $(1-\nu^2)$ term in the denominator. For steel, this is equivalent to increasing Young's Modulus by about 10%. Thus, inclusion of plate rigidity will tend to stiffen the model for bending in the plane of the crankthrows. In the formulation of the sub-element for web bending in the x-y plane (see Figure 3.1(c)) the $(1-\nu^2)$ term is also included.

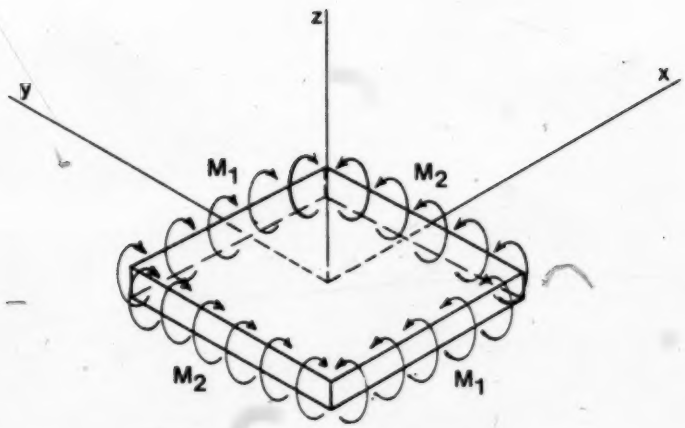

Figure 3.3 Plate Bending

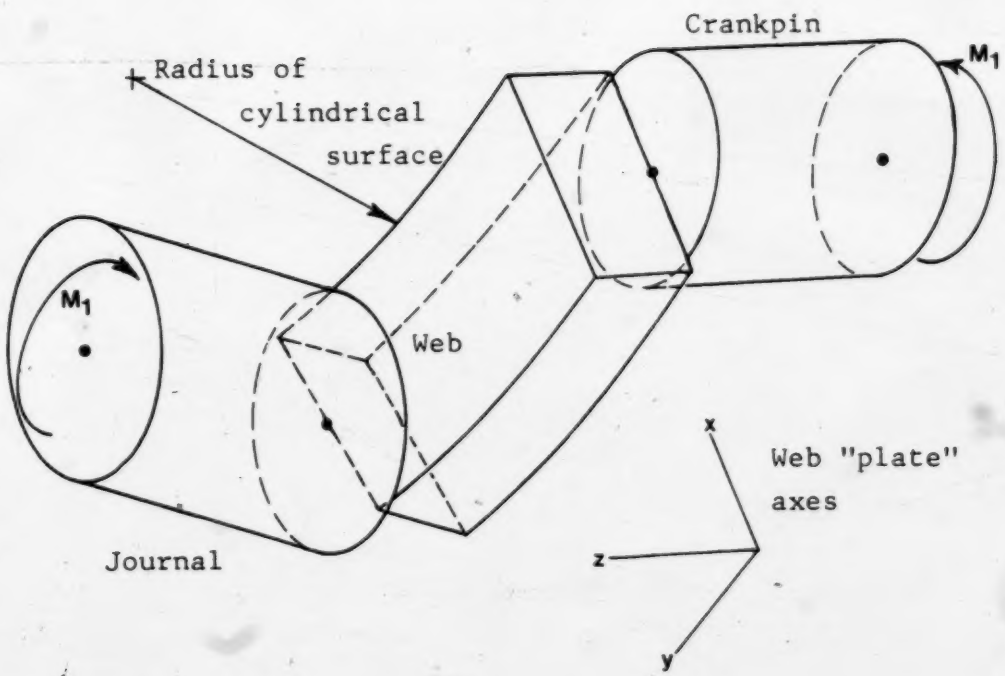

Figure 3.4 Web Curvature for In-Plane Bending

3.3 Transformations and Assembly

Having formulated the elements with the necessary degrees of freedom the problem of assembly into the correct geometry required by the crankshaft is now considered. This requires that each element be oriented to its correct position by a coordinate transformation procedure and then joined at its nodes to the neighboring elements. First, the element and global axis systems are defined. The element axis system is shown at the top of Figure 3.5. The global axis system refers to the set of axes applied to the crankshaft as a whole. The global x axis is the crankshaft centerline and the global y axis is directed parallel to the crankthrow for cylinder number one. The global z axis is determined from the global x and y axes using the right hand rule. The element mass and stiffness matrices describe the same physical element regardless of the orientation of the element. However, the numerical form of these matrices depends on which axis system the nodal coordinates are expressed in. The following transformation procedure shows how the element mass and stiffness matrices expressed in the element axis system are changed to matrices defined in the global axis system.

The relationship between element and global axis systems will, in general, be different for each element comprising the crankshaft model. This relationship is best stated in the form of a matrix of direction cosines. That is, the cosines of the angles between each of the element

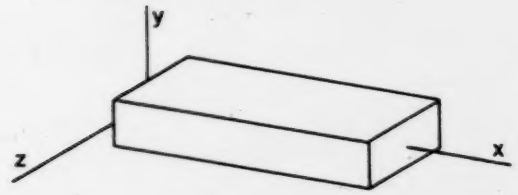

Original axis system

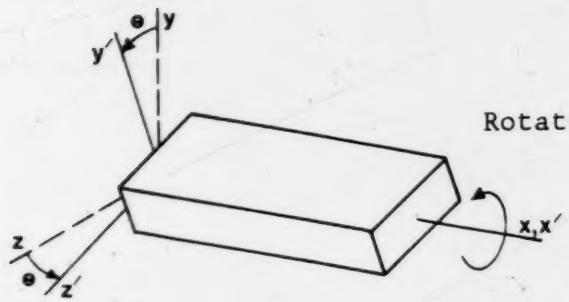

Rotate θ degrees about x axis

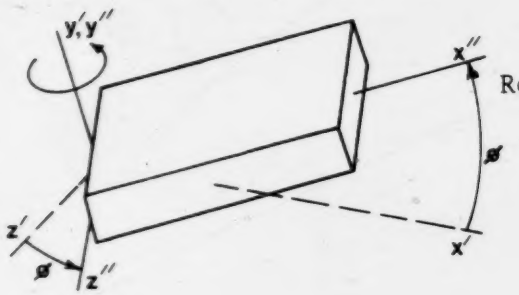

Rotate ϕ degrees about y' axis

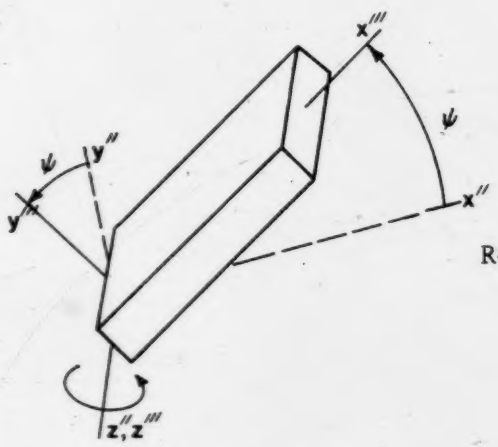

Rotate ψ degrees about z'' axis

Figure 3.5 Coordinate Transformation of Elements

axes and each of the global axes. A total of nine values for 3-D axis systems requires a 3x3 matrix (called $[T]_e$). These nine values are not independent since both axis systems consist of three mutually orthogonal axes providing a total of six constraints. Thus, only three independent values are needed to completely define any orientation of the element axis system relative to the global axis system. A set of three angles or rotations, known as the Tait-Bryan angles [29], are ideally suited for this purpose. These angles, which are used to compute the nine direction cosines, are best understood by referring to Figure 3.5.

Proceeding to formulate $[T]_e$, unit vectors are assigned to each axis system shown in Figure 3.5. Let $\{\hat{w}\}$ be the column of unit vectors, $\hat{x}$, $\hat{y}$ and $\hat{z}$ for the original element axis system. These vectors are related to the unit vectors $\hat{x}'$, $\hat{y}'$ and $\hat{z}'$ by the relation,

$$\{\hat{w}'\} = [A]\cdot\{\hat{w}\} \qquad [A] = \begin{bmatrix} 1 & 0 & 0 \\ 0 & \cos\theta & \sin\theta \\ 0 & -\sin\theta & \cos\theta \end{bmatrix} \tag{3.9}$$

Likewise, for the next two successive rotations of ϕ and ψ the following relations apply.

$$\{\hat{w}''\} = [B]\cdot\{\hat{w}'\} \qquad [B] = \begin{bmatrix} \cos\phi & 0 & -\sin\phi \\ 0 & 1 & 0 \\ \sin\phi & 0 & \cos\phi \end{bmatrix} \tag{3.10}$$

$$\{\hat{w}'''\} = [C]\cdot\{\hat{w}''\} \qquad [C] = \begin{bmatrix} \cos\psi & \sin\psi & 0 \\ -\sin\psi & \cos\psi & 0 \\ 0 & 0 & 1 \end{bmatrix} \tag{3.11}$$

By combining the relations in equations 3.9, 3.10 and 3.11 the matrix $[T]_1$ is calculated.

$$\{\hat{w}'''\} = [C]\cdot[B]\cdot[A]\cdot\{\hat{w}\} = [T]_1\cdot\{\hat{w}\} \qquad (3.12)$$

where, $[T]_1 = [C]\cdot[B]\cdot[A]$

In subroutine COTRAN, listed in Appendix B3, the general explicit form of matrix $[T]_1$ is given as a function of θ, ϕ and ψ.

The element coordinates are composed of the nodal deflections and end face rotations which act along and about the element axis unit vectors. The nodal coordinates must be treated as vectors if the transformations described above are to be applied. This is no problem for the linear degrees of freedom but could pose a problem for the end face rotational degrees of freedom. Finite rotations are distinct from infinitesimal rotations in that they may not be treated as vector quantities. However, it is understood that the vibrating crankshaft undergoes only small oscillations and thus the rotational degrees of freedom may be assumed to be infinitesimal rotations. Therefore, element coordinates may be transformed to global coordinates by the matrix $[T]_1$. The composite finite element has a total of 12 nodal coordinates and requires matrix $[T]_1$ to be applied four times. This is done by constructing the element transformation matrix [T] (12x12) from the axis transformation matrix $[T]_1$.

$$[T] = \begin{bmatrix} [T]_1 & & & \\ & [T]_2 & & \\ & & [T]_3 & \\ & & & [T]_4 \end{bmatrix} \qquad (3.13)$$

For an element in its correct orientation, it is most convenient to define the Tait-Bryan angles in terms of rotations from the global axis system to the element axis system. Thus, the relation between coordinates in the two systems is given by:

$$\{p\} = [T] \cdot \{r\} \qquad (3.14)$$

$\{p\}$ Nodal displacements in the element axis system.

$\{r\}$ Nodal displacements in the global axis system.

By differentiating equation 3.14 the transformation for nodal velocities is obtained.

$$\{\dot{p}\} = [T] \cdot \{\dot{r}\} \qquad (3.15)$$

$\{\dot{p}\}$ Nodal velocities in the element axis system.

$\{\dot{r}\}$ Nodal velocities in the global axis system.

And differentiating again to obtain the transformation for nodal accelerations:

$$\{\ddot{p}\} = [T] \cdot \{\ddot{r}\} \qquad (3.16)$$

$\{\ddot{p}\}$ Nodal accelerations in the element axis system.

$\{\ddot{r}\}$ Nodal accelerations in the global axis system.

Equations 3.14 and 3.16 are substituted into the equations of motion in element coordinates (equation 3.3) to obtain the equations of motion in global coordinates. In order to retain the symmetry of the element mass and stiffness matrices, the matrix equation is then pre-multiplied by $[T]'$. The resulting equations of motion for an element expressed in global coordinates is written as,

$$[MT]\cdot\{\ddot{r}\} + [KT]\cdot\{r\} = \{0\} \qquad (3.17)$$

[MT] Transformed element mass matrix (12x12)

[KT] Transformed element stiffness matrix (12x12)

The manner in which the element mass and stiffness matrices, [ME] and [KE], are transformed so that they express the mass and stiffness properties of an element in global coordinates is by "similarity transformations" given by:

$$[MT] = [T]'\cdot[ME]\cdot[T] \qquad (3.18a)$$

$$[KT] = [T]'\cdot[KE]\cdot[T] \qquad (3.18b)$$

The similarity transformations may also be derived by considering the kinetic and potential energy to be the same scalar quantities regardless of the axis system the nodal coordinates are expressed in. The kinetic and potential energy expressed in element coordinates are respectively:

$$K.E. = 0.5\langle\dot{p}\rangle\cdot[ME]\cdot\{\dot{p}\} \qquad (3.19a)$$

$$P.E. = 0.5\langle p\rangle \cdot [KE] \cdot \{p\} \qquad (3.19b)$$

Likewise, the same quantities may be written for global coordinates.

$$K.E. = 0.5\langle \dot{r}\rangle \cdot [MT] \cdot \{\dot{r}\} \qquad (3.20a)$$

$$P.E. = 0.5\langle r\rangle \cdot [KT] \cdot \{r\} \qquad (3.20b)$$

Equating the kinetic and potential energy expressions in equations 3.19 and 3.20 to obtain:

$$\langle \dot{r}\rangle \cdot [MT] \cdot \{\dot{r}\} = \langle p\rangle \cdot [ME] \cdot \{p\} \qquad (3.21a)$$

$$\langle r\rangle \cdot [KT] \cdot \{r\} = \langle p\rangle \cdot [KE] \cdot \{p\} \qquad (3.21b)$$

At this point the displacement and velocity coordinate transformations given in equations 3.14 and 3.15 are substituted into equations 3.21.

$$\langle \dot{r}\rangle \cdot [MT] \cdot \{\dot{r}\} = \langle \dot{r}\rangle \cdot [T]' \cdot [ME] \cdot [T] \cdot \{\dot{r}\} \qquad (3.22a)$$

$$\langle r\rangle \cdot [KT] \cdot \{r\} = \langle r\rangle \cdot [T]' \cdot [KE] \cdot [T] \cdot \{r\} \qquad (3.22b)$$

By inspection of equations 3.22 it is evident that the similarity equations (3.18) are true.

In the case of crankshafts, the elements used are often so short that the largest cross-sectional dimension is of the same size as the length of the element. For elements that are not colinear, this would mean large geometric incompatibility if elements were forced to join at the mid-points of the end faces. To alleviate the problem, a

transformation may be used whereby the nodes of the elements representing the webs are moved to the edges of the elements. This type of transformation has been presented by Stickler [63] for transforming the element stiffness matrix. The coordinate systems, transformation matrix and element matrix transformations for a web element are shown in Figure 3.6. The transformation for nodal accelerations may be given by $\{\ddot{q}\} = [T]\cdot\{\ddot{p}\}$ if the second order, non-linear terms due to centripetal acceleration are neglected. Thus, the element mass matrix is transformed by the same transformation matrix [T]. In the computer program the edge node transformation for webs is performed before the general coordinate transformation.

After an element has been formed in terms of its mass and stiffness matrix and then transformed to global coordinates it must be assembled with all other elements that make up the crankshaft model. The chain assembly procedure is used whereby only two elements join at a node and the crankshaft becomes a "chain" of finite elements. At such a node the two adjoining end faces remain in the same position relative to each other during vibration as when first assembled and in the undeformed position. Mathematically, the global equations of motion are derived from the element equations of motion expressed in transformed coordinates. The principles of displacement compatibility and force equilibrium are applied at each node where two elements are joined. If there are "N" elements in

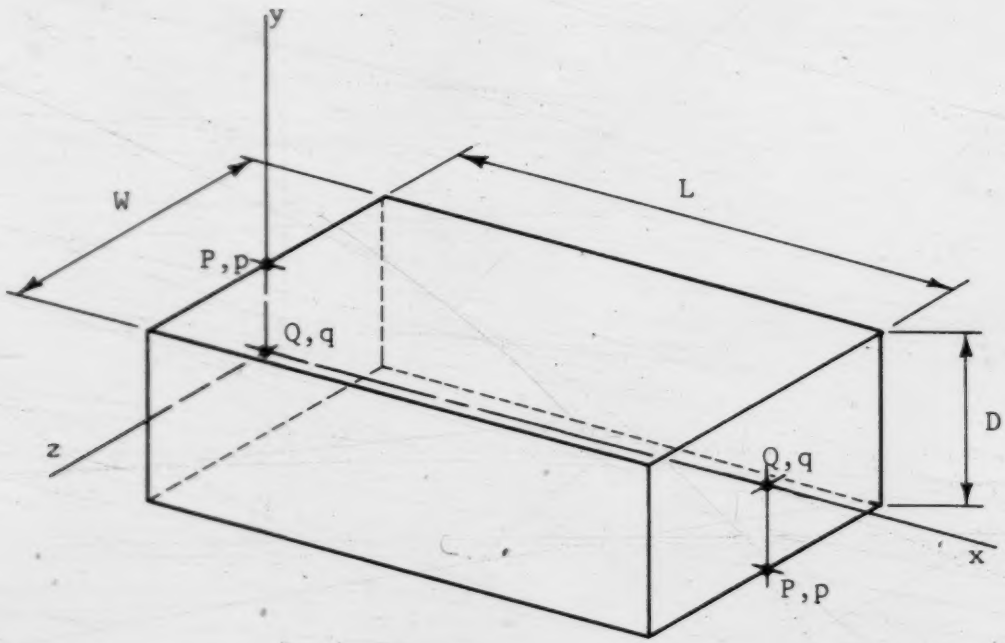

Transformation of Nodal Coordinates

$$\{q\} = [T]\{p\} \qquad \{\dot{q}\} = [T]\{\dot{p}\}$$

where,

$$[T] = \begin{bmatrix} I & A & 0 & 0 \\ 0 & I & 0 & 0 \\ 0 & 0 & I & -A \\ 0 & 0 & 0 & I \end{bmatrix} \qquad [I] = \begin{bmatrix} 1 & 0 & 0 \\ 0 & 1 & 0 \\ 0 & 0 & 1 \end{bmatrix}$$

$$[A] = \begin{bmatrix} 0 & 0 & \frac{1}{2}D \\ 0 & 0 & 0 \\ -\frac{1}{2}D & 0 & 0 \end{bmatrix}$$

Element Matrix Transformations

Stiffness, $[K_p] = [T]^t \cdot [K_q] \cdot [T]$

Mass, $[M_p] = [T]^t \cdot [M_q] \cdot [T]$

Figure 3.6 Edge Node Transformation

a crankshaft finite element model there will be 6·(N+1) degrees of freedom for the system. The global equations of motion may be expressed in matrix form as

$$[MG]\cdot\{\ddot{r}\} + [KG]\cdot\{r\} = \{0\} \qquad (3.23)$$

[MG] Global mass matrix

[KG] Global stiffness matrix

The global matrices, [MG] and [KG], may easily be obtained by adding the coefficients of the element matrices, [MT] and [KT], of each element that correspond to the same force-displacement conditions. Essentially, this amounts to placing the element matrices into the global matrices such that the upper left quadrant of a 12x12, transformed, element matrix is added to the lower, right quadrant of the transformed mass or stiffness matrix of the previous element.

During the assembly procedure the mass and inertia values of material outside the boundaries of the elements must also be added to the global mass matrix. With the relatively large 1-D elements the crankshaft will only be roughly modelled in places such as the web area. Consider Figure 3.4 which shows that a web element has a length that extends only from the journal axis to the crankpin axis. In their experimental tests, Fessler & Sood ([24], p.571) found no bending of the webs below the journal. Thus, parts of the crankshaft such as counterweights, which do not affect the stiffness and sometimes have very irregular geometry, are

treated as rigid bodies and are not represented by finite elements. At each node where an "extra-element" mass is situated the appropriate mass and inertia values are added to the mass matrix. The extra terms are evaluated by forming the kinetic energy expression for the mass in terms of the nodal coordinates.

$$K.E._i = 0.5m_i V_i \cdot V_i + 0.5\dot{\theta}_i \cdot H_i \qquad (3.24)$$

m_i = mass of "extra-element" material at node i

V_i = velocity of the center of gravity of mass m_i

$\dot{\theta}_i$ = angular velocity vector of the rigid body mass

H_i = angular momentum vector about the center of gravity of mass m_i

For counterweights of uniform thickness the derived figures method described in Section 2.4 may be used to obtain inertia and center of gravity data.

3.4 Constraints and Solution

In order for the equations to be solved numerically certain conditions of constraint must be applied to the system degrees of freedom. The constraints may be applied to the system equations in either one or both of the following two ways. First, by rigidly constraining certain degrees of freedom so that they are eliminated entirely from the model. In equation 3.23 above this is done by removing the variables corresponding to these freedoms from $\{r\}$ and $\{\ddot{r}\}$ and by deleting the corresponding rows and columns from [MG]

and [KG]. A second method involves constraining by linear or torsional springs at specified degrees of freedom. This is done mathematically by adding the spring constant to the appropriate element or DOF on the diagonal of the stiffness matrix.

For the example crankshafts modelled in this thesis, two constraint systems have been used: free-free and simple bearing constraints. Free-free refers to a crankshaft suspended from soft springs and simple bearings to the approximate constraints a crankshaft is subjected to in an engine. For the free-free mode of constraint springs with very small spring constants are attached to the crankshaft. It should be noted that any rigid body has six independent parameters that will completely describe its position and orientation in space. Thus, at least six degrees of freedom must be constrained. The six rigid body vibration modes of the crankshaft should have frequencies considerably less than the lowest flexible mode. This is so that the flexible modes will not be affected by the presence of the spring constraints and so simulate a truly free structure.

In an engine the crankshaft is not a free structure but rather is part of a controlled system and constrained by other components of the engine such as the main bearings. The simple bearing constraint model assumes no oil film damping or position dependent stiffness in the main bearing. Instead, a method is used whereby all lateral movement at the journal centers is prohibited while the journal is left

free to tilt, rotate and move axially. A more sophisticated method is to simulate the stiffness effect of the main bearings and bulkheads by appropriate linear and rotary springs. Values for spring constants may be obtained by experimental methods and some have been suggested in the literature (see Hodgetts [35],[36] and Welsh & Booker [74]).

As well as lateral constraint of the crankshaft at the main bearings there are other important constraints that deserve attention. If the flywheel mass and inertia is to be included in the crankshaft model then only a light torsional spring at the flywheel node is necessary to constrain the rigid body torsional mode. If no flywheel is included, the torsional DOF at the flywheel end of the crankshaft should be rigidly constrained. In either case (with or without flywheel), a thrust bearing must also be modelled and this is usually done at the flywheel end by rigidly constraining the axial DOF. Finally, consideration must be given to the two rotary freedoms, θ_y and θ_z at the flywheel end of the shaft. The degree of stiffness here is crucial in affecting the bending modes of the crankshaft and rotary spring constants must be chosen with care. For a first approximation it would be rational to place rigid constraints on the two freedoms considering the effect of flywheel inertia on rotation about these two degrees of freedom.

Once the system equations (equations 3.23) have been constrained they are ready to be solved. From Appendix A the

general solution has the form,

$$\{r\} = \{X\}\sin(\omega t) \tag{3.25}$$

$$\{\ddot{r}\} = -\omega^2\{X\}\sin(\omega t) \tag{3.26}$$

$\{X\}$ Amplitudes of global nodal coordinates.

Equations 3.25 and 3.26 are substituted into the system matrix equation (3.23).

$$\begin{aligned} -\omega^2[MG]\cdot\{X\} + [KG]\cdot\{X\} &= \{0\} \\ [KG]^{-1}\cdot[MG]\cdot\{X\} &= (1/\omega^2)\cdot\{X\} \end{aligned} \tag{3.27}$$

Equation 3.27 is in the form of a standard eigenvalue problem where $1/\omega^2$ is the eigenvalue and $\{X\}$ the eigenvector. For a system with N degrees of freedom there will be N eigenvalues and eigenvectors. The n-th eigenvector, $\{X\}_n$, represents the relative magnitudes of the nodal displacement coordinates for a characteristic mode shape of the crankshaft. From the n-th eigenvalue, $(1/\omega^2)_n$, comes the corresponding natural frequency, f_n (Hz).

$$f_n = \frac{1}{2\pi\sqrt{(1/\omega^2)_n}} \tag{3.28}$$

In the computer code a prepackaged routine (EIGZS in the IMSL library) was used to extract all the eigenvalues and eigenvectors for a given crankshaft model. This was found to be a more economical method for the size of the models investigated (150 degrees of freedom or less) than by using an iterative approach whereby only the lowest modes

are extracted. The numerical accuracy of the solution decreases with increasing frequency or mode number but only the lowest six to fourteen modes are of interest and therefore, this should not pose a problem.

3.5 Modelling Deficiencies

A prior consideration was that the theoretical, numerical method proposed here is one that will sacrifice some accuracy for the sake of economy of time, effort and money. The Timoshenko beam and other sub-elements are in themselves a sound, reasonable description for crankshaft materials. The complex geometry of a crankshaft, and especially the web parts, is what introduces the error. A number of points will now be discussed with regard to the assumptions and deficiencies of the model.

A very significant problem concerns element compatibility at the web faces, even for webs with edge nodes. Whether cast or forged, a crankshaft is manufactured as a single structural member. If a forged crankshaft were shown in a cut-away view, the grain flow lines would show the material continuity between journal, web and crankpin. The composite finite element model breaks up this continuum and thus the large joining surface areas between webs and journals are not mathematically described. The basic theory behind the elements demands that any cross-section remains plane. There is no warping or bending of a cross-section except for a rectangular section in torsion. Hence, for a

crankshaft in bending, where a journal or crankpin node joins to an edge node of a web that is at right angles to the journal, geometric incompatibility will result. Figure 3.7 shows the potential gap or overlap that may result in bending of the elements. This incompatibility would tend to make the model overly flexible. For torsion of crankthrows, a similar principle would apply. Instead of boundary geometric incompatibility there is relative slip between the joining element surfaces.

When considering a web of a crankthrow it seems reasonable to think that there may be shearing action in a longitudinal direction rather than just transversly. The large firing and inertia forces occur when the crankthrow is close to top dead center or bottom dead center and thus the web is closely alligned lengthwise with these forces. This mode of flexibility is not built into the web element and could potentially overstiffen the model.

One deficiency of the model results from the fact that a physically three dimensional beam element is seen mathematically as a "line" element. In most cases this is of no real consequence but for the case of torsional vibration this does introduce an error. The true moment of inertia of the crankpin about the crankshaft axis has a radius of gyration slightly greater than the crank radius. For solid sections the radius of gyration is calculated from:

$$k_{xx}^2 = CR^2 + R^2/2 \qquad (3.29)$$

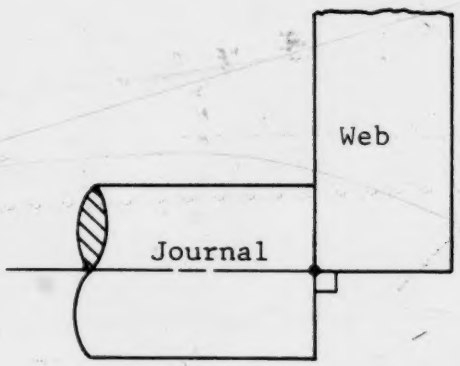

(a) Undeformed Elements

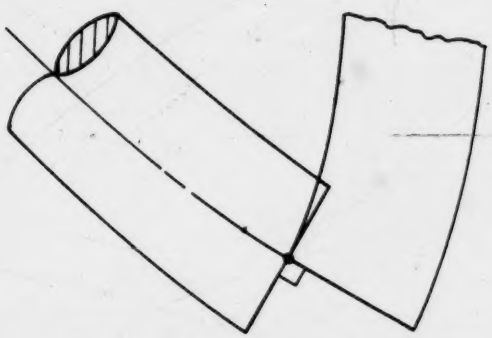

(b) Boundary Overlap

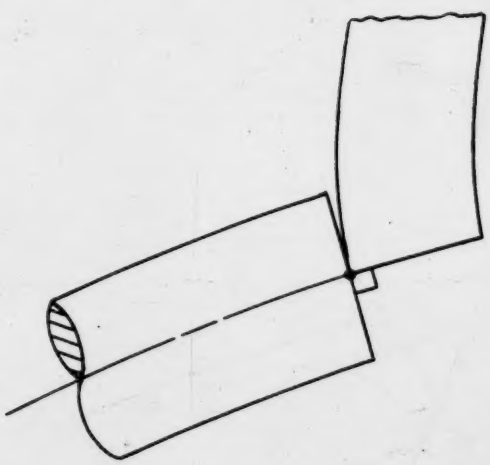

(c) Boundary Gap

Figure 3.7 Potential Incompatibilities at Web Joints

k_{xx}= radius of gyration of crankpin about the crankshaft axis

CR = crankthrow radius

R = crankpin radius

Other problem areas encountered when attempting to model a crankshaft are the presence of such things as oil holes, bored counterweights, web curvatures, gear drives and flanges for bolting to flywheels or transmissions. The oil holes are neglected altogether since the small diameter of these holes (about 0.2 inches) would seem to affect the stresses more than the mass or stiffness of the shaft. Bored holes in the ends of counterweights may be taken into account when calculating the masses and inertias of the counterweights. This is done more or less accurately depending on the resources and investment of the analyst. Webs with curvatures and shapes such as gears and flanges that cannot be modelled by a simple cylinder or rectangular block must be reduced to these simple shapes.

These shortcomings in the model could ultimately raise or lower the modal frequencies. If the computed frequencies and mode shapes for a specific crankshaft differ greatly from the measured ones then a decision must be made on whether to modify the existing model or to resort to a new approach. This decision is discussed in Chapter 4 after computed and experimental results for some example crankshafts have been presented.

3.6 Example Crankshaft Models

It would be appropriate at this point to demonstrate the capabilities of the numerical model by presenting results (modal frequencies and shapes) for a variety of example crankshafts. A single throw and two, four throw, coplanar crankshafts were obtained for the purpose of modelling and testing experimentally. Before presenting computed results some pertinent details of each model will be clarified. Using the results of one crankshaft model, a short discussion on the effects of shear deformation and rotary inertia included in the Timoshenko beam elements is also given.

The four cylinder engine crankshaft, mentioned in Section 2.4 for the Holzer tabulation and coded "ATX5" has a main bearing between each crankthrow. It is shown again in Figure 3.8 along with its finite element model. A number of approximations were made for this model. An oil pump/distributor drive gear as well as the reduced diameter of the front end pulley shaft was all made into one uniform cylindrical element (element 1). The rear end, which consists of a large diameter flange with threaded holes for connecting to the flywheel, was similarly converted (element 24). Four counterweights at nodes 4, 12, 14 and 22 had inertia values calculated by means of the derived figures method. Other material, such as back chamfers, at nodes 5, 6, 7, 9, 10, 11, 15, 16, 17, 20 and 21 were approximated by simple rectangular prisms. At node 19 the material was in

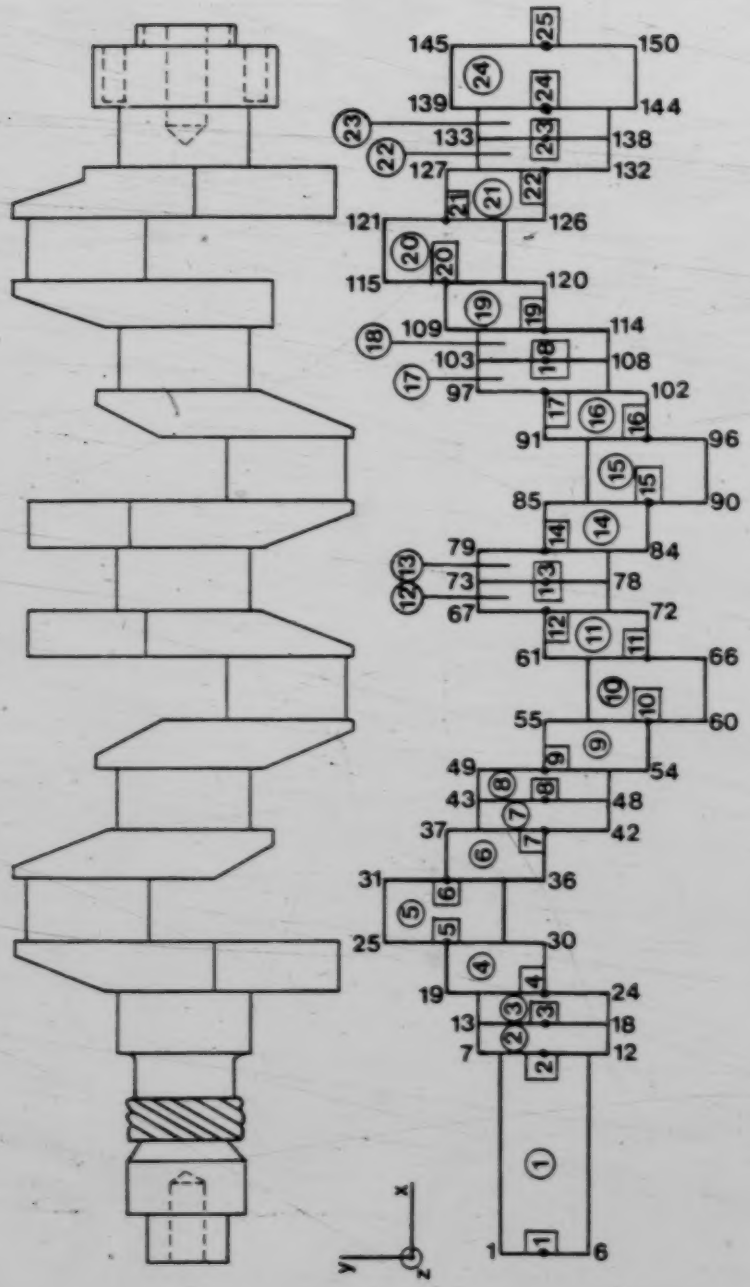

(24) Elements [25] Nodes 150 Degrees of Freedom

Figure 3.8 Finite Element Model for Crankshaft ATX5

the shape of a half circle of uniform thickness. The inertia values for these various shapes and the degrees of freedom to which they are added in the mass matrix were determined using equation 3.24.

A three bearing, four throw crankshaft, coded as "DT3", was also modelled. This shaft had much simpler counterweight geometry and, in addition, both ends of the crankshaft were machined to a smooth finish. A side view of this crankshaft and its finite element representation is shown in Figure 3.9.

Finally, a crankshaft from a single cylinder engine was obtained (model "SL2"). Its ends were also machined for easier modelling. The two counterweights were of such a geometry that it was thought best to model them by two differently sized rectangular prisms. The crankshaft and the finite element model are shown in Figure 3.10.

Data for each model was prepared according to the input parameters given in Appendix B1. The material properties used were a mixture of nominal values for steel ($E=30.0\times10^6$ lb/in^2, $\nu=0.3$) and actual measured values (density, ρ). Average density for each shaft was the measured mass over the measured volume (determined by water displacement tests). Other data includes the system description (number, type and angle of crankthrow), constraints, geometrical dimensions and the mass, inertia, and center of gravity of the counterweights and other lumped nodal masses. A free constraint condition was simulated by the method described

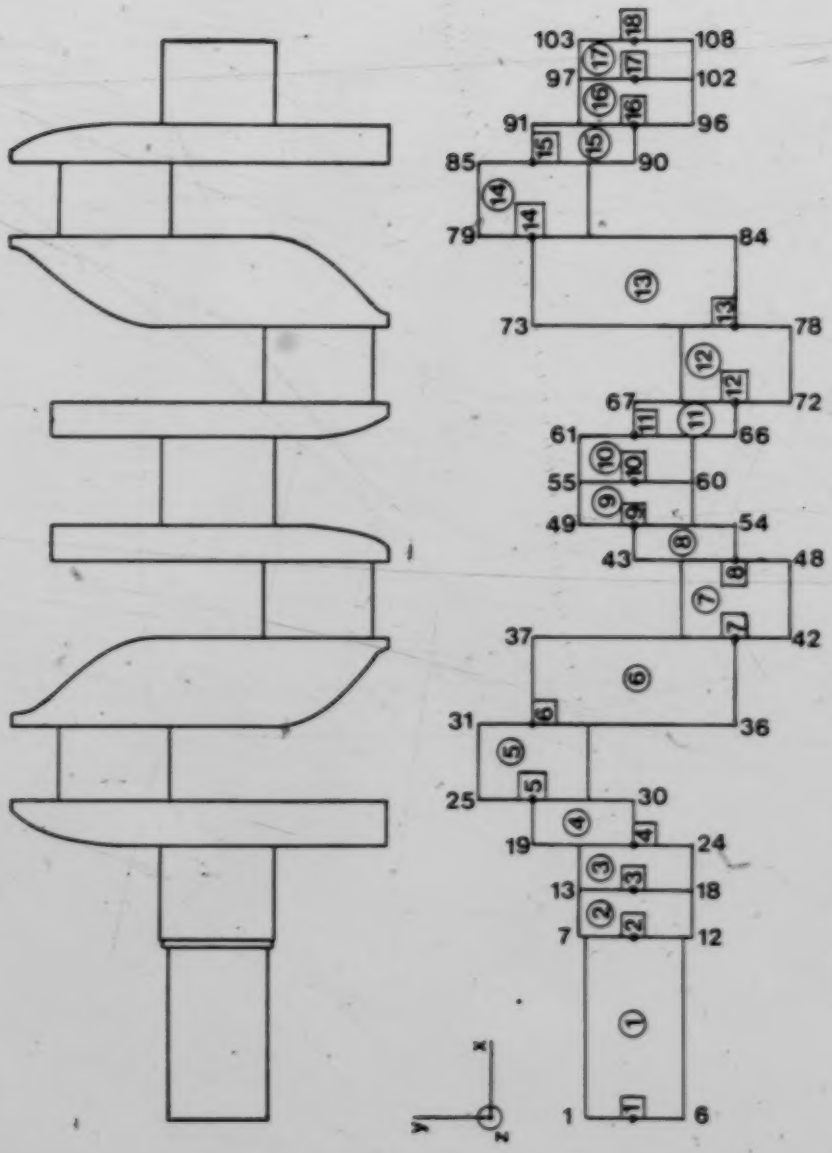

(17) Elements [18] Nodes 108 Degrees of Freedom

Figure 3.9 Finite Element Model for Crankshaft DT3

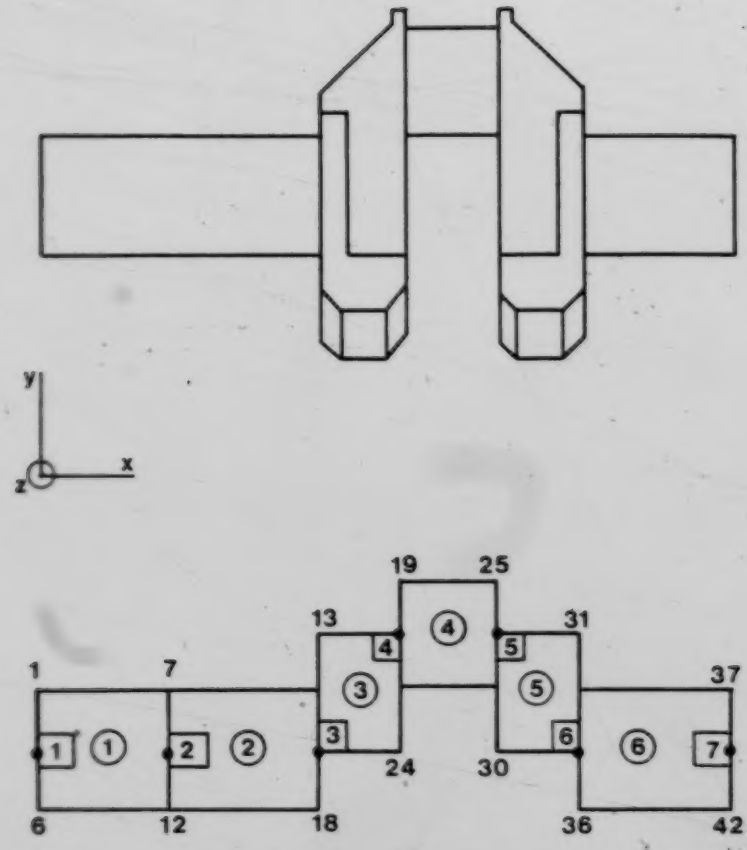

⑥ Elements [7] Nodes 42 Degrees of Freedom

Figure 3.10 Finite Element Model for Single Cylinder Engine Crankshaft (SL2)

in Section 3.4. The actual data is given in Appendix B2.

Appendix B3 contains a listing of the computing codes, written in standard FORTRAN, that were used to calculate natural modes for the crankshafts. Routine "CRANK" is the main structural analysis program which reads in the data, assembles the elements for the crankshaft and solves for the natural mode solution. An Amdahl 5860 mainframe computer at the University of Alberta required less than 30 seconds to compute the solution for crankshaft ATX5, the largest of the three models. The results are shown along with the experimentally determined counterparts in Section 4.2.3. All computed mode shapes include the undeformed shape of the crankshaft centerline shown as a dashed line to aid in visual reference. For ATX5 and DT3 crankshafts the first eight flexible modes are shown in figures 4.6 and 4.7 respectively. The six rigid body modes which result from the free constraint condition are of no interest and are not shown. For SL2 crankshaft the first four flexible modes are shown in Figure 4.8.

Detailed classification and analysis of the modes constitutes the discussion in Chapter 5. However, from observation of the computed modes for each crankshaft, two general classifications are apparent. The first one may be identified as in-plane (IP) modes since all the deformation is in the plane of the crankthrow(s). The other may be classified as out-of-plane (OP) modes since all modal distortion is in a direction normal to the plane of the

crankthrow(s). Note that these distinctions apply specifically to the coplanar crankshafts modelled here.

The effects of shear deformation and rotary inertia in the Timoshenko beam sub-elements will be quantitatively assessed for crankshaft ATX5 in free-free constraint. Figure 3.11 depicts the change in frequency level of each mode when the effects of shear deformation and rotary inertia are included separately and then together. The modes are designated according to the test modes. Inclusion of shear deformation makes the model more flexible and accounting for rotary inertia effectively increases the resistance to angular rotation within each element; thus the natural frequency decreases in every case. The influence becomes more pronounced for higher modes as one might expect since there is more deformation and higher angular velocity associated with these modes. An explanation may be given for the observation that OP modes are more influenced by inclusion of rotary inertia than are the IP modes. Crankshaft webs are usually designed so that their width to thickness ratios are larger than unity. In ATX5 the ratio averages at about 3.78 for all throws. Consequently, the rotational inertia of the web undergoing angular oscillations in an OP mode would be greater than for vibration in an IP mode. The effect of shear deformation on frequency change is not clearly biased towards either OP or IP modes.

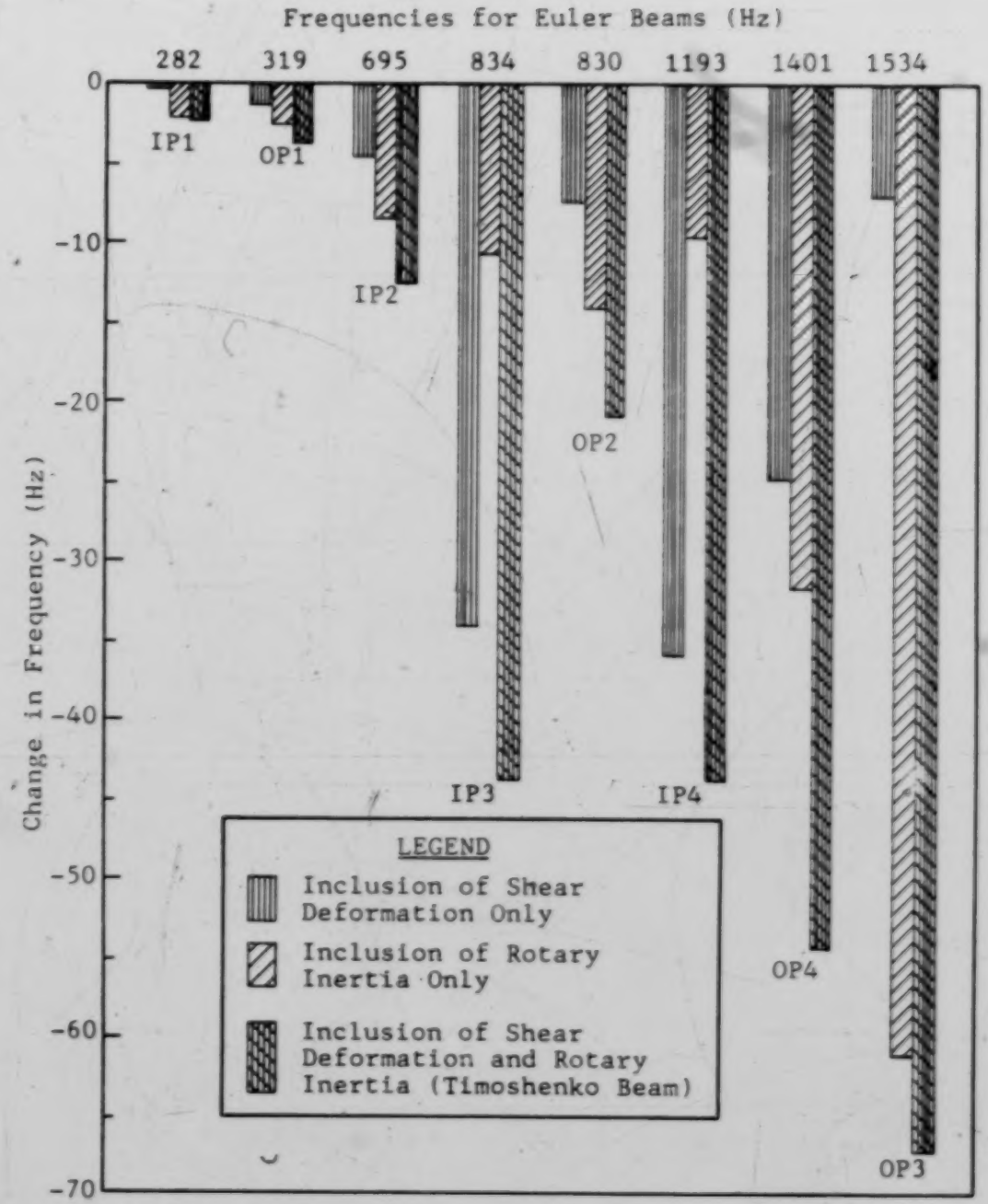

Figure 3.11 The Effects of Shear Deformation and Rotary Inertia on the Natural Frequencies of Crankshaft ATX5

In the following chapter the computed results will be compared with the results of actual tests used to obtain the same modal information from the crankshafts constrained by equivalent boundary conditions.

4. VERIFICATION OF THE COMPUTER MODEL

A numerical model for calculation of natural modes and frequencies of a crankshaft may stand by its own merits insofar as the theoretical basis is sound and complete. However, to gain assurance in the results of a model it is helpful to verify the model against a standard which has a known and sufficient accuracy. This applies to the finite element approximation in general and especially when a model contains known deficiencies due to causes other than the finite element theory (Section 3.5). Experimental tests performed on actual crankshafts with dependable instrumentation should yield the same type of information as the computer model. Comparisons of the results may be made if boundary conditions are equivalent and the effects of instrumentation are minimal.

Two general types of tests were performed on the example crankshafts: static and dynamic. In Section 1 of this chapter the results of an axial compression test performed on crankshaft DT3 are presented and in Section 2 the description and results of resonance tests performed on all three example crankshafts are given.

4.1 Axial Compression Test

Crankshaft DT3 was first machined so that the ends were smooth and flat for positioning in the 50,000 lb. Instron testing machine. A total of three tests were performed with loading rates of 0.01, 0.05 and 0.10 in/min. The maximum

load in each case was well over 30,000 lb. and it was observed that the crankshaft had a permanent decrease in length of about 0.014 inches after each test. From the loading and unloading curves drawn on an integrated chart recorder an average axial stiffness of 221,000 lb/in was computed. It was observed that slight bowing of the crankshaft centerline in the plane of the throws occurred during the test. The results from program CRANK give the axial stiffness as 222,000 lb/in, which is only 0.5% higher than the test result. A plot of the computed deformations is shown in Figure 4.1.

4.2 Resonance Testing

In a resonance test the analyst seeks to extract the modal parameters for each mode of a physical structure constrained by known boundary conditions. This is done by exciting the structure with a known force and then measuring the response of the structure.

4.2.1 Boundary Conditions and Test Methods

The boundary condition most easily achieved experimentally and also easily modelled numerically is the free-free condition. The crankshafts were hung by rubber straps or bands that resulted in an up and down rigid body mode with a frequency of only a few Herz. This is well below the fundamental flexible mode for a crankshaft which is usually of the order of a few hundred Herz.

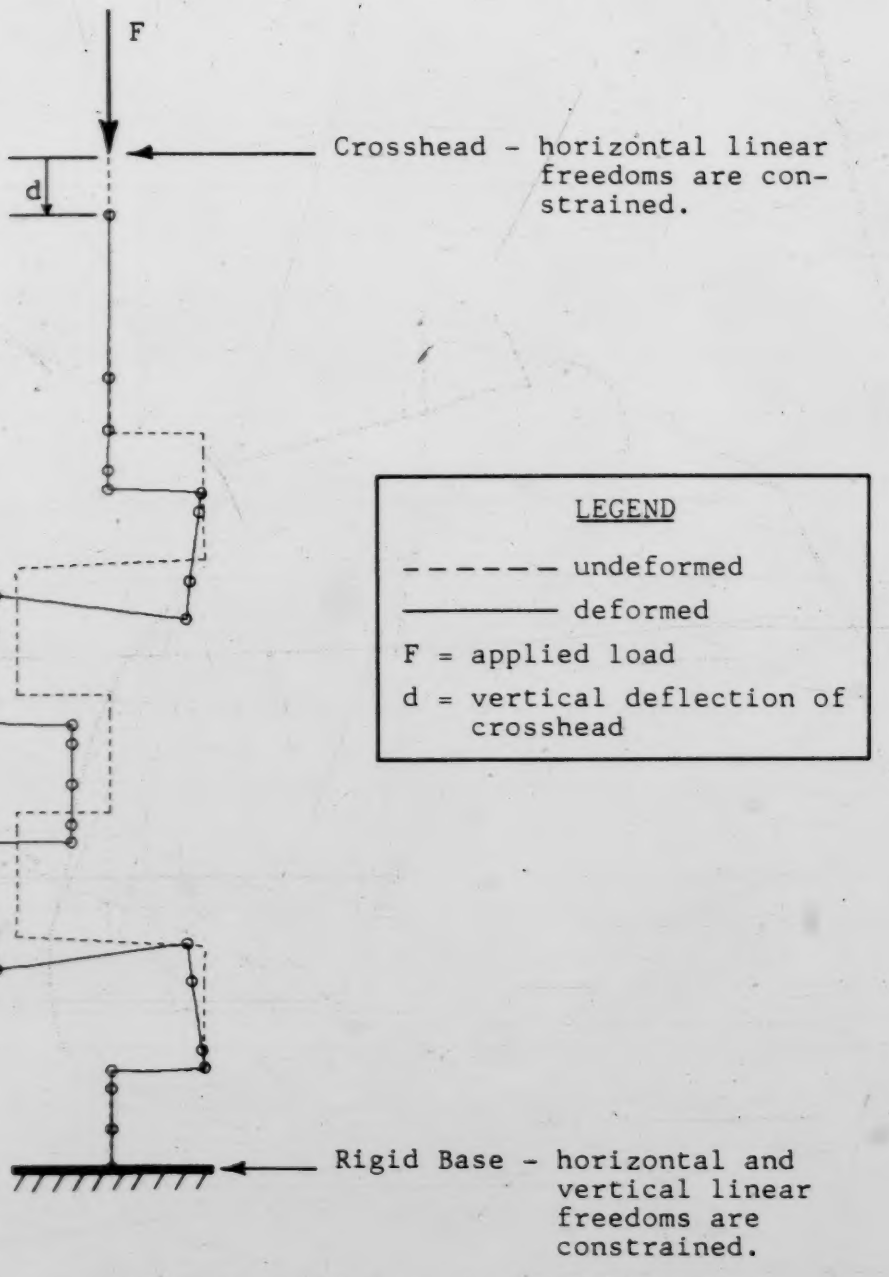

Figure 4.1 Crankshaft DT3 Under Compressive Static Load

One method of resonance testing called Experimental Modal Analysis involves an impulse technique that uses the Fourier transform of both the excitation and response to obtain the frequency response spectrum. The modal parameters may be extracted from the impedance curve. Theoretical and practical aspects of this method are detailed in theses written by Fyfe [28] and Beamish [5].

A simpler, although more tedious, method involves applying a single frequency, sinusoidally varying force through a pre-determined range of frequencies. The lower bound of this frequency range must be less than the fundamental mode of the structure and the upper bound is largely determined by instrumentation capability. One then proceeds to scan through the range in discrete frequency steps, pausing at each frequency long enough for the system to reach steady state conditions, and then recording force and response. Resonant peaks require a secondary scan entailing a smaller step size in order that a more accurate definition of the frequency response curve is obtained when the data is finally plotted. The modulus that is plotted against frequency is called the inertance and is obtained by dividing the acceleration at each frequency step by the corresponding force. A comprehensive and practical guide to resonance testing is given in a three part paper by Ewins [21],[22],[23] and is well worth consulting.

The latter type of resonance test was chosen in this work for determination of modal parameters for crankshafts

DT3, ATX5 and SL2. Details of exactly how these paramenters were obtained and a note to their accuracy is to be discussed in the following subsection.

Standard, available vibration equipment was used except for the force transducer where a specialized device employing strain gages was manufactured and calibrated for force measurement. Figure 4.2 shows a schematic of the test equipment used.

4.2.2 Determination of Modal Parameters and Accuracy

From an analysis of frequency response plots, modes may be identified by significant peaks in the curves and are easily detected for structures with light damping and widely spaced modes. The crankshafts tested may be classified as this type of structure. The frequencies for which the inertance is a maximum are the system natural frequencies.

Another technique for locating natural frequencies is done by scanning the forcing frequency range with only the shaker and force transducer attached; no accelerometer or response measuring device is connected to the crankshaft. At a forcing frequency slightly less than the natural frequency the force reaches a maximum value. At resonance the force signal has decreased to a point where virtually no waveform can be seen on the oscilloscope. The small amount of force being applied at this frequency is only that needed to overcome the damping forces present in the vibrating crankshaft.

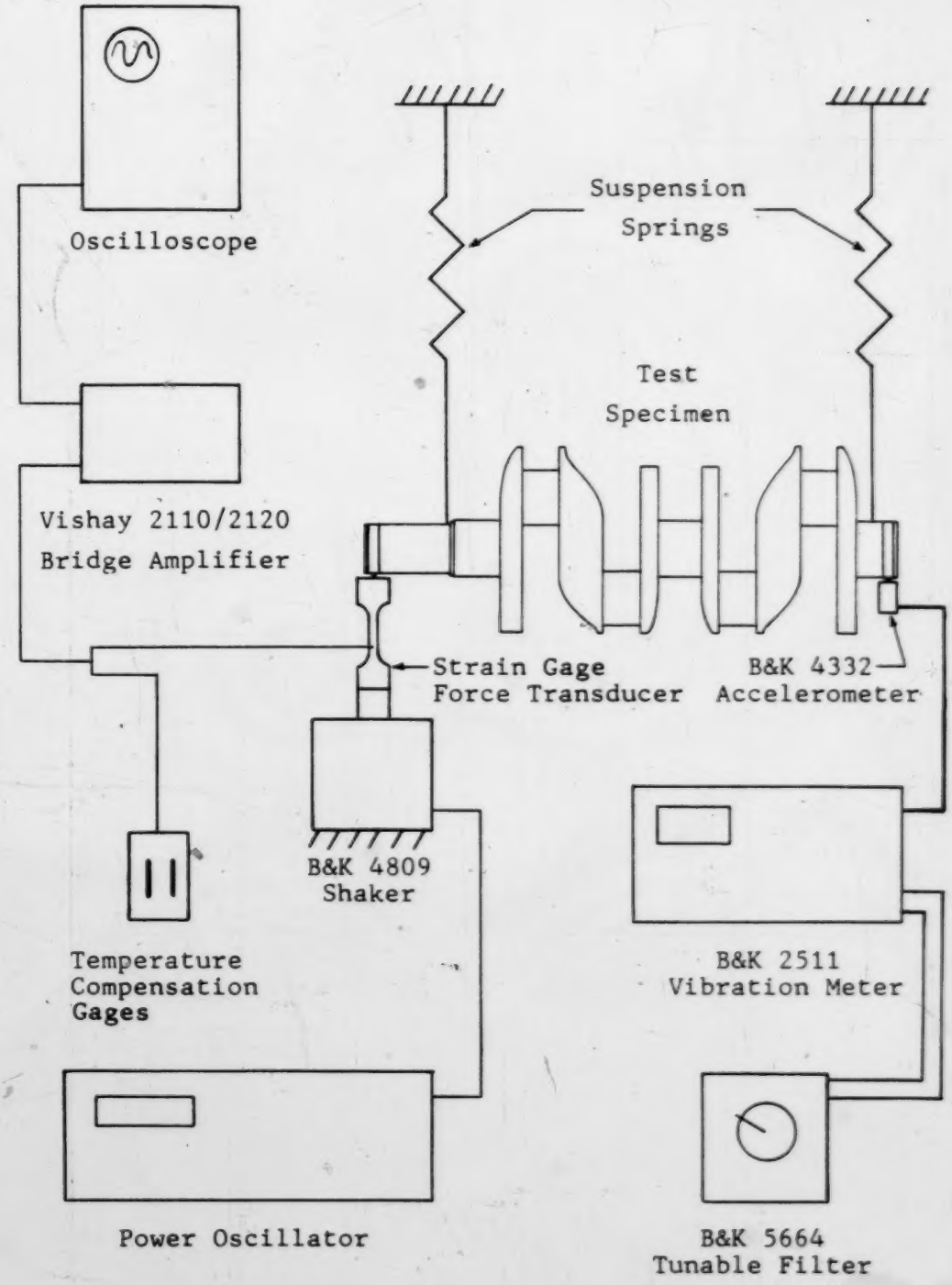

Figure 4.2 Apparatus for Resonance Testing in Free Constraint Mode

An indication of the magnitude of instrumentation effects on natural frequency is gained by observing the change in frequencies when different testing procedures are used. For example, crankshaft DT3 was also tested using an impulse technique whereby only an accelerometer was attached to the structure. The frequencies obtained in this way for modes IP1, OP1 and IP2 were compared with those from two other methods. That is, the maximum inertance method and the minimum force method described above. Between these three methods the natural frequency for any given mode varied from 8 to 17 Hz depending on the mode. Each of these methods involved different instrumentation and thus, an estimation may be made for the range within which the true natural frequency for a mode may lie. It is estimated that the true natural frequency for a crankshaft mode lies within 10 Hz on either side of the minimum force frequency.

The minimum force frequency was used as the basis for comparison with computed results. Reasons for choosing frequencies obtained using this method are as follows.

1. There are no effects due to attachment of response measuring devices.
2. Without additional calibration, the impulse technique was limited to frequencies lower than 1000 Hz.
3. Resonances are easy to identify because only a true mode exhibits the max/min behavior previously described for the forcing signal.
4. Some modes do not exhibit a clear peak and the minimum

force method fixes the frequencies more precisely.

The modal damping factor, ζ_n, may be determined from the frequency response curve according to the half-power method.[4] The result is given as,

$$\zeta_n = \frac{\theta_2 - \theta_1}{2 \cdot f_n} \qquad (4.1)$$

ζ_n = viscous damping factor for the n-th mode

f_n = natural frequency for the n-th mode located at peak inertance

θ_i = oscillator frequency for which the inertance amplitude is $\sqrt{2}/2$ times the peak amplitude. For i =1 and 2, $\theta_1 < f_n < \theta_2$

The accuracy of damping factors was not assessed and remains of little concern since they are not necessary for verification of computed results. They are included only for the sake of presenting complete sets of experimentally determined modal parameters.

Mode shapes may also be determined using the force and response measurements if the response is measured at enough points on the crankshaft. This would require a rather lengthy testing program. However, a mode shape may also be determined by sensing the relative magnitude of vibrations at a natural frequency with a small, hand-held, sharp-tipped probe that is brought into contact with the crankshaft surface. This rather subjective approach was deemed to be sufficiently accurate as it clearly indicated the presence of nodes and locations of increasing or decreasing vibration

---

[4]Derived by Craig [17], p.96,97

amplitude. In spite of the subjective nature of such a method, independent tests revealed good repeatability for any given mode.

In order that changes in vibration amplitude could be adequately detected by the sensing probe the mode shapes had to be sensed at frequencies offset from their corresponding natural frequencies. This is because a natural frequency is located whenever the inertance is a maximum quantity which is not necessarily at the same frequency for maximum acceleration or displacement response. Ewins [23] points out how a mode shape may change when there is such a frequency offset. The average deviance in frequency for eight modes for crankshafts DT3 and ATX5 was 5.7 Hz and 7.1 Hz respectively. It is not expected that any significant error in mode shape is introduced for these two shafts. For crankshaft SL2 the average frequency offset for four modes was 78 Hz. This rather large difference could possibly mean some alteration of the mode shapes from their true forms.

Since computed mode shapes showed either all IP or all OP deflections it was assumed that this was the case and the tests were performed accordingly. For this reason two frequency scans were conducted, with force and response measured at the extreme ends of the crankshafts: one measuring strictly within the plane of throws (IP) and the other only in the OP direction. A third scan was employed on the multi-throw crankshafts, DT3 and ATX5, with an OP force applied at one crankpin and OP response measured at another.

This arrangement was specifically designed to better excite the torsional type modes.

4.2.3 Test Results

Crankshafts ATX5, DT3 and SL2 were tested according to the sine scanning method previously outlined. The frequency response plots are shown in figures 4.3 to 4.5 and the mode shapes are shown in figures 4.6 to 4.8. It should be noted that although computed mode shapes had been plotted prior to the sensing probe tests they were not consulted during the testing procedure so as to prohibit any possible bias. The frequencies given with each mode are those obtained by the minimum force method explained in the previous sub-section. The dark shading on each crankshaft represents the relative magnitude of displacement that is felt with the sensing probe. Shading marks drawn beside the counterweights are indications of vibrations perpendicular to the surface that lies in a plane normal to the paper. The torsional mode, OP3 for DT3 and ATX5, is taken from the torsional scan performed on these crankshafts.

All three crankshafts show that the fundamental mode is of the IP type. For the four throw crankshafts, DT3 and ATX5, the fundamental frequency of about 400 Hz is much lower than IP1 for the single throw crank (SL2) which is over 1300 Hz. The first OP mode (OP1) appears at an average 33% higher frequency than IP1. For any given scan, the modes are usually well spaced and a clear resonant peak is evident

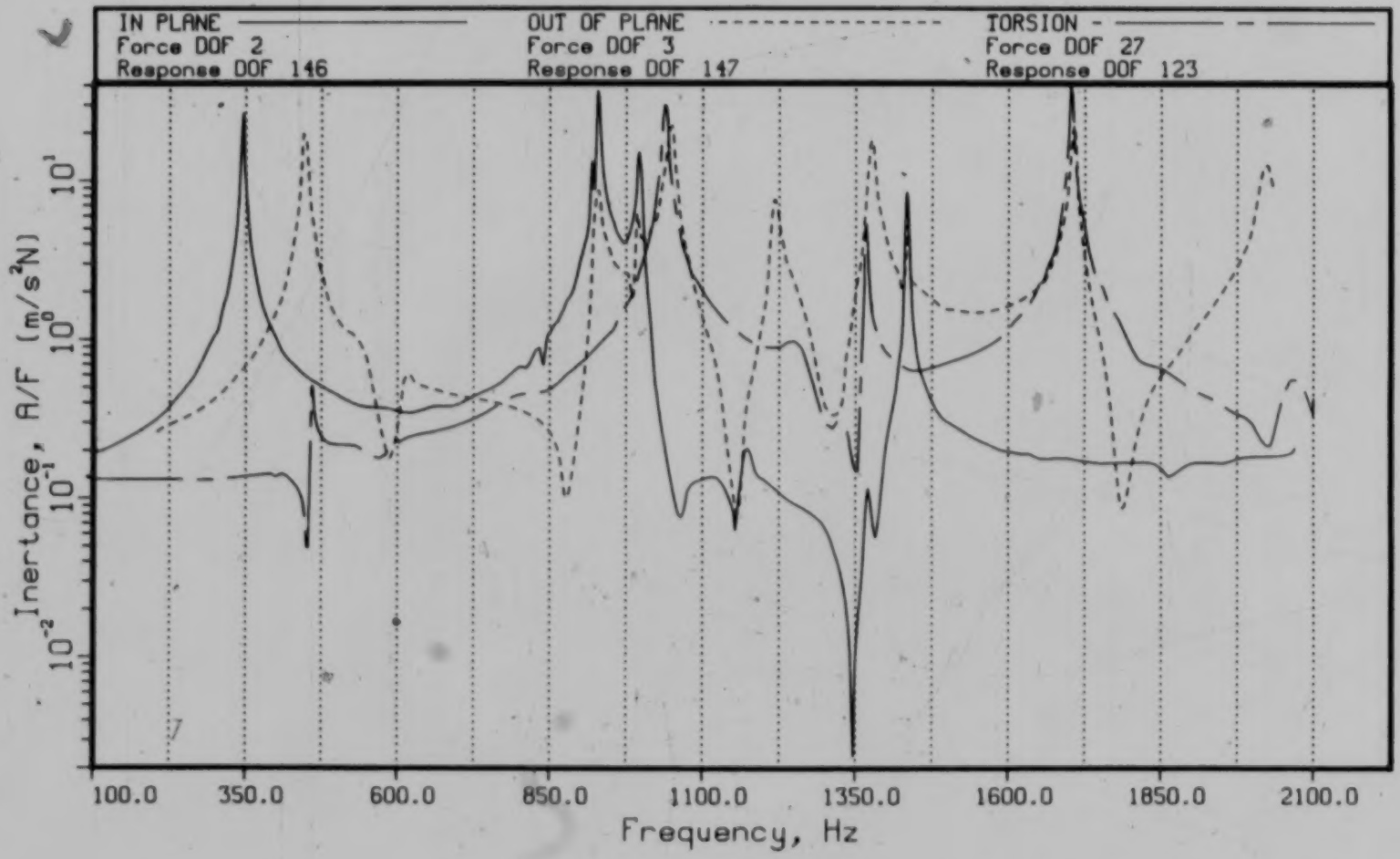

Figure 4.3 Measured Frequency Response for Crankshaft ATX5 in Free Constraint

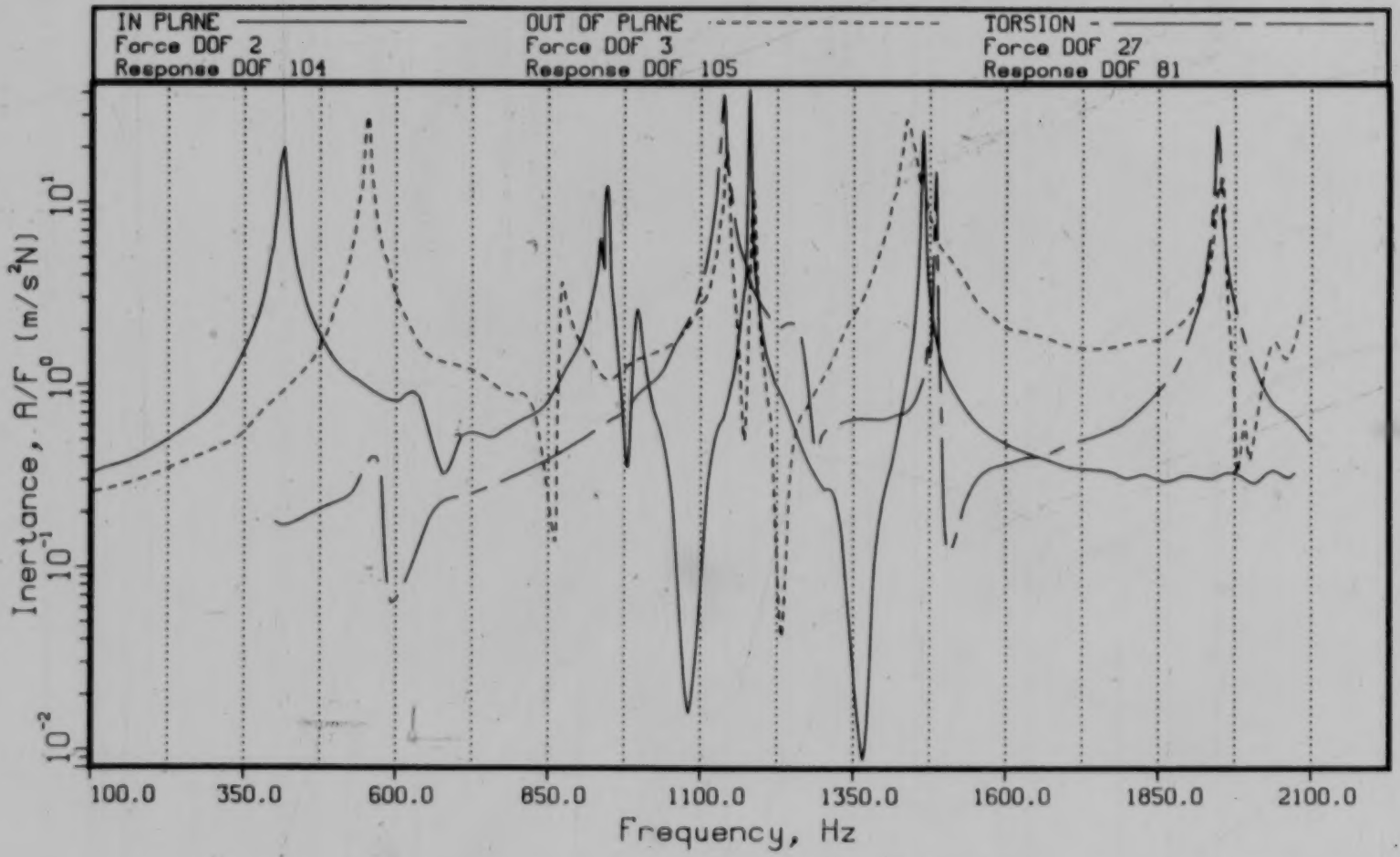

Figure 4.4 Measured Frequency Response for Crankshaft DT3 in Free Constraint

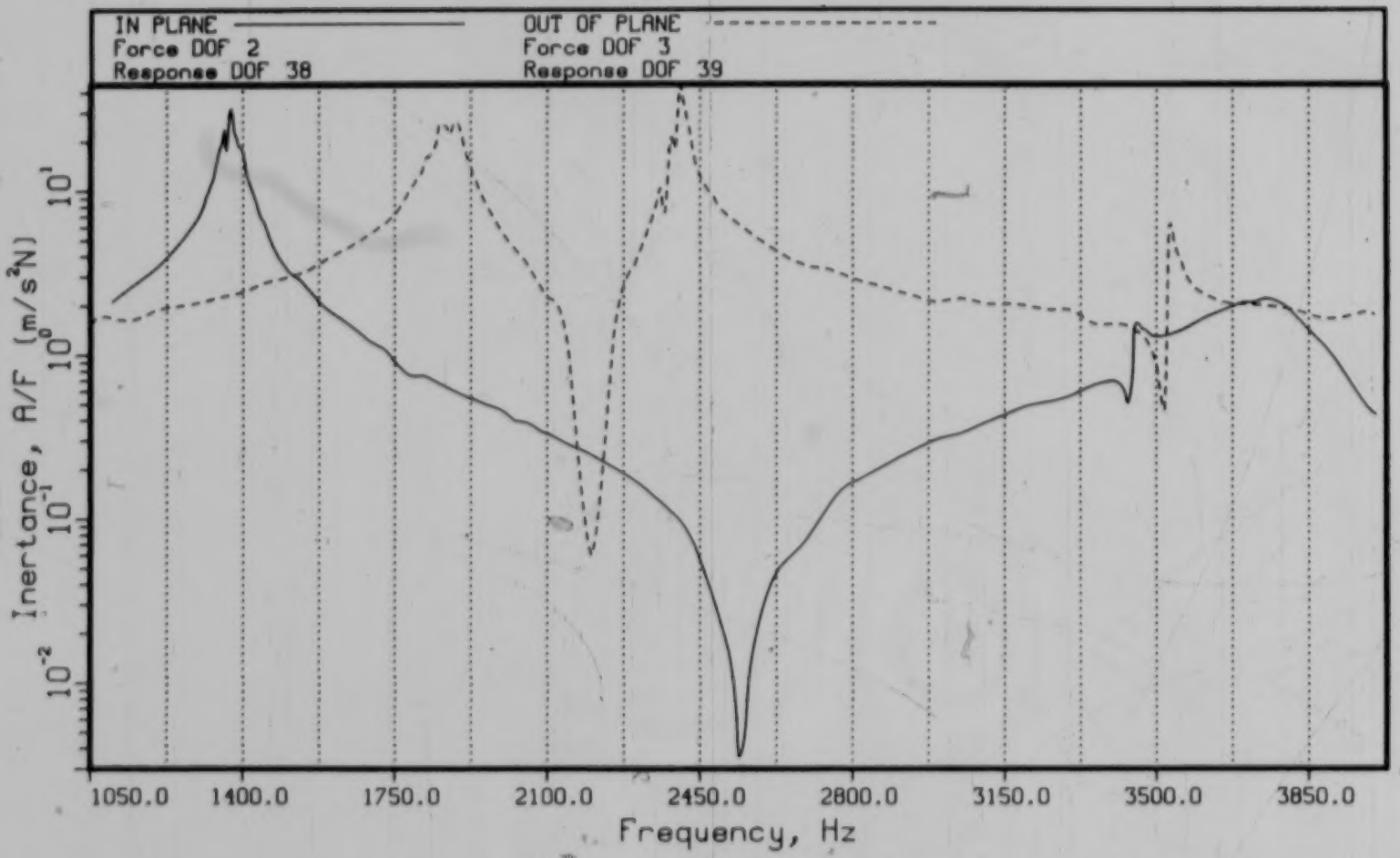

Figure 4.5 Measured Frequency Response for Crankshaft SL2 in Free Constraint

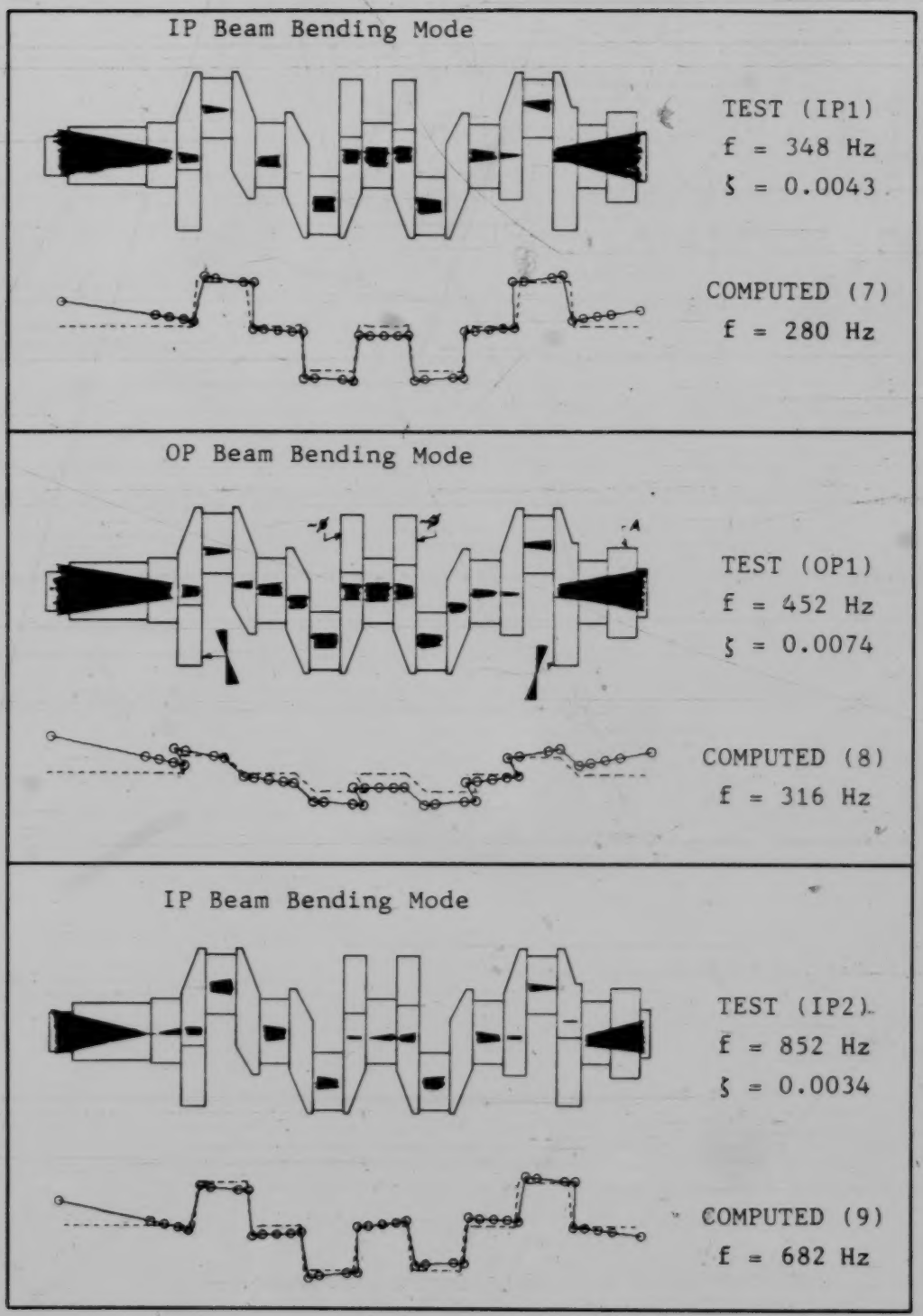

Figure 4.6 Experimental and Computed Modes for ATX5 Crankshaft in Free-Free Constraint

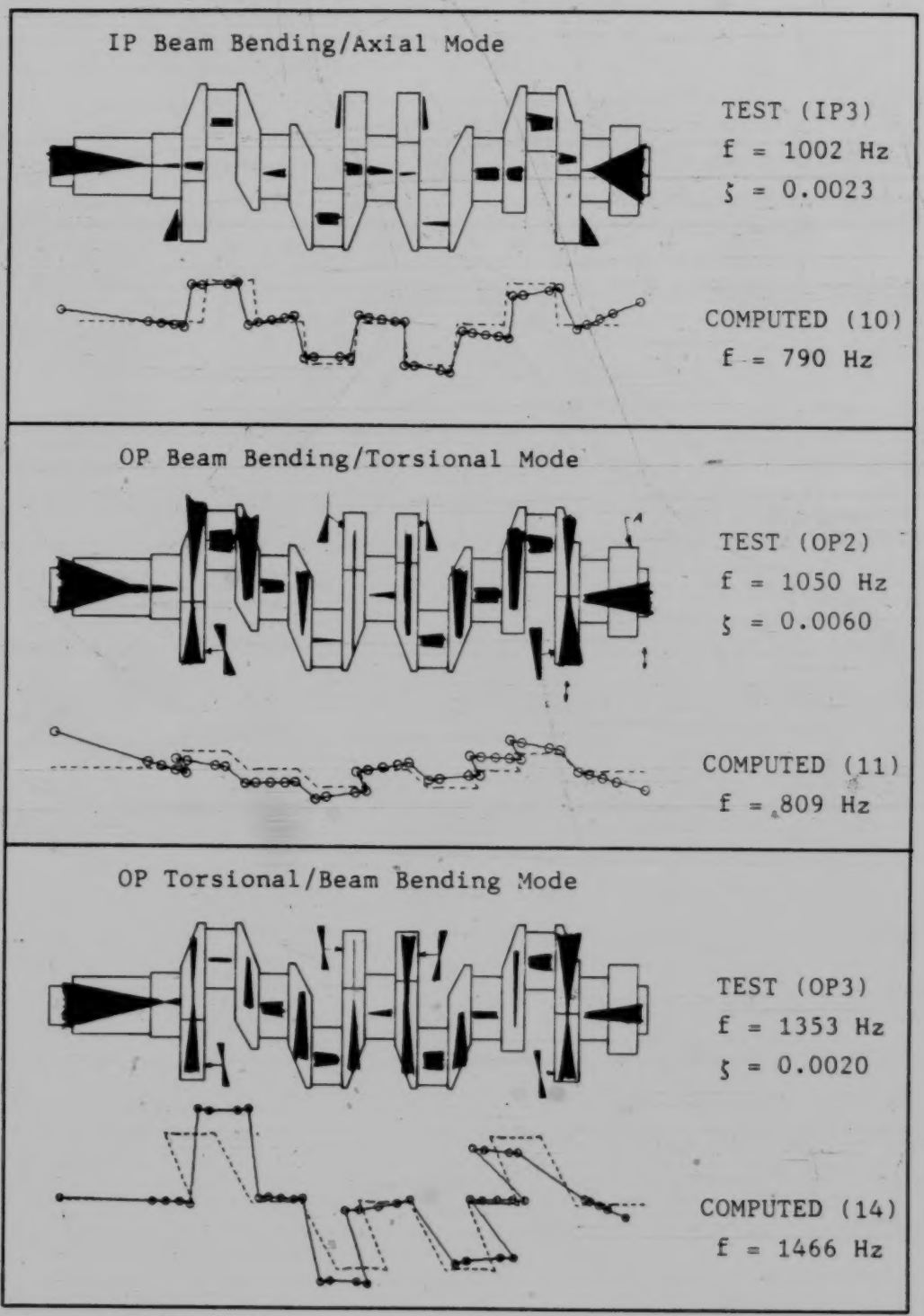

Figure 4.6 (cont'd) Experimental and Computed Modes for ATX5 Crankshaft in Free-Free Constraint

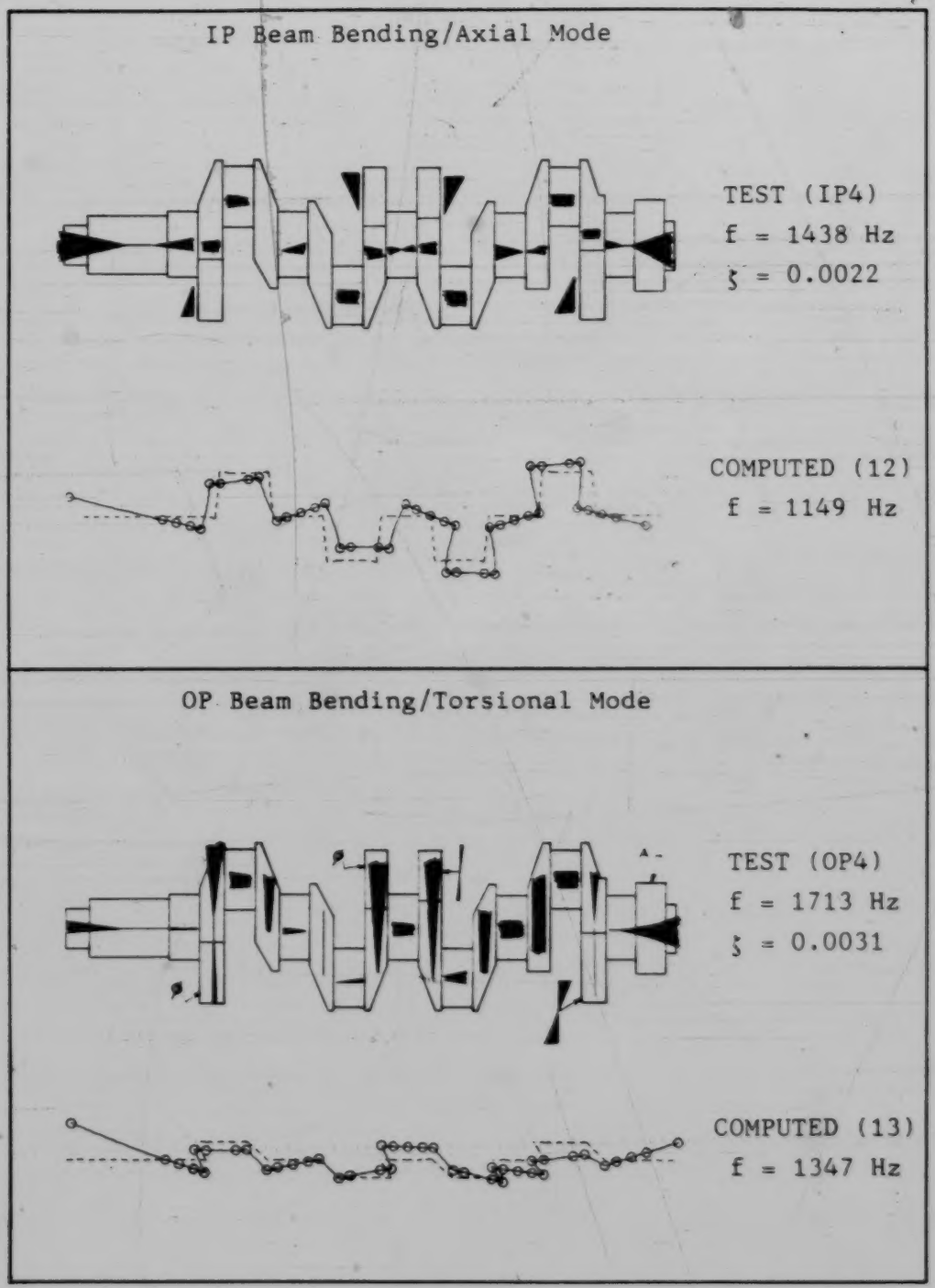

Figure 4.6 (cont'd) Experimental and Computed Modes for ATX5 Crankshaft in Free-Free Constraint

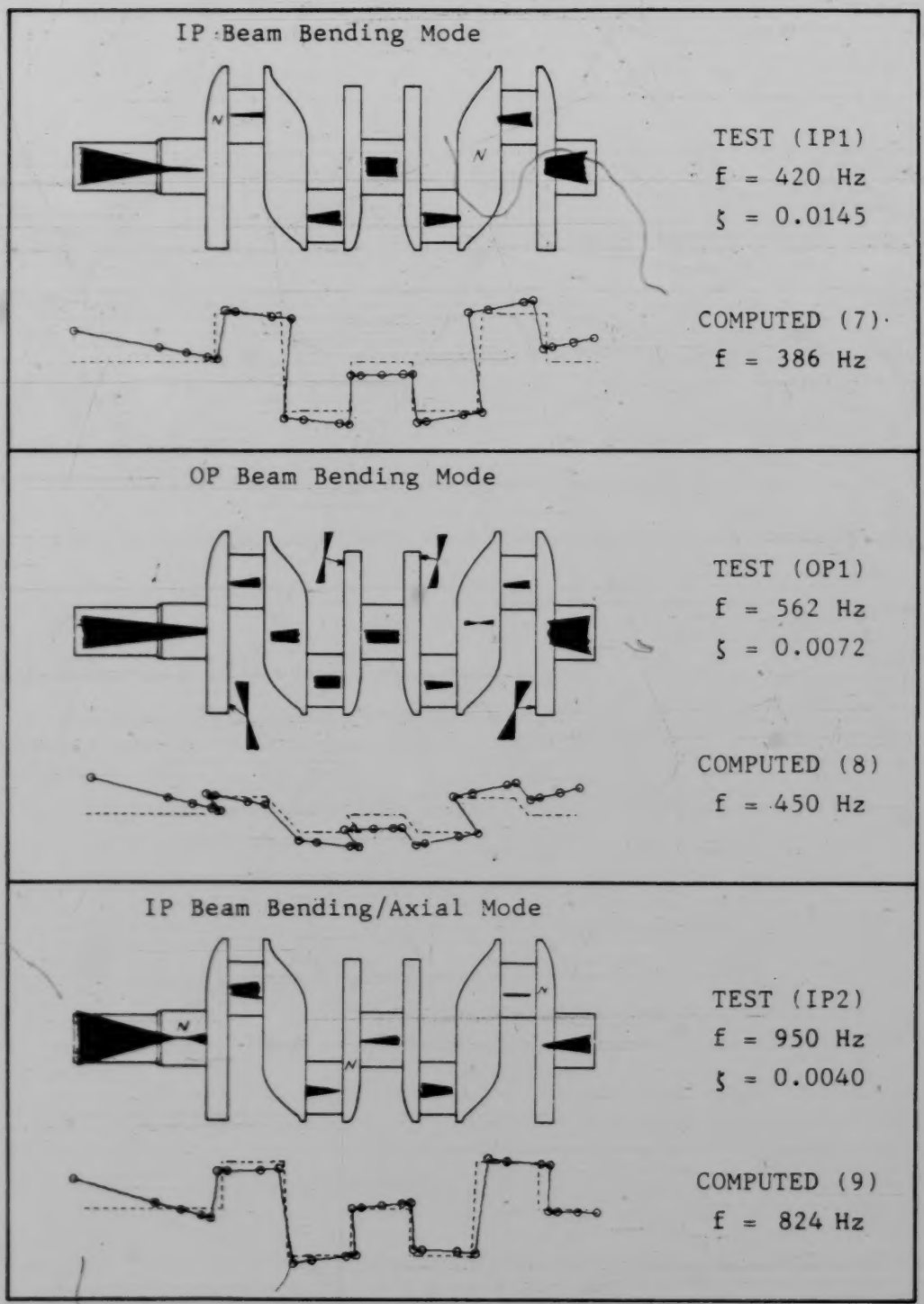

Figure 4.7 Experimental and Computed Modes for DT3 Crankshaft in Free-Free Constraint

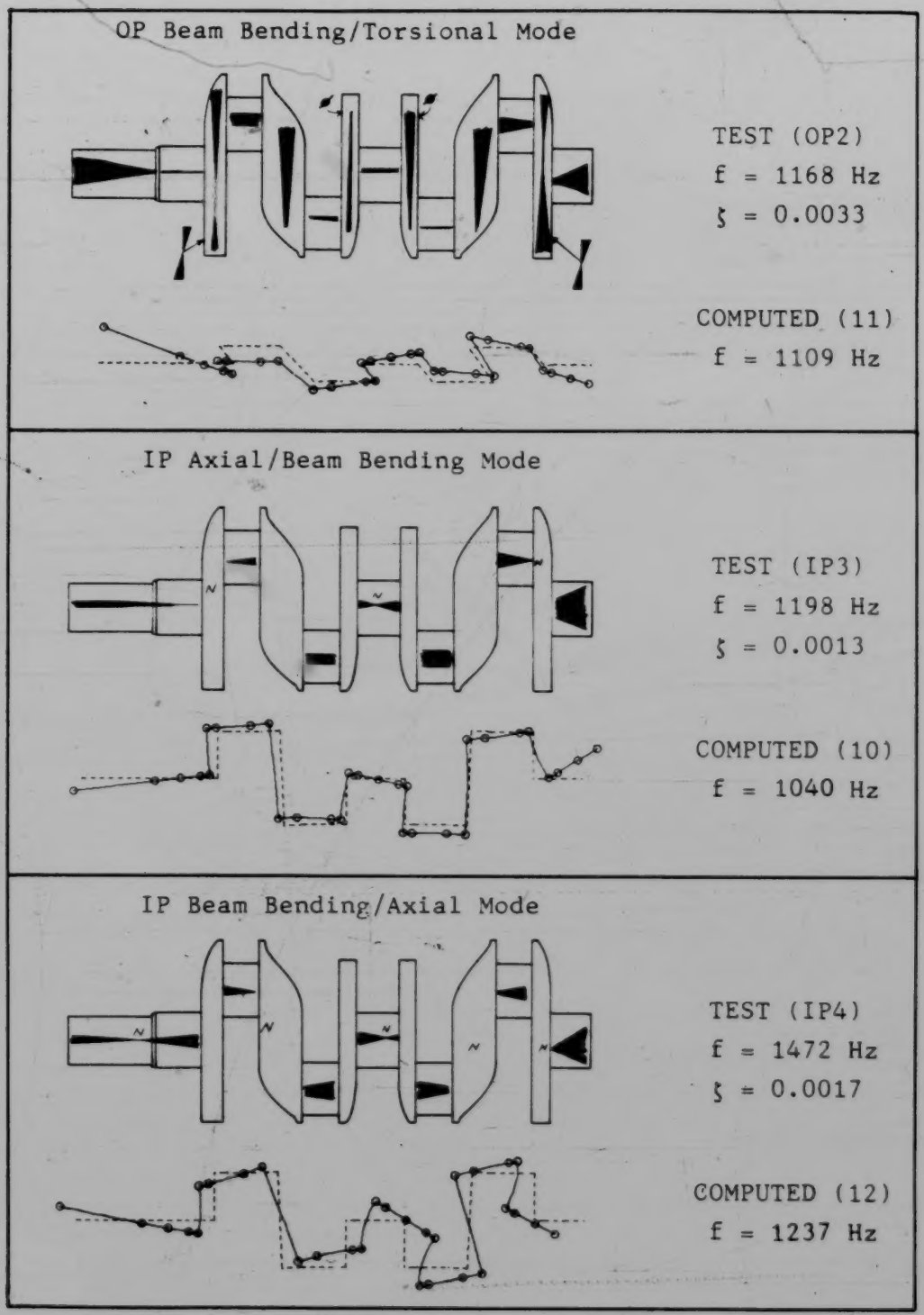

Figure 4.7 (cont'd) Experimental and Computed Modes for DT3 Crankshaft in Free-Free Constraint

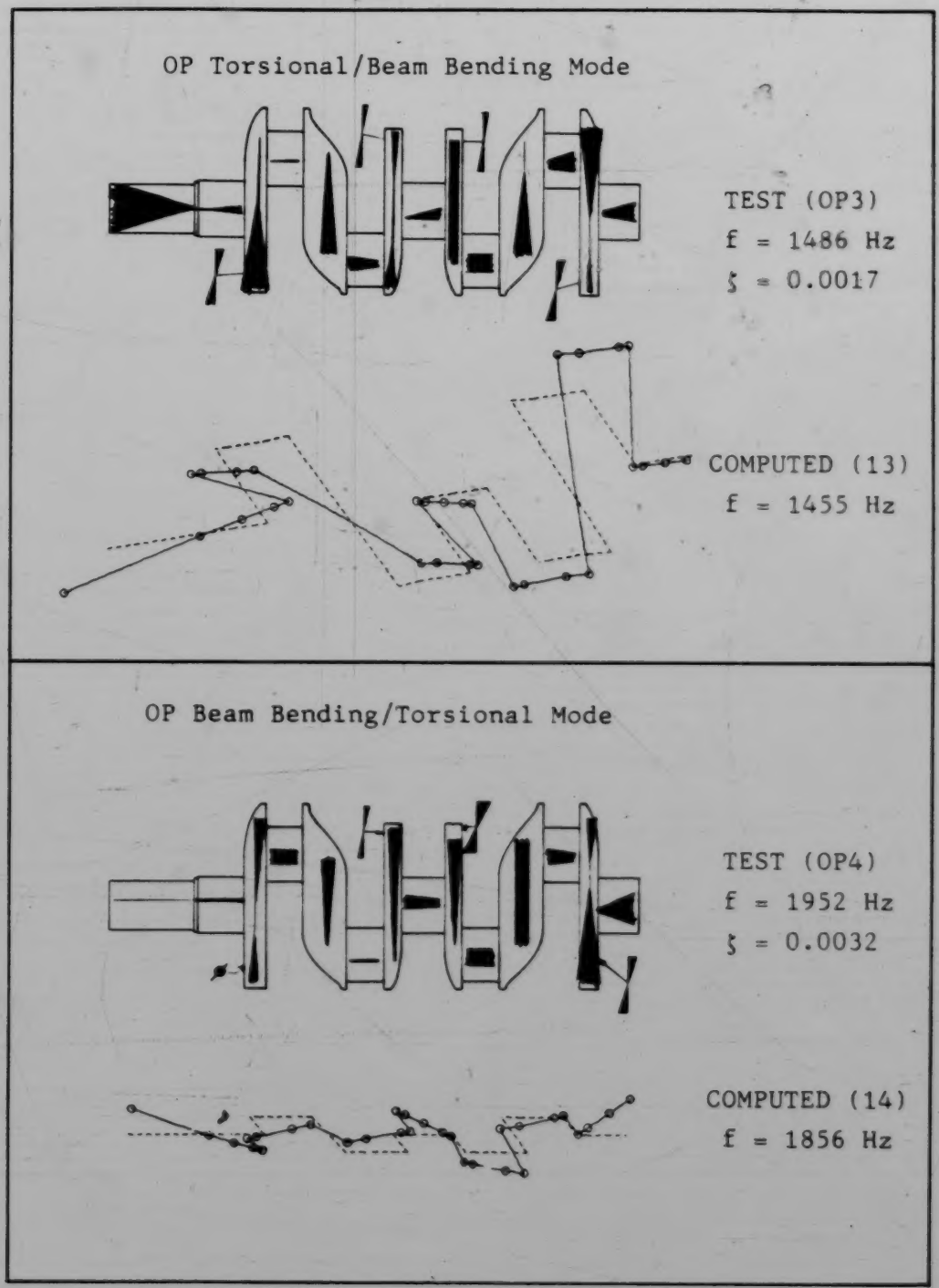

Figure 4.7 (cont'd) Experimental and Computed Modes for DT3 Crankshaft in Free-Free Constraint

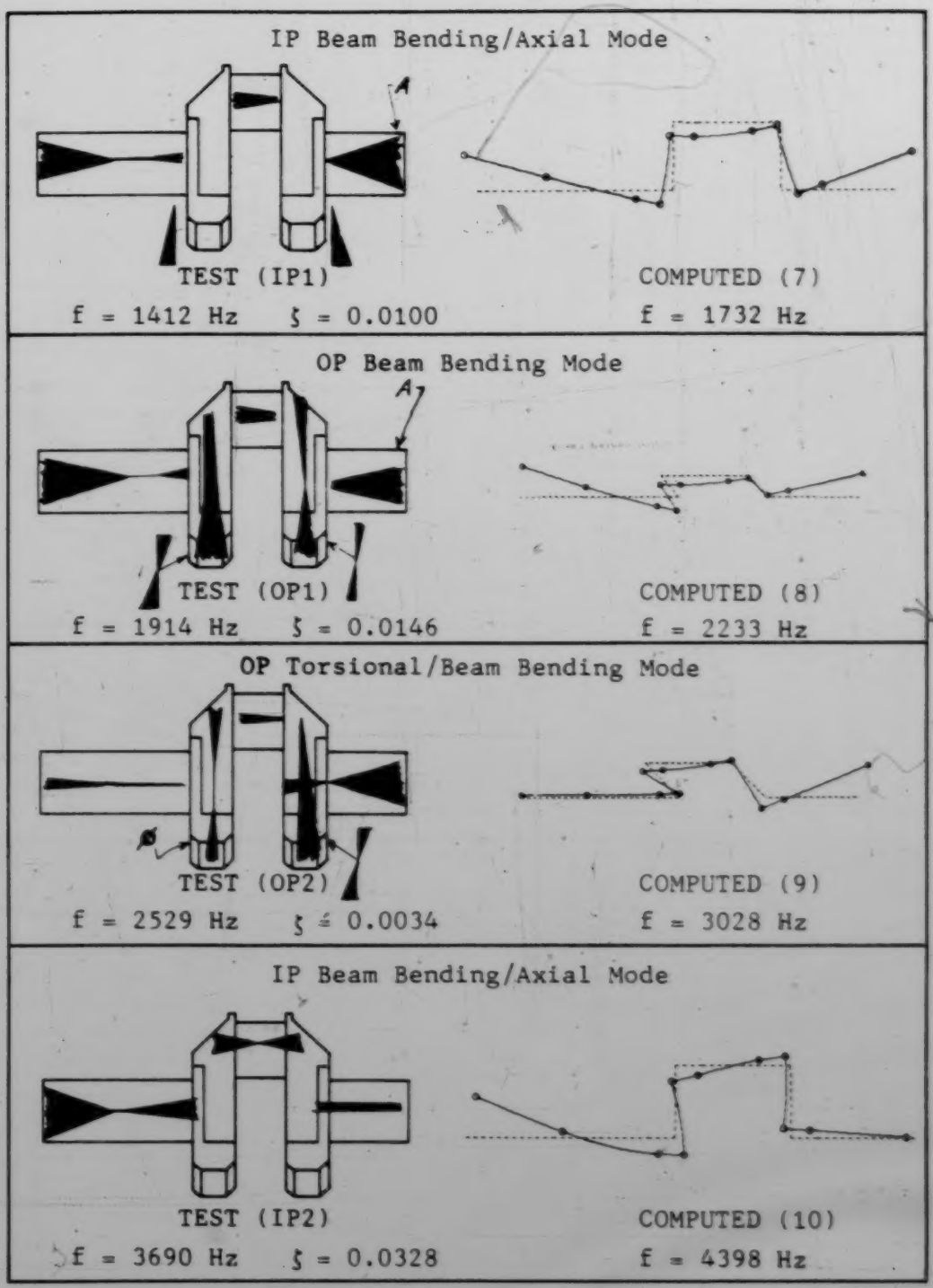

Figure 4.8 Experimental and Computed Modes for SL2 Crankshaft in Free-Free Constraint

for each mode. Notable exceptions are IP2 and IP3 of crankshaft ATX5 which are relatively closely spaced with a 150 Hz frequency separation. Also, IP2 of crankshaft SL2 shows up as a broad "hump" on the curve rather than the expected peak. Another observation taken from the natural frequency values is that a pair of modes, one IP the other OP, may occur quite close together. Thus, modes IP4 and OP3 of crankshaft DT3 have only a 14 Hz frequency difference. Other examples of such paired modes are IP3 and OP2 of crankshaft ATX5 and modes OP2 and IP3 of crankshaft DT3.

The response curves show that the OP curve may, for some modes, follow the IP curve to some degree. This raises the question of coupling between IP and OP modes and challenges the validity of the previous assumption predicted by the model, that is, that modes are strictly of the IP or OP type. It is obvious that more conclusive testing is needed to clarify the whole issue of coupling of vibrations in orthogonal planes of the crankshaft.

Experiments were conducted on each crankshaft whereby only a force was applied at an angle of approximately 45° to the plane of throws. The appropriate frequency range was scanned and the frequency where force became a minimum was recorded. Thus, by using this single scan all modes, IP, OP or any coupled ones, would be detected. At the minimum force frequencies the sharped-tipped probe was used to determine the planes in which there was vibration. These tests revealed that vibrations at a natural frequency were

predominant in either the IP or OP direction with very little or none at all apparent in the opposite direction. When there is vibration in the direction perpendicular to the major modal vibration it is likely a direct response due to the excitation force and not a condition of resonance due to a coupled mode. Another possibility is that an IP/OP mode pair, having close natural frequencies, influence each other at the respective natural frequencies. For example, crankshaft ATX5 in Figure 4.6 shows mode OP2 (f=1050 Hz) with some IP vibration at the flywheel end. This behavior could be due to the close proximity of mode IP3 (f=1002 Hz). Sufficient evidence has been found to conclude that the modes for these three crankshafts are uncoupled with respect to IP and OP vibrations.

Damping factors were extracted from the frequency response curves according to the theoretical method described (equation 4.1). The modal damping factor is given with each mode in figures 4.6 to 4.8. These damping factors may be used in a numerical, dynamic response model in conjunction with calculated natural frequencies and mode shapes. Hawkins & Southall [32] did measurements on engine materials and engine systems and found that for such lightly damped structures the damping ratio is about 0.010 for most modes.

4.3 Comparisons of Computed and Experimental Results

The calculated frequencies and mode shapes for the three crankshafts in free-free constraint may be compared with their counterparts determined by the resonance tests. Expressing the differences between the two sets of frequencies as percentage quantities, the following figures are obtained:

Average for 8 modes of DT3	10.3%
Average for 8 modes of ATX5	19.6%
Average for 4 modes of SL2	20.5%
Average for three crankshafts	16.2%

With mode OP3 of ATX5 as the exception, the frequencies computed for crankshafts DT3 and ATX5 came out lower than the corresponding test frequencies.

Computed frequencies for crankshaft DT3 correlated better with test frequencies than did crankshaft ATX5. Two identifiable reasons can be given for this.

1. Crankshaft DT3, with three main bearings, has less web-joint interaction than ATX5, which has five such bearings. The web-bearing interfaces are one of the most critical regions that determine the accuracy of the numerical model.
2. The crankpin-journal overlap (see Figure 4.9) in DT3 is less than that of ATX5 (0.182 in. and 0.406 in. respectively). Since the numerical model has no way of accounting for this kind of overlap it will more accurately reflect the actual situation as the amount of

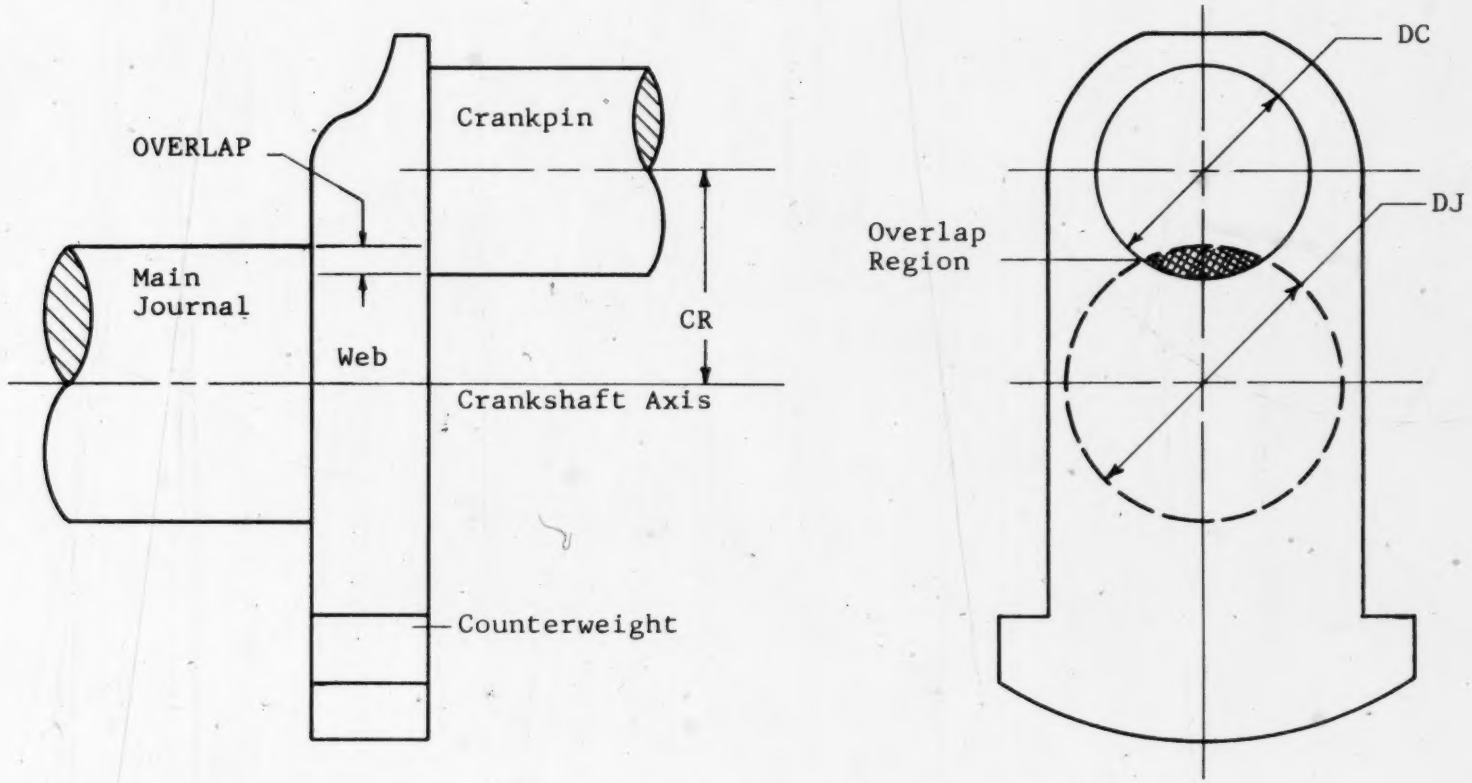

$$OVERLAP = \tfrac{1}{2}(DJ + DC) - CR$$

Figure 4.9 Crankpin-Journal Overlap Geometry

overlap decreases.

For crankshafts DT3 and ATX5, the mode exhibiting mostly torsional behavior (OP3) was among the modes having the lowest frequency difference. This is an encouraging result since the torsional mode is usually considered to be of primary importance in engine vibration analysis.

The torsional mode for ATX5 (OP3) in free-free constraint has been evaluated by three independent methods. The equivalent shaft technique yields a frequency of 1292 Hz for this mode while the finite element model produces a value of 1466 Hz and the test result was 1353 Hz. If the test result is chosen as the standard, it follows that the equivalent shaft method underpredicts the frequency by 4.5% while the finite element model overshoots by 8.4%. However, the equivalent shaft model predicts a mode shape that gives only the torsional deformation of each crankthrow. The finite element model is more realistic in its mode shape prediction since it also shows the bending and tilting of journals and crankpins.

Turning now to the single throw crankshaft, SL2, it is evident that the model consistently overpredicts the natural frequencies given by experiment. Crankshaft SL2 has only 0.005 inches overlap which is considerably less than that for the four throw shafts. If it is true that the accuracy of a model increases as the overlap decreases then the results for SL2 should be closer to test results than the results of the other two models. However, this is not the

case and basically two reasons may be offered as an explanation. One, there are factors other than overlap which have significant influence on the accuracy of computed results. Secondly, and possibly the case for SL2, is the effect that instrumentation mass may have on experimental results. Since SL2 is a specimen having a much lower mass than either DT3 or ATX5 the mass of the attached force transducer will have a greater effect on the natural frequencies. Another experimental method applied to SL2, such as the impulse technique, would be helpful in determining if this is the case.

Verification of the model includes not only a comparison of natural frequencies but also investigating the relationship between computed and experimental mode shapes. A close observation of the mode shapes depicted in figures 4.6 through 4.8 reveals a high degree of correlation. For the in-plane modes especially, there is almost no difference between modal deformations in the two cases. The most significant deviations are present for the higher OP modes of crankshafts DT3 and ATX5. For these modes the tests showed a greater degree of torsional deformation than predicted by the model. The comparison between mode shape results for SL2 is excellent even for the predominantly torsional mode, OP2.

It is now apparent that significant differences exist between computed and experimental frequencies and, to a lesser degree, between the corresponding mode shapes. In

most cases, these differences are more than can be accounted for by the effects of instrumentation. Although the static test would indicate that there is no problem in representing the stiffness of crankshaft DT3, the evidence offered by the results of resonance tests on all three crankshafts seems to suggest modelling problems that could originate with both the stiffness and mass representation of the crankshafts. Three suggestions for improving the model, in accuracy and consistency, may be made based on the assumption that all the error is attributed to modelling of the web and web-journal interfaces.

1. Model the web by using smaller 3-D elements and employ reduction and boundary techniques to join the web to the straight circular shaft parts. This was done by Nagamatsu & Nagaike [51],[52] who had fairly good comparison with experiment for the lower modes ($n \leq 4$).
2. Derive a theoretical procedure that alters the existing beam type web element by taking into consideration the known deficiencies and attempts to correct them. For example, the use of Lagrangian multipliers to constrain the web surface to the journal end faces.
3. Introduce empirical web modification factors as described by Hodgetts [36]. Numerous crankshafts of varying geometry would need to be tested with the objective of finding a generalized correlation between the modifying factors and some pertinent geometrical parameter. This approach has been used for analysis of

portal frames, for example (see [60], p.151-152).

All of these options are beyond the scope of the present project work. However, some work was done using the modification method in suggestion (3) above which involves altering the flexibility of the web for bending and twist in different planes. Formal results for this modifying method will not be given in this thesis since the investigation remains rather inconclusive. However, it did become clear that the modificaton factors depend not only on crankshaft geometry but on the mode number or frequency level as well.

Ideally then, the next step would be to introduce one of the modification schemes with the objective of arriving at a more accurate model. For dynamic response analysis this would be essential; however, the existing model may be utilized to analyze the mode shapes and give a perspective on the type and ordering of modes for a crankshaft. This forms the basis of the discussion in the following chapter.

5. MODE CLASSIFICATION

Mode shapes of crankshafts in free vibration may be classified by their recognizable patterns of distortion. In the present study, only coplanar crankshafts were investigated although the numerical model may be applied to a crankshaft having crankthrows in more than one plane. For example, a crankshaft for a six-cylinder engine, having three throw-planes at angles of 120° relative to each other, would most likely have some mode classifications which differ from those of the four throw coplanar crankshaft. Classifications will also change for different modes of constraint. Two cases of constraint are investigated here: free-free constraints and simple bearing constraints.

5.1 Free - Free Constraints

The distinction between in-plane (IP) and out-of-plane (OP) modes is a general one observed for both computed and test results. The mode shape results shown in figures 4.6 to 4.8 may be classified more specifically. All the modes shown may be identified in one or more of the four categories described in Table 5.1. The classifications are generally easier to derive from the computed mode shapes but experimental results were also consulted whenever the predictions differed from test shapes by a noticable amount. The term "Beam Bending" used to classify IP or OP modes in Table 5.1 is a meaningful description of crankshaft modes when they are compared to the natural modes of a uniform,

Mode Classification	Examples (Fig. 4.6 to 4.8) Crankshaft & Mode	Characteristics of the Deformation
IP Beam Bending	ATX5 IP1, IP2, IP3, IP4 DT3 IP1, IP2, IP3, IP4 SL2 IP1, IP2	Journals and crankpins bend and deflect in the plane of the crankthrows. Webs bend about axes parallel to the global z axis.
IP Axial	ATX5 IP3, IP4 DT3 IP2, IP3, IP4 SL2 IP1, IP2	Linear movement of journals and crankpins along their axes. Webs bend about axes parallel to the global z axis.
OP Beam Bending	ATX5 OP1, OP2, OP3, OP4 DT3 OP1, OP2, OP3, OP4 SL2 OP1, OP2	Journals and crankpins bend and deflect in planes perpendicular to the plane of throws. Webs twist about their length axes.
OP Torsional	ATX5 OP2, OP3, OP4 DT3 OP2, OP3, OP4 SL2 OP2	Journals and crankpins experience twist deformation and may displace in the OP direction. Webs bend and rotate about axes parallel to the global x axis.

Table 5.1 Mode Classifications for Coplanar Crankshafts in Free Constraint

free-free beam.[5] Imagine the crankshaft to be imbedded in a uniform, rectangular beam having a depth of twice the crank radius and a thickness equal to the web width. The deformation of the beam in its characteristic modes could conceivably show the mode shapes of the imbedded crankshaft for the Beam Bending classification.

As indicated in the table, a single mode may come under two classifications. This is especially so for the free constraint case where there are no rigid constraints to cause the crankshaft to vibrate in a single type of modal shape. IP Axial and IP Beam Bending are often coupled as in mode IP3 of crankshaft ATX5. In fact, a pure axial mode does not seem to exist for crankshafts in free constraint. Another example of coupling is mode OP4 of crankshaft DT3 where a combination of OP Torsion and OP Beam Bending is evident. Mode OP3 of crankshafts DT3 and ATX5 are the closest to pure torsion but even these had some OP Beam Bending type deformation inherent in them.

From the plotted OP mode shapes there is virtually no observable axial deflection. In actuality, torsion of a shaft is inseparably linked with an axial deformation. This phenomenon is described in a paper by Wilson [79]. A shaft, cranked or straight, vibrating in its torsional mode will experience axial vibrations at twice the torsional frequency. The finite elements developed for torsion and axial vibration act independent of each other and therefore

---

[5]These can be found in standard vibration textbooks, see Tse, et al. [72], p.276 for instance.

the numerical model does not predict this coupled behavior.

For all three crankshafts, half of the modes that were calculated are IP type and the other half are OP type. Of the OP modes there is one that displays significant torsional behavior. For the two four-throw crankshafts this mode is the third OP mode and for the single throw crankshaft it is the second OP mode. In any case, the torsional mode for free-free constraints is at a frequency in the higher end of the range of interest. Generally, the pattern for the lowest modes is one that alternates between IP and OP type modes. At higher frequencies it is common for two successive modes to be of the IP or OP type.

5.2 Simple Bearing Constraints

Hodgetts [35] concluded that the assumption of "pinned" journals was adequate for prediction of natural frequencies of a crankshaft. The simple bearing constraint model used here is based on this assumption. This constraint system has been described in detail in Section 3.4. Briefly again, simple bearing constraint means that only transverse freedoms at all journal centers are constrained. In addition, the axial (δ_x), torsional (θ_x), and two rotary freedoms (θ_y, θ_z) at the flywheel end of the crankshaft are rigidly constrained.

Figures 5.1 to 5.3 show the first six modes of the crankshafts with simple bearing constraints. The results presented here have value in that they predict the

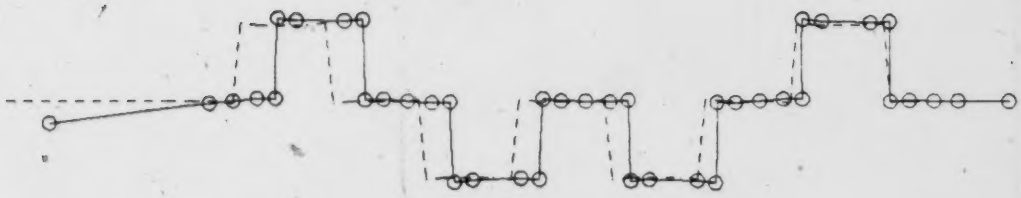

IP Axial Mode (1)
f = 486 Hz

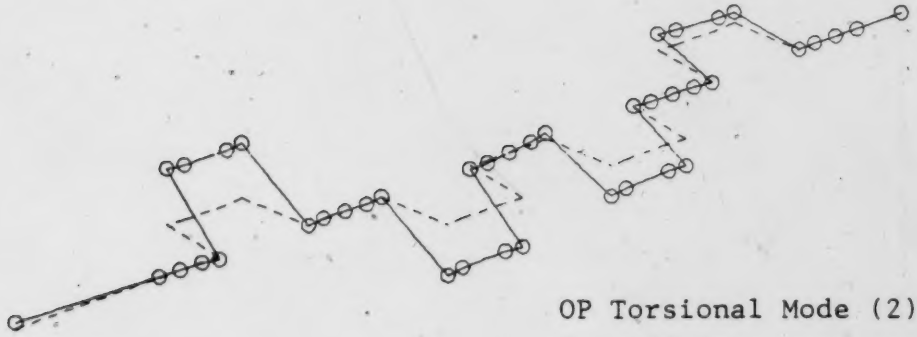

OP Torsional Mode (2)
f = 678 Hz

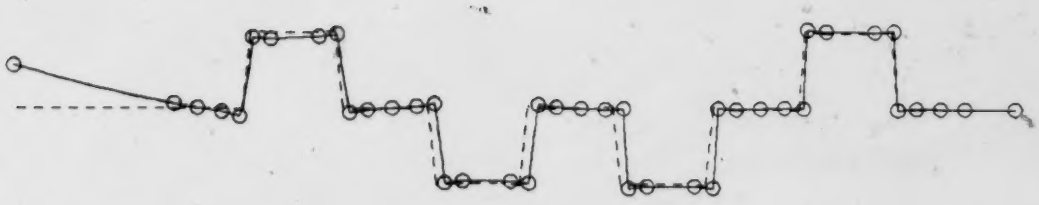

IP Nodding Mode (3)
f = 737 Hz

Figure 5.1 Natural Modes of Crankshaft ATX5 in Simple Bearing Constraints

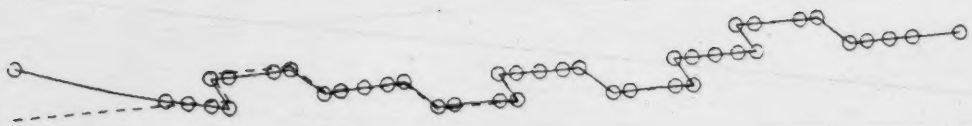

OP Nodding Mode (4)
f = 757 Hz

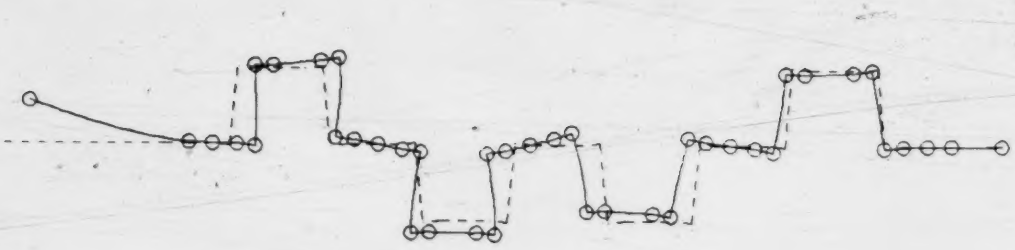

IP Axial/Beam Bending Mode (5)
f = 1244 Hz

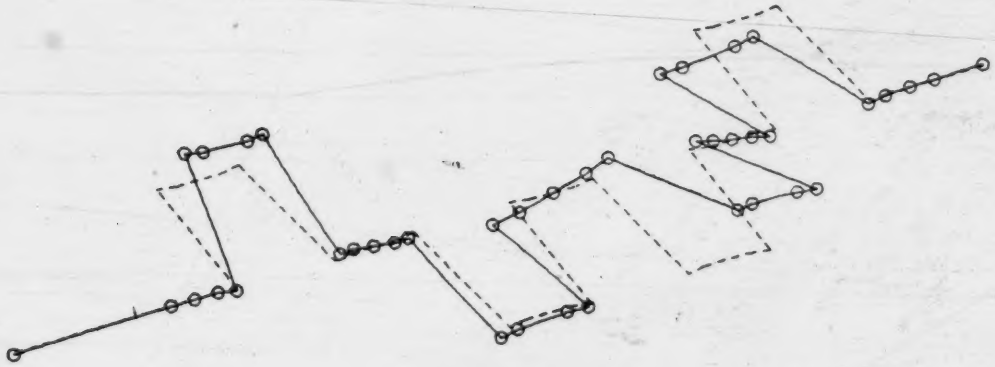

OP Torsional/Beam Bending Mode (6)
f = 1878 Hz

Figure 5.1 (cont'd) Natural Modes of Crankshaft ATX5 in Simple Bearing Constraints

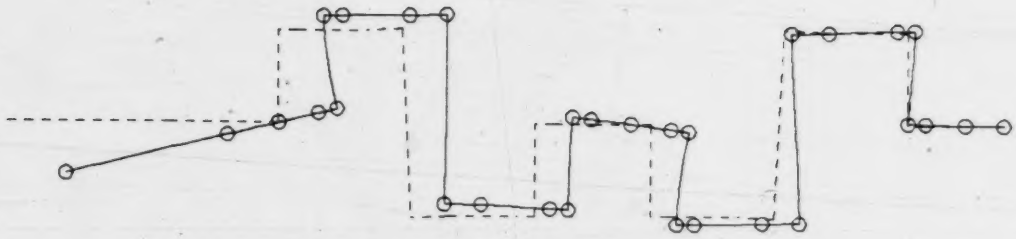

IP Axial Mode (1)
f = 564 Hz

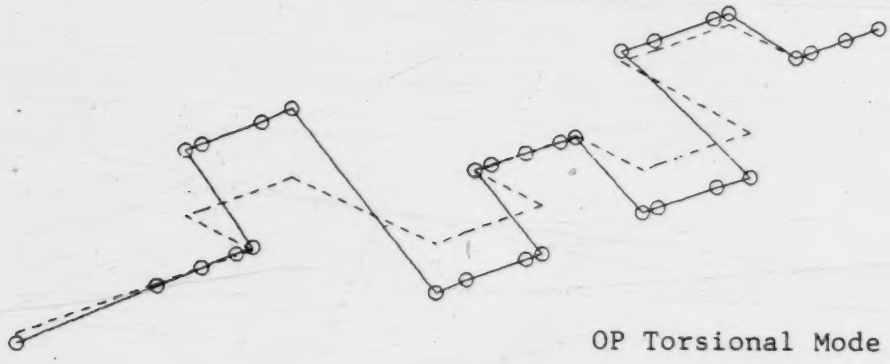

OP Torsional Mode (2)
f = 698 Hz

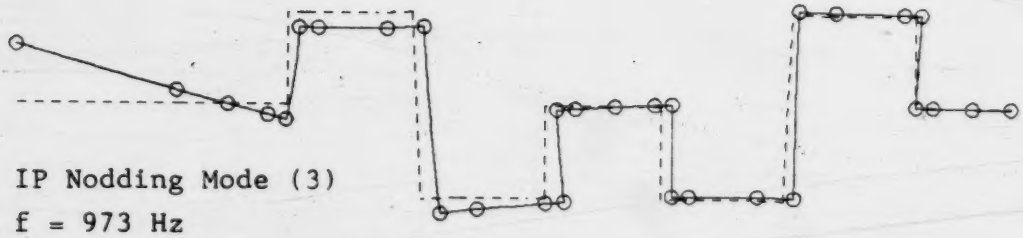

IP Nodding Mode (3)
f = 973 Hz

Figure 5.2 Natural Modes of Crankshaft DT3 in Simple Bearing Constraints

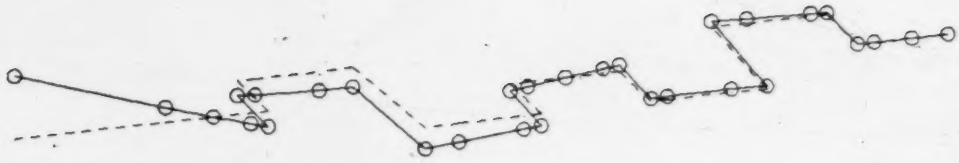

OP Nodding Mode (4)
f = 1030 Hz

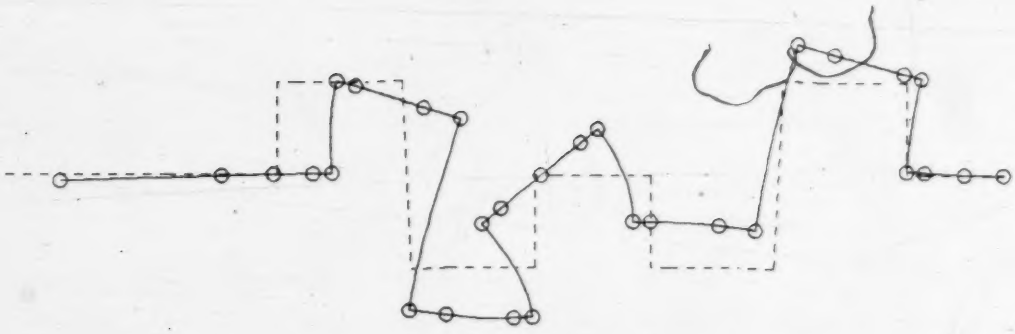

IP Beam Bending/Axial Mode (5)
f = 1151 Hz

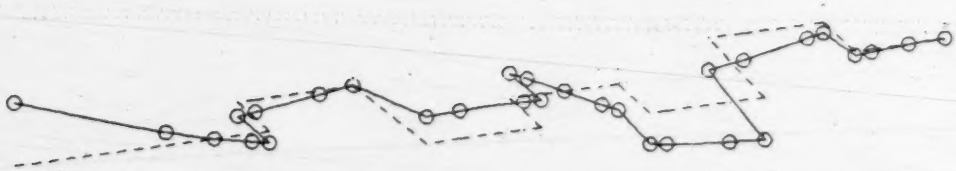

OP Beam Bending Mode (6)
f = 1751 Hz

Figure 5.2 (cont'd) Natural Modes of Crankshaft DT3 in Simple Bearing Constraints

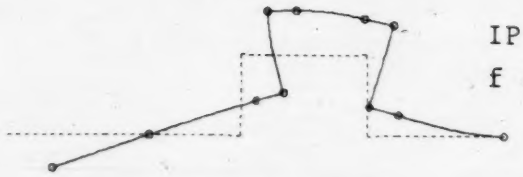

IP Axial/Beam Bending Mode (1)
f = 1559 Hz

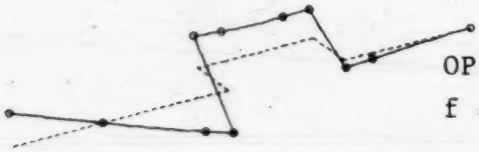

OP Torsional/Beam Bending Mode (2)
f = 1638 Hz

OP Beam Bending Mode (3)
f = 1996 Hz

IP Beam Bending/Axial Mode (4)
f = 3280 Hz

OP Torsional/Beam Bending Mode (5)
f = 3704 Hz

IP Beam Bending Mode (6)
f = 5115 Hz

Figure 5.3 Natural Modes of Crankshaft SL2
in Simple Bearing Constraints

classifications of modes and the ordering of the frequencies. The frequencies themselves may be expected to be accurate within the bounds stated for the free constraint case (see Section 4.3).

Crankshafts DT3 and SL2 differ from their free constraint modes only by the constraints themselves. Crankshaft ATX5 in the simple bearing model has major additions to its mass and inertia properties. These come about because the mass of the front end pulley and timing-belt gear, the rotating mass of the connecting rod and the effective mass of the reciprocating parts are included with the crankshaft. The mass and inertia is added to the finite element model in a way similar to that already described for the second case of the equivalent torsional system for ATX5 (Section 2.4).

Analysis of the pinned bearing modes reveals the mode classifications. These have been summarized and described in Table 5.2. There are now two additional categories for the multi-throw crankshafts not present with the free-free modes: IP and OP Nodding modes. "Nodding" refers to relatively large deflections of either flywheel or pulley end shafting when compared to the crankthrows. Wilson ([77], p.81) hinted at their existence in his discussion of the bending flexibility of single and double throw crankshafts. These modes would likely have important acoustical significance as the nodding vibration excites the pulley or flywheel thus causing ringing noises to emanate from their

Mode Classification	Examples (Fig. 5.1 to 5.3) Crankshaft & Mode	Characteristics of the Deformation
IP Axial	ATX5 (1), (5) DT3 (1), (5) SL2 (1), (4)	Axial movement of journals and crankpins. Webs bend about axes parallel to the global z axis.
OP Torsional	ATX5 (2), (6) DT3 (2) SL2 (2), (5)	Rotation of crankthrows about crankshaft axis. Journals (and sometimes crankpins) twist along their length axes. Webs bend about axes parallel to the global x axis.
IP Beam Bending	ATX5 (5) DT3 (5) SL2 (1), (4), (6)	Main journals tilt and bend. Webs bend about axes parallel to the global z axis. Tilting, bending and lateral deflection of crankpins in the IP plane.
OP Beam Bending	ATX5 (6) DT3 (6) SL2 (2), (3), (5)	Tilting and bending of main journals. Webs twist along their length axes. Crankpins tilt, bend and displace laterally in their OP planes.
IP Nodding	ATX5 (3) DT3 (3) SL2 none	Pulley end shafting vibrates laterally with large amplitude. The remainder of the crankshaft (crankthrows) has relatively small or no deflection.
OP Nodding	ATX5 (4) DT3 (4) SL2 none	Same as "IP Nodding" except that the pulley end vibrates laterally in the OP direction.

Table 5.2 Mode Classifications for Coplanar Crankshafts in Simple Bearing Constraints

surfaces. The rigid constraint approximations at the flywheel end prohibit any flywheel nodding in the present model.

The Beam Bending modes are similar to those found for the free-free case of constraint. The important attribute of these modes is that almost all parts of the crankshaft vibrate with significant amplitude. Beam Bending modes may also have large lateral deflections at the ends of the crankshaft which force the pulley and flywheel parts in vibration. In crankshaft design it is generally favored to include a main bearing between each throw rather than between each pair of throws so that the crankshaft will have greater bending rigidity. Therefore, the modes of crankshaft DT3 generally show more bending than the corresponding modes of ATX5.

With the rigid constraints it is evident that Axial modes may exist independently. For crankshaft ATX5, the fundamental mode is almost pure axial; the pulley end has only slight lateral deflection. Crankshaft DT3, having less bending restraint because of fewer main bearings, has greater pulley end nodding in the fundamental, axial mode of vibration. As well as pure axial modes, the IP Beam Bending mode in most cases is coupled with significant axial deflection.

All three crankshafts show a distinctive, isolated torsional mode. In each case the torsional mode is the second one in the frequency spectrum. For each example

crankshaft, the modal frequencies are generally well spaced. The closest pair of frequencies are modes (3) and (4) of crankshaft ATX5 where a difference of 20 Hz exists.

The coupling behavior between axial and torsional vibrations was briefly discussed in the last section on free-free constraints. In a running engine, this coupling of modes would have special significance if, by some "chance" in design, the axial natural frequency of the crankshaft was approximately twice its torsional natural frequency. With the engine running at one of the corresponding critical speeds, there would be a much larger dynamic magnification because of such coupling of modes. However, from the calculated mode shapes shown in figures 5.1 to 5.3 it is evident that the fundamental, axial mode has a frequency that is lower than the first torsional mode. This indicates that the problem of torsional-axial coupling is a remote one, at least for the fundamental modes of torsion and axial vibration. This does not mean that the torsional mode could not couple with another axial mode. It is noteworthy that the second axial mode (actually a coupled Axial/Beam Bending mode) for the three crankshafts has a frequency that is approximately 1.8 times the lowest torsional natural frequency for the crankshaft. Since this factor is close to 2.0, a degree of coupling may occur. A limiting influence on the dynamic magnification due to this mode of coupling is the fact that, for the four throw crankshafts at least, the axial mode has nodes along the length of the crankshaft.

Thus, the axial vibrations due to torsional oscillation would not always constructively interfere with the direct Axial/Beam Bending mode.

Finally, the torsional mode for ATX5 may be compared with the result for the same system modelled by the equivalent shaft method. Table 2.3 shows a frequency of 526 Hz while the finite element model predicts a value of 678 Hz as shown in Figure 5.1. If it is assumed that the same differences between calculated and measured results exist for the pinned constraints as for free-free constraints then the calculated torsional frequencies for pinned constraints may be adjusted accordingly. Thus, the equivalent shaft frequency becomes 587 Hz and the finite element prediction drops to 565 Hz. If the bearing constraint and reciprocating mass approximations have been modelled correctly, a frequency of 575 Hz would be a reasonably good estimate of the torsional natural frequency for crankshaft ATX5.

6. APPLICATION AND CONCLUSIONS

Before summarizing the results of the research and analysis presented in this thesis, the use of the numerical model as a tool in prediction of dynamic response to periodic forces will be discussed. Consideration will be given as to how the problem should be approached and solved.

6.1 Application: Dynamic Response Prediction

In order to better understand the problem of predicting crankshaft response to engine forces, a comprehension of "critical speed", which was touched upon in the last chapter, would be helpful. A critical engine speed occurs when one of the harmonics of the engine forces has a frequency equal to one of the natural frequencies of the crankshaft. Since there are many natural frequencies and force harmonics, a plethora of critical speeds are possible within the speed range of a running engine. However, an engine designer is usually concerned with only a few of them. For a critical speed to be considered "dangerous" a number of ingredients or requirements are necessary.

First, the forcing harmonic must have sufficient amplitude or strength to be able to excite a natural mode into resonance. The forcing harmonic spectrum generally decreases in strength with increasing frequency. For this reason, orders higher than 12 are usually not considered. "Order" here refers to the number of frequency cycles, for the forcing harmonic or vibrational response, per revolution

of the crankshaft.‘

Secondly, a critical speed may be significant if the relationship between the force harmonic and the mode shape deflection at each crankthrow is close to being in-phase. Phasing between forces and crankshaft mode shapes depends on the engine cylinder firing sequence, on the relative deflections of crankthrows in a particular natural mode, and on the particular order of force harmonic.

Finally, since the vibration energy required for a crankshaft mode increases with mode number, critical speeds need only be considered for the lowest few modes of the structure. The modes with higher vibrational energy have frequencies well above the high energy forcing harmonics. In other words, the higher order forcing harmonics, having frequencies comparable to those of the higher natural modes, have insufficient power to excite these modes. For example, a crankshaft torsional mode with a natural frequency of 1000 Hz would require forcing harmonics of 12 or greater for excitation at engine speeds less than 5000 rpm. Therefore, it seems that only modes with frequencies below 1000 Hz are significant.

Consider the lowest torsinal mode of crankshaft ATX5, shown in Figure 5.1, which has a frequency of 678 Hz. A perspective on the spacing between the various orders of critical speed due to the presence of this natural mode is an important part of the dynamic analysis of the engine.

‘Order Number = Frequency (cpm)/Engine Speed (rpm)

Figure 6.1 shows a typical critical speed analysis for the torsional response of crankshaft ATX5. The phase and vector diagrams are helpful in ascertaining how the oscillations of each of the crankthrows combine in the different orders. The arrows in the circular phase diagrams rotate clockwise at a speed equal to the order number times engine speed. Their projections on the vertical axis represent the twists at the pulley end due to a harmonic torque (at this point, of arbitrary magnitude) applied at each crankthrow. However, as the mode shape shows, each crankthrow deflects a different amount requiring the arrows to be of different lengths and hence, the vector diagrams are also needed. Included in the critical speed spectrum is information regarding the relative susceptibility of each order; this being obtained directly from the vector diagrams. It is important to note that the speed spectrum in Figure 6.1 is not a complete indication of response at engine speeds where critical vibrations occur since there is no information regarding the magnitude of the forcing harmonic at each of the critical orders shown.

Up to this point only torsional critical speeds have been discussed although a comprehensive analysis would include criticals due to bending and axial vibrations as well. The following paragraphs discuss additional information that is required before an accurate prediction of general response amplitudes can be made. Aspects such as forcing function, bearing restraint, and friction are

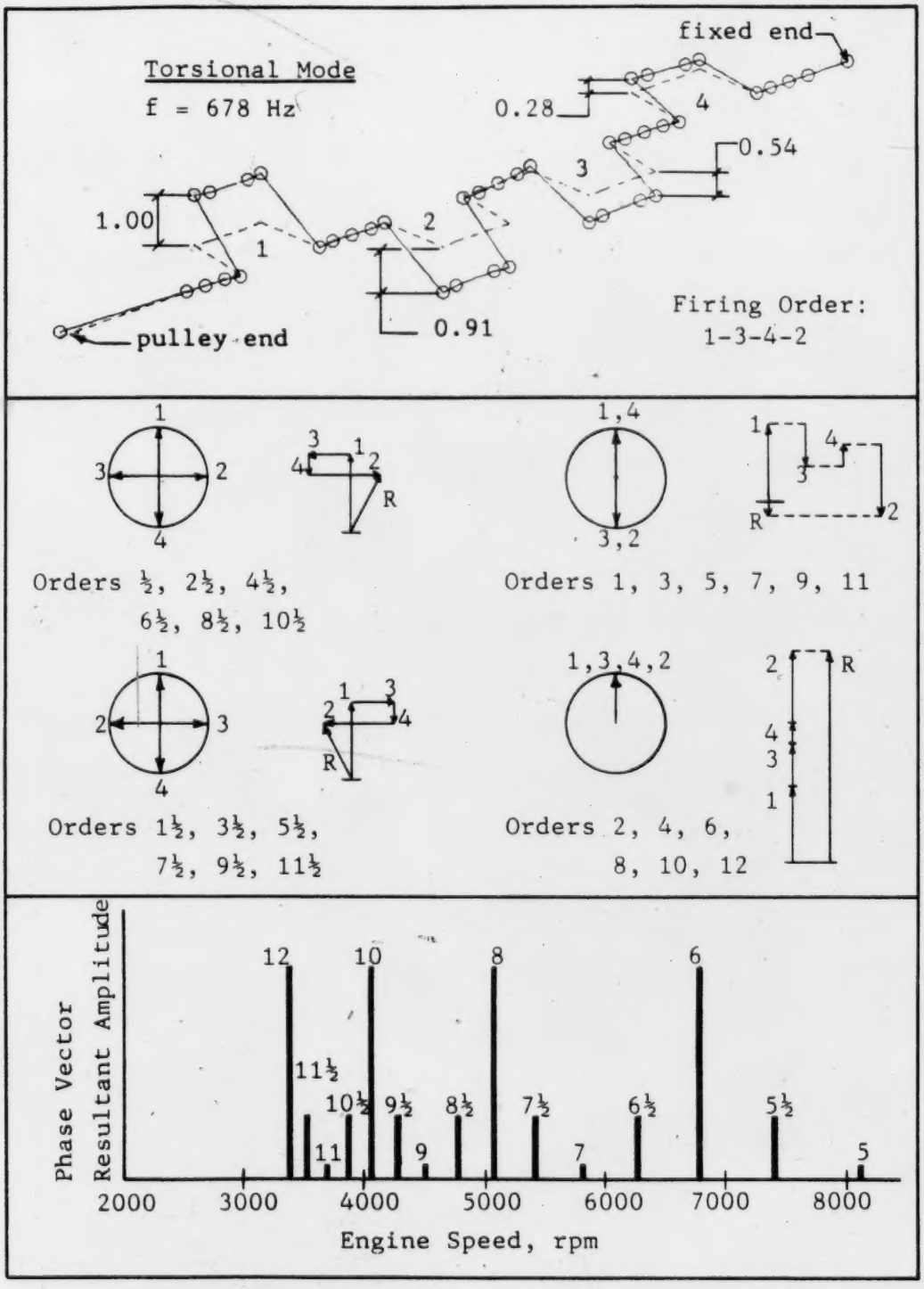

Figure 6.1 Critical Speed Analysis for Lowest Torsional Mode of Crankshaft ATX5.

considered.

When considering realistic engine forces, the source, line of action, phases between harmonic orders and between points of force application, and the magnitude of the force must all be known. The two main sources of fluctuating load are the inertia forces of the reciprocating parts and the combustion explosion force. The resultant line of action has components parallel to and perpendicular to each crankthrow producing a bending force and torque, respectively. The cylinder pressure-time curve, and the relation between linear piston movement and crankthrow rotation, are used to obtain curves of the force components versus crank angle. Fourier analysis, performed on these curves, yields the magnitudes and phases of the forcing harmonics for a particular engine speed. For any one order, the harmonic forces between crankthrows also have a phase relationship. The circular, vector diagrams shown in Figure 6.1 are helpful in identifying this phase relationship for each order. References found helpful in this area are books by Wilson [78] and Taylor [65].

Modelling the bearing restraints is crucial in the dynamic response model. This was proven by Hodgetts [35],[36] who tested the flexibility of the bearing supports and used oil film stiffness and damping coefficients from a paper by Kikuchi [42]. If sufficient theoretical and experimental knowledge of the bearing is known the crankshaft may be modelled independently of the other engine

components. Alternatively, a component mode synthesis as described in Section 1.1, could be used in a broader, all inclusive engine response analysis.

Finally, friction and damping are crucial in determining dynamic response since forces due to these elements are the ones that limit the vibrational amplitudes, especially at resonance. Hysteretic or material damping within the crankshaft itself has some influence, but more important are the external effects due to friction and pumping loss. Friction occurs in the bearings, at the piston rings and at gear and pulley drives on the crankshaft. Pumping loss refers to the work needed for the intake and exhaust strokes of a four-stroke engine. In a purely torsional response model of the crankshaft, Kamath, et al. [41] included piston friction as a damper-like device attached to each crankthrow. As the subject of damping and friction is a rather involved one, no further details will be pursued here.[7]

In a general sense, consideration has been given to the problem of predicting dynamic response of the crankshaft to gas pressure and inertia forces. The finite element model developed in this thesis is more comprehensive than many presented in the literature because all types of modes are computed. Thus, with accurate representation of exciting forces, bearing restraint, friction and damping, dynamic response in any plane or direction may be predicted.

---

[7]See also Taylor [64] for an extensive treatment of mechanical friction in engines.

6.2 Conclusions and Recommendations

In the introductory chapter, four major objectives were outlined. The format in this section is to summarize how these objectives were fulfilled and what conclusions and recommendations may be drawn for each one.

First, the survey of literature showed a general progression in the research work done on crankshaft vibrations. Initially, with large, slow speed engines, the concern was with designing for loads and mass balance. As early as 1920, when engine speeds and cylinder numbers were increasing, critical engine speeds due to the occurrence of torsional, bending and axial crankshaft vibrations began to be observed and studied. This led to an extensive search for analytical methods of predicting the natural frequencies of crankshafts as well as for apparatus which would measure the same value experimentally. The analytical methods largely involved simplification of the actual system and subsequent application of elementary beam theory equations. The accuracy of one such method, the equivalent shaft-disc system for torsional modes, was checked and found to be fairly reliable with only a 4.5% difference from a corresponding test result. This period in the history of crankshaft analysis continued until the introduction of the high speed digital computer and relevant software in the 1960's. This meant that crankshafts could then be modelled more precisely and the desired solutions solved numerically.

The most common approach in computer modelling was to use 1-D or 3-D finite elements to represent the crankshaft geometry. The finite element method is still being used in all aspects of crankshaft design including stress analysis, calculation of modal parameters and prediction of dynamic response.

Finally, from the early 1960's on to the present, the literature reveals a considerable volume of research into engine noise. Researchers probed into the sources of engine noise and succeeded in identifying distinct noise patterns such as rumble, thud and roughness for which the various modes of crankshaft vibration have a direct influence. In the last decade, experimental and finite element methods have been used to construct comprehensive engine models for prediction of vibration transfer paths and noise. These models are the tools used to find ways of reducing vibration and noise.

The second and third objectives were, respectively: to formulate a numerical model for calculating natural modes of crankshafts and then, to verify the accuracy of the model by means of experiment. As a direct result of the relatively large elements that were used, two problems became apparent when modelling a crankshaft. One is the flexibility of the model, especially at the web-journal interface and also in the journal-crankpin overlap region. The other concern was to correctly represent the mass and inertia of any material not readily modelled by a simple cylindrical or rectangular

finite element. The latter problem may be alleviated by refining both the measurements of "extra-element" material and calculation of their mass and inertia properties. To rectify the stiffness misrepresentation in the web area, it is recommended that a sub-structuring approach be used, wherein the web is modelled with a finer, 3-D finite element mesh. As it is, the model predicts frequencies which differ from test results by as much as 30% and as little as 2% depending on the mode.

Mode shapes for in-plane vibrations may be considered as very reliable. Confidence in the out-of-plane mode shapes for crankshafts in free-free constraint and which have torsional deformations is not as strong. For the single throw crankshaft, both IP and OP mode shapes were accurately predicted by the model.

Verification of the model was performed only for the crankshafts in free-free constraints. It would be recommended that verification also be made for results of the crankshaft model in bearing restraint, as shown in figures 5.1 to 5.3. Improvements in the representation of bearing constraint would be a necessary addition to the existing model. A progression from "pinned" bearings would be to account for bulkhead stiffness and oil film stiffness and damping properties. The tests, in this case, would still be done on a stationary crankshaft but with journals seated in their bearings, connecting rods attached to crankpins and bearing clearances pressurized with oil. The vibration

exciter could be attached in such a way that torsional and bending modes could be induced (see Okamura, et al. [55]). Axial modes may need to be excited by a separate connection to the end of the crankshaft and with the exciter oriented in the axial direction.

The final objective of this thesis was the classification of crankshaft modes. This was done by analyzing the plots of predicted and experimental mode shapes and determining how each mode could be described in a simplified and standardized manner. For coplanar crankshafts, the model predicts that modal deflections for any given mode are either all in the plane of throws or all perpendicular to the plane of throws. Within these two broad definitions a mode shape may be further classified according to specific deflections of journals, crankpins and crankwebs. These specific categories have been listed in tables 5.1 and 5.2 for free-free and pinned constraints respectively. For free-free constraints there are axial, torsional and bending classifications. For pinned constraints the "nodding" classification is an additional one that appears for both IP and OP types of modes. The analysis for pinned constraints confirms the existence of a distinct axial mode. The four-throw crankshafts, although having different geometries, had very similar modal ordering. The fundamental mode for each of these crankshafts was the axial one, followed by the torsional, the IP and OP nodding and then the IP and OP beam bending modes. In

summary, the descriptions given in tables 5.1 and 5.2 may be used to identify any coplanar crankshaft mode; even a complex deformation may be seen as the superposition of simpler distinct classifications.

The thesis would not be entirely complete without giving some recommendations as to potential usage of the model in its present state. The model could be used in an economical "first try run" to investigate what possible modes and ordering sequence exists for any crankshaft constrained by given boundary conditions. Knowledge of expected deformations under resonant conditions would be helpful in design of not only the crankshaft parts but also other connected engine parts. If the frequencies themselves were uncertain, the change in frequency due to variation in geometry or constraint may still be an accurate reflection of the actual case. Finally, if a critical speed is known or suspected in an operating engine, the model could be used to help identify the mode, by its classification and harmonic order, contributing to the resonant condition.

BIBLIOGRAPHY

1. Andon, Jerar and Marks, Craig (1964) "Engine Roughness - the Key to Lower Octane Requirement", SAE Transactions, Paper No. 647A, v.72, pp.636-658.

2. Andrews, S.A., and Anderton, D. (1979) "The Analysis and Mechanism of Engine 'Crank Rumble'", I. Mech. E. Conference Publications, Noise and Vibrations of Engines and Transmissions, pp.99-109.

3. Bagci, C. and Falconer, D.R. (1981) "Spatial Finite Line Element Method for Determining Critical Speeds of Multi-Throw Crankshafts Considering Actual Throw Geometry", ASME Publication 81-DET-141, 15 pages.

4. Barbiero, D.; Chiosso, T.; Garro, A. and Roberi, G. (1979) "Combustion Engine Stiffness Distribution and Dynamic Response", SAE Paper 790987, pp.153-168.

5. Beamish, David (1984) Structural Dynamics Modification from Experimental Modal Analysis, M.Sc. Thesis, Department of Mechanical Engineering, University of Alberta.

6. Belgaumkar, B.M. and Ahuja, B.K. (1958) "Crankshaft Failure", Proc. 4th Congress on Theoretical and Applied Mechanics in Howrah (Calcutta), pub. by the Indian Society of Theoretical and Applied Mechanics, Kharagpur, India, pp.271-278.

7. Bickley, I.J. and McCallion, H. (1968) "On Predicting Crankshaft Stiffnesses and Frequencies", Proc. Instn. Mech. Engrs. 1967-68, Paper 6, v.182, Pt.3L, pp.52-57.

8. Bradbury, C.H. (1968) "A Saga of Sound and Vibration", Proc. Instn. Mech. Engrs. 1967-68, v.182, Pt.2A, pp.1-14.

9. Bradbury, Cyril Henry (1938) Torsional Vibration in Diesel Engines, Charles Griffin and Company Ltd., London.

10. Brandeis, J.P. and Graison, J. (1984) "Determining Noise Radiation of a Diesel Engine due to Bearing Excitation Using Analytical and Experimental Techniques", I. Mech. E., Vehicle Noise and Vibration, Paper C146/84, pp.173-188.

11. Braund, D.F. (1959) "Torsional Vibration", Proc. I. Mech. E., Automobile Division Proceedings, No.2,

pp.63-72.

12. Brown, Ross K. and Mischke, Charles R. (1970) "Whirling of a Four-Cylinder Engine Crankshaft", SAE Transactions, Paper 700121, pp.473-484.

13. Buma, C.J. (projected completion 1986) Multiple-source Excitation of Acoustic Cavity Resonances of Damped Small-room Enclosures, M.Sc. Thesis, Department of Mechanical Engineering, University of Alberta.

14. Butler, J.F. and Ørbeck, F. (1966) "Design Aspects of Large Marine Engines", Proc. Instn. Mech. Engrs., Paper 5, v.181, Pt.3H, pp.10-19.

15. Carter, B.C. (1928) "An Empirical Formula for Crankshaft Stiffness in Torsion", Engineering, July 13, 1928, pp.36-39.

16. Cowper, G.R. (1966) "The Shear Coefficient in Timoshenko's Beam Theory", Journal of Applied Mechanics in the Transactions of the ASME, June/1966, pp.335-340.

17. Craig Jr., Roy R. (1981) Structural Dynamics, John Wiley & Sons, Inc., New York.

18. Davis, R.; Henshell, R.D. and Warburton, G.B. (1972) "A Timoshenko Beam Element", Journal of Sound and Vibration, 22(4), pp.475-487.

19. DeJong, R.G. and Parsons, N.E. (1980) "High Frequency Vibration Transmission Through the Moving Parts of an Engine", SAE Transactions, Paper 800405, pp.1598-1604.

20. Dorey, S.F. (1939) Strength of Marine Engine Shafting, The North East Coast Institution of Engineers and Shipbuilders, London.

21. Ewins, D.J. (1975) "Measurement and Application of Mechanical Impedance Data", Journal of the Society of Environmental Engineers, Part 1 - Introduction and Ground Rules, v.14-4, No.67, Dec./1975, pp.3-12.

22. Ewins, D.J. (1976) "Measurement and Application of Mechanical Impedance Data", Journal of the Society of Environmental Engineers, Part 2 - Measurement Techniques, v.15-1, No.68, Mar./1976, pp.23-33.

23. Ewins, D.J. (1976) "Measurement and Application of Mechanical Impedance Data", Journal of the Society of Environmental Engineers, Part 3 - Interpretation and Application of Data, v.15-2, No.69, June/1976, pp.7-17.

24. Fessler, H. and Sood, V.K. (1973) "Deformations of Some

Medium Speed Diesel Engine Crankshafts", CIMAC, pp.563-590.

25. Ford, Dean M.; Hayes, Paul A. and Smith, Stephen K. (1979) "Engine Noise Reduction by Structural Design Using Advanced Experimental and Finite Element Methods", SAE Transactions, Paper 790366, pp.1299-1306.

26. Foulds, K. and D'Olier, V. (1973) "Factors Contributing to Crankshaft Fillet Stresses and Their Influence on Crankshaft Design", CIMAC, pp.591-610.

27. Fox, J.F. (1920) "Torsional Vibration and Critical Speeds in Crankshafts", SAE Journal, vol. VII, No.5, November, pp.413-417, 435.

28. Fyfe, Ken (1983) Practical Implementation of Modal Analysis, M.Sc. Thesis, Department of Mechanical Engineering, University of Alberta.

29. Goldstein, Herbert (1980) Classical Mechanics, 2nd Edition, Addison-Wesley Publishing Company, Reading, Mass.

30. Guyan, Robert J. (1965) "Reduction of Stiffness and Mass Matrices", AIAA Journal, v.3, p.380.

31. Haddad, S.D. and Watson, N. - editors (1984) Design and Applications in Diesel Engineering, Ellis Horwood Ltd., Chichester, England.

32. Hawkins, M.G. and Southall, R. (1975) "Analysis and Prediction of Engine Structure Vibration", SAE Transactions, Paper 750832, pp.2123-2133.

33. Hayashi, Yoshimasa; Sugihara, Kunihiko; Toda, Akira and Ushijima, Yuji (1981) "Analytical Study on Engine Vibration Transfer Characteristics Using Single-Shot Combustion", SAE Transactions, Paper 810403, pp.1539-1548.

34. Hodgetts, D. and McDonald, A.M. (1979) "The Transmission of Piston Forces to the Mounts of an Engine", I. Mech. E., Paper C116/79, 8 pages.

35. Hodgetts, D. (1976) "The Whirl Modes of Vibration of a Crankshaft", I. Mech. E., Paper C216/76, pp.255-261.

36. Hodgetts, D. (1972) "Vibrations of a Crankshaft", I. Mech. E. publication, Vibrations and Noise in Motor Vehicles, Paper C99/71, pp.35-50.

37. Hopkins, R. Bruce (1967) "Torsional Vibrations in Agricultural Tractors", SAE Journal, Paper 670193,

pp.1051-1057.

38. Howarth, M.H. (1966) The Design of High Speed Diesel Engines, American Elsevier Publishing Company, Inc., New York.

39. Ishihama, Masao; Hayashi, Yoshimasa and Kubozuka, Takao (1981) "An Analysis of the Movement of the Crankshaft Journals during Engine Firing", SAE Transactions, Paper 810772, Section 3, pp.2343-2353.

40. Kabele, D.F. (1984) "A New Approach in the Simulation of Crankshaft Torsional Vibration", I. Mech. E. publication, Vehicle Noise and Vibration, Paper C140/84, pp.131-140.

41. Kamath, M.; Narasimhan, R.; Nataraj, C. and Ramamurti, V. (1982) "Dynamic Response of Multicylinder Engines With a Viscous or Hysteretic Crankshaft Damper", Journal of Sound and Vibration, Letters to the Editor, 81(3), pp.448-452.

42. Kikuchi, Katsuaki (1970) "Analysis of Unbalance Vibration of Rotating Shaft System with Many Bearings and Discs", Bulletin of the JSME, v.13, No.61, pp.864-872.

43. Kliebhan, Frank H. (1966) "Considerations in Crankshaft Design", SAE Paper 660472, pp.22-33.

44. Kubozuka, Takao; Hayashi, Yoshimasa; Hayakawa, Yoshikazu and Kikuchi, Kazuhiro (1983) "Analytical Study on Engine Noise Caused by Vibration of the Cylinder Block and Crankshaft", SAE Transactions, Paper 830346, pp.1.1191-1.1199.

45. Lack, Arnold and Jahnke, Charles B. (1925) "Torsional Vibrations and Critical Speeds of Shafts", ASME Transactions, v.47, No.1969, pp.493-523.

46. Lewis, F.M. (1920) "The Critical Speeds of Torsional Vibration", SAE Journal, vol.VII, No.5, pp.418-431.

47. Liljedahl, John B.; Carleton, Walter M.; Turnquist, Paul K. and Smith, David W. (1979) Tractors and Their Power Units, 3rd Edition, John Wiley and Sons, New York.

48. Lürenbaum, Karl (1936) "Vibration of Crankshaft-Propeller Systems", SAE Journal (Transactions), v.39, No.6, pp.469-479.

49. Mehta, L.C.; Farr, M.K. and DeWitt, R.L. (1978) "Computer Simulation and Verification of I.C. Engine Vibration Characteristics", ASME Publication 78-DGP-24,

9 pages.

50. Myklestad, N.O. (1956) Fundamentals of Vibration Analysis, McGraw-Hill Book Co., Inc., New York.

51. Nagamatsu, Akio and Nagaike, Masaru (1981) "Vibration Analysis of Movable Part of Internal Combustion Engine", Bulletin of the JSME, Part I - Crankshaft, v.24, No.198-11, Dec./1981, pp.2141-2146.

52. Nagamatsu, Akio and Nagaike, Masaru (1983) "Vibration Analysis of Movable Part of Internal Combustion Engine", Bulletin of the JSME, Part II - Combined System of Crank Shaft and Flywheel, v.26, No.215-20, May/1983, pp.827-831.

53. Nestorides, E.J. - compiler (1958) A Handbook on Torsional Vibration, British Internal Combustion Engine Research Association (BICERA), Cambridge University Press, London, England.

54. Ochiai, Kazuomi and Nakano, Mitsuo (1979) "Relation Between Crankshaft Torsional Vibration and Engine Noise", SAE Transactions, Paper 790365, pp.1291-1298.

55. Okamura, Hideo; Sogabe, Kiyoshi; Sato, Yoshihiro; Suzuki, Yukio and Arai, Susumu (1983) "Experiments on the Coupling and Transmission Behavior of Crankshaft Torsional Bending and Longitudinal Vibrations in High Speed Engines", SAE Paper 830882, pp.205-218.

56. Poole, Ralph (1941) "The Axial Vibration of Diesel Engine Crankshafts", Proc. Instn. Mech. Engrs., v.146, pp.167-182.

57. Priede, T.; Dixon, J.; Grover, E.C. and Saleh, N.A. (1984) "Experimental Techniques Leading to the Better Understanding of the Origins of Automotive Engine Noise", I. Mech. E. publication, Vehicle Noise and Vibration, Paper C151/84, pp.141-159.

58. Roeder, James W. and Doane, James K. (1962) "Determining the Strength of a Large Crankshaft", ASME - Latest Technology in Oil and Gas Power, 34th Conference, Paper 62-OGP-5, 7 pages.

59. Shaw, Terry M. and Richter, Ira B. (1979) "Crankshaft Design Using a Generalized Finite Element Model", SAE Technical Paper 790279, 7 pages.

60. Srinivasulu, P. and Vaidyanathan, C.V. (1977) Handbook of Machine Foundations, Tata McGraw-Hill Publishing Company Ltd., New Delhi, pp.151-152.

61. Stansfield, R. (1942) "The Measurement of Torsional Vibrations", Proc. I. Mech. E., vol.148, pp.175-193.

62. Starkman, E.S. and Sytz, W.E. (1960) "The Identification and Characterization of Rumble and Thud", SAE Transactions, v.68, pp.93-100.

63. Stickler, Albert Craig (1974) Calculation of Bearing Performance in Indeterminate Systems, Ph.D. Thesis, Cornell University.

64. Taylor, Charles Fayette (1977) The Internal Combustion Engine in Theory and Practice, Volume I - Thermodynamics, Fluid Flow and Performance, 2nd Edition, M.I.T. Press, Cambridge, Mass.

65. Taylor, Charles Fayette (1968) The Internal Combustion Engine in Theory and Practice, Volume II - Combustion, Fuels, Materials, Design, M.I.T. Press, Cambridge, Mass.

66. Thomas, D.L.; Wilson, J.M. and Wilson, R.R. (1973) "Timoshenko Beam Finite Elements", Journal of Sound and Vibration, 31(3), pp.315-330.

67. Thomson, William T. (1981) Theory of Vibration with Applications, 2nd Edition, Prentice-Hall, Inc., New Jersey.

68. Timoshenko, S.P. and Goodier, J.N. (1970) Theory of Elasticity, 3rd Edition, McGraw-Hill Book Company, New York.

69. Timoshenko, S. (1923) "The Bending and Torsion of Multi-Throw Crankshafts on Many Supports", ASME Transactions, v.45, No.1907, pp.448-471.

70. Timoshenko, S. (1922) "Torsion of Crankshafts", ASME Transactions, v.44, No.1864, pp.653-667.

71. Timoshenko, Prof. S.P. (1921) "On the Transverse Vibrations of Prismatic Bars", Philosophical Magazine, v.41, pp.744-746.

72. Tse, Francis S., Morse; Ivan E. and Hinkle, Rolland T. (1978) Mechanical Vibrations Theory and Applications, 2nd Edition, Allyn and Bacon, Inc., Boston.

73. Tuplin, W.A. (1934) Torsional Vibration, John Wiley and Sons Inc., New York.

74. Welsh, W.A. and Booker, J.F. (1983) "Dynamic Analysis of Engine Bearing Systems", SAE Technical Paper 830065, International Congress and Exposition, Detroit, Michigan, 9 pages.

75. White, R.G. and Walker, J.G. - editors (1982) Noise and Vibration, Ellis Horwood Limited, Chichester, England.

76. Wilson, W. Ker (1971) "Some Early Experiences of Mechanical Vibration in Marine Engine Systems", James Clayton Lecture, Proc. Instn. Mech. Engrs. 1970-71, v.185 75/71, pp.1023-1089.

77. Wilson, W. Ker (1963) Practical Solution of Torsional Vibration Problems, 3rd Edition, Volume 1 - Frequency Calculations, John Wiley and Sons, New York.

78. Wilson, W. Ker (1963) Practical Solution of Torsional Vibration Problems, 3rd Edition, Volume 2 - Amplitude Calculations, John Wiley and Sons, New York.

79. Wilson, W. Ker (1958) "Crankshaft Vibrations", Gas and Oil Power, v.53, April, pp.98-101.

80. Yang, T.Y. and Sun, C.T. (1973) "Axial-flexural vibration of frameworks using finite element approach", The Journal of the Acoustical Society of America, v.53, Number 1, pp.137-146.

APPENDIX A - Energy Formulations for Sub-elements

Nomenclature used in Appendix A:

- a polynomial coefficient in element shape function
- A cross-sectional area of an element
- E Young's Modulus
- F transverse shearing force
- G shear modulus
- I_y second moment of area about the y axis
- I_z second moment of area about the z axis
- J_{xx} polar second moment of area
- K shear coefficient
- ℓ length of the element
- M bending moment
- p general element nodal coordinate
- t time variable
- u nodal displacement coordinate for axial sub-element
- v nodal transverse displacement for beam sub-elements
- x distance along an element
- β_y EI_y/GKA
- β_z EI_z/GKA
- θ bending slope
- ρ density
- ϕ nodal twist for torsional sub-element
- ψ shear slope
- ω angular frequency of vibration (rad/s)

A1 Axial Extension Element

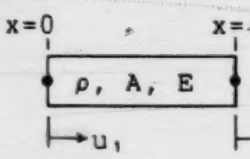

$$u(x,t) = (a_0 + a_1 x)\sin(\omega t)$$

$$u_1 = u(0,t) = p_1$$

$$u_2 = u(\ell,t) = p_7$$

$$\text{P.E.} = 0.5\int_0^{\ell} AE(\partial u/\partial x)^2 dx = 0.5\langle u_1, u_2\rangle [KA] \begin{Bmatrix} u_1 \\ u_2 \end{Bmatrix}$$

$$\text{K.E.} = 0.5\int_0^{\ell} \rho A(\partial u/\partial t)^2 dx = 0.5\langle \dot{u}_1, \dot{u}_2\rangle [MA] \begin{Bmatrix} \dot{u}_1 \\ \dot{u}_2 \end{Bmatrix}$$

where,

$$[KA] = \frac{AE}{\ell}\begin{bmatrix} 1 & -1 \\ -1 & 1 \end{bmatrix} \qquad [MA] = \rho A\ell \begin{bmatrix} 1/3 & 1/6 \\ 1/6 & 1/3 \end{bmatrix}$$

A2 Torsional Element

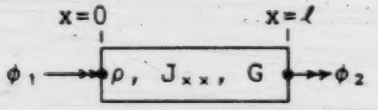

$$\phi(x,t) = (a_0 + a_1 x)\sin(\omega t)$$

$$\phi_1 = \phi(0,t) = p_8$$

$$\phi_2 = \phi(\ell,t) = p_{10}$$

$$\text{P.E.} = 0.5\int_0^{\ell} GJ_{xx}(\partial\phi/\partial x)^2 dx = 0.5\langle \phi_1, \phi_2\rangle [KB] \begin{Bmatrix} \phi_1 \\ \phi_2 \end{Bmatrix}$$

$$\text{K.E.} = 0.5\int_0^{\ell} \rho J_{xx}(\partial\phi/\partial t)^2 dx = 0.5\langle \dot{\phi}_1, \dot{\phi}_2\rangle [MB] \begin{Bmatrix} \dot{\phi}_1 \\ \dot{\phi}_2 \end{Bmatrix}$$

where,

$$[KB] = \frac{GJ_{xx}}{\ell}\begin{bmatrix} 1 & -1 \\ -1 & 1 \end{bmatrix} \qquad [MB] = \rho J_{xx}\ell \begin{bmatrix} 1/3 & 1/6 \\ 1/6 & 1/3 \end{bmatrix}$$

A3 Timoshenko Beam Element (x-y plane)

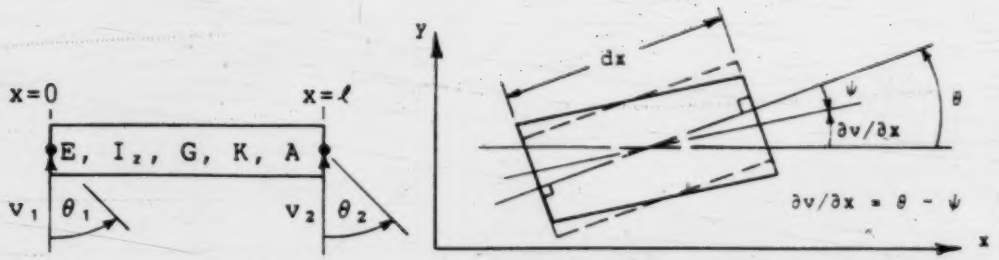

$$v(x,t) = (a_0 + a_1x + a_2x^2 + a_3x^3)\sin(\omega t)$$

$$\psi(x,t) = \psi(x)\sin(\omega t)$$

$$\theta(x,t) = \partial v/\partial x + \psi = (a_1 + 2a_2x + 3a_3x^2 + \psi(x))\sin(\omega t)$$

$$v_1 = v(0,t) = p_2 \qquad \theta_1 = \theta(0,t) = p_6$$

$$v_2 = v(\ell,t) = p_8 \qquad \theta_2 = \theta(\ell,t) = p_{12}$$

Determine $\psi(x)$ from the force-moment relationship in a beam,

$$\partial F/\partial x = 0 \qquad F = \partial M/\partial x$$

$$GKA(\partial\psi/\partial x) = 0 \qquad GKA\psi = EI_z \cdot \partial^3 v/\partial x^3$$

$$\psi(x) = \text{const.} \qquad \psi(x) = \beta_z \cdot 6a_3$$

$$\text{P.E.} = 0.5\int_0^{\ell}\{EI_z(\partial^2 v/\partial x^2)^2 + GKA\psi^2\}dx$$

$$= 0.5\langle v_1\ \theta_1\ v_2\ \theta_2\rangle[KC]\begin{Bmatrix} v_1 \\ \theta_1 \\ v_2 \\ \theta_2 \end{Bmatrix}$$

$$\text{K.E.} = 0.5\int_0^{\ell}\{\rho A(\partial v/\partial t)^2 + \rho I_z(\partial\theta/\partial t)^2\}dx$$

$$= 0.5\langle \dot{v}_1\ \dot{\theta}_1\ \dot{v}_2\ \dot{\theta}_2\rangle[MC]\begin{Bmatrix} \dot{v}_1 \\ \dot{\theta}_1 \\ \dot{v}_2 \\ \dot{\theta}_2 \end{Bmatrix}$$

Matrices [KC] and [MC] may be found in a paper by Thomas, et al. [66] and are listed in routine ELKM in Appendix B3.

A4 Timoshenko Beam Element (x-z plane)

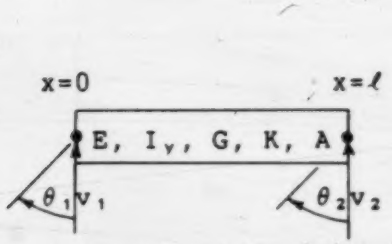

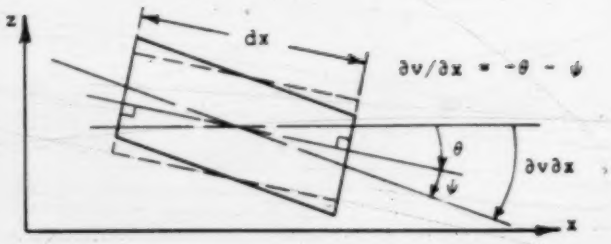

$$v(x,t) = (a_0 + a_1x + a_2x^2 + a_3x^3)\sin(\omega t)$$

$$\psi(x,t) = 6\beta_y a_3 \sin(\omega t) \qquad \text{(see Section A3)}$$

$$\theta(x,t) = -\partial v/\partial x - \psi = -(a_1 + 2a_2x + 3a_3x^2 + 6\beta_y a_3)\sin(\omega t)$$

$$v_1 = v(0,t) = p_3 \qquad \theta_1 = \theta(0,t) = p_5$$

$$v_2 = v(\ell,t) = p_9 \qquad \theta_2 = \theta(\ell,t) = p_{11}$$

$$P.E. = 0.5\int_0^{\ell}\{EI_y(\partial^2 v/\partial x^2)^2 + GKA\psi^2\}dx$$

$$= 0.5\langle v_1\ \theta_1\ v_2\ \theta_2\rangle[KD]\begin{Bmatrix} v_1 \\ \theta_1 \\ v_2 \\ \theta_2 \end{Bmatrix}$$

$$K.E. = 0.5\int_0^{\ell}\{\rho A(\partial v/\partial t)^2 + \rho I_y(\partial\theta/\partial t)^2\}dx$$

$$= 0.5\langle \dot{v}_1\ \dot{\theta}_1\ \dot{v}_2\ \dot{\theta}_2\rangle[MD]\begin{Bmatrix} \dot{v}_1 \\ \dot{\theta}_1 \\ \dot{v}_2 \\ \dot{\theta}_2 \end{Bmatrix}$$

Matrices [KD] and [MD] are similar to those in reference [66] except for the following sign changes: elements of the 4x4 matrices, KD(i,j) and MD(i,j), where i+j is an odd integer, must be negated. These matrices are listed in routine ELKM in Appendix B3.

APPENDIX B - Computer Program Input, Output and Codes

In the first section the input data necessary to calculate natural frequencies and mode shapes of a crankshaft are described. Physical data may be in English or S.I. units but must remain consistent throughout. The next section describes how the main structural analysis and plotting routines are executed. Output data for crankshafts ATX5, DT3 and SL2 is given for reference. The final section contains listings of the computer codes and should be consulted when preparing input data.

B1 INPUT

Variable	Description
TITLE	Self-explanatory. If plots are included, a dollar sign ($) must be the last character in TITLE.
IJOB	Static problems: IJOB is a negative integer; |IJOB| denotes the number of static loads. Dynamic problems: IJOB=0 if only natural frequencies are calculated. IJOB=1 if natural frequencies and mode shapes are desired.
IPLOT	IPLOT=0 for no plotted modes or deformations. IPLOT=1 for plottng static deformation. For plotting mode shapes, IPLOT takes on the number of the highest mode to be plotted.
Plot data (if IPLOT>0)	
I1	First mode to be plotted. Use in case of unwanted rigid body modes. I1≤IPLOT and if IJOB<0 then I1=1.

VP, VT, VR — Viewpoint for 3-D plots in spherical coordinates (see DISSPLA user's manual). Suggested first try: VP = -160., VT = 30. and VR two orders of magnitude larger than the length of the crankshaft.

SF — Scale Factor. Scales the plotted deformations such that the largest deflection is SF times the average element length. First try: 0.5 to 0.8.

System Data

NT — Number of throws or sub-structures. The crankshaft is built up from the segments shown in figures B.1 to B.3.

NC — Number of rigid constraints. NC≥0

NS — Number of non-rigid constraints. NS≥0

NM — Number of annular discs as shown in Figure B.4 which are attached at specified nodes of the crankshaft. NM≥0

NTYP(NT) — Array specifying segments as shown in figures B.1 to B.3. For "A" type, NTYP=1; for "D" type, NTYP=-2; for "E" type, NTYP=0. Order from left to right in crankshaft model.

TA(NT) — Segment angles in degrees relative to a fixed global axis system, for each segment specified in NTYP.

C_x, C_y, C_z — Web length modifiers. Use zeroes for an unmodified model. Altered Length = Original Length - $C_{x/y/z}$(Journal Dia. + Crankpin Dia.). See Section 4.3.

E — Young's Modulus of the crankshaft material.

RHO — Density of crankshaft material. Units of $lb/s^2/in^4$ or kg/m^3.

PR — Poisson's Ratio of the crankshaft material.

"A" Type Throw Data

CL, CR, DC DJ, PL, SP WT, WW	Geometrical parameters as shown in Figure B.1. Webs are assumed to be identical and allowance is made for angling of the webs.
CM	"Extra-element" mass information matrix. Each of four rows contains the mass, x, y and z mass moments of inertia about the centroid and x, y and z coordinates of the centroid relative to the node. Relevant nodes are the 2nd, 3rd, 4th and 5th of this throw type.

"D" Type Throw Data

CL, CR, DC DJ, PL, SP ST, SW, WT WW	Geometrical parameters as shown in Figure B.2. Outside webs are identical and upright; center web may be slanted.
CM	"Extra-element" mass informatin matrix. Each of six rows contains the mass, x, y and z mass moments of inertia about the centroid and x, y and z coordinates of the centroid relative to the node. Relevant nodes are the 2nd through 7th of this throw type.

"E" Type Shaft Data

XL, XD	Geometrical parameters as shown in Figure B.3. Used for crankshaft ends or spacer shafting between throws.

Disc Mass Data (if NM>0)

M(NM)	Array of node numbers for annular discs.
P(NM,3)	Each row contains the thickness, the inside and the outside diameter of an annular disc as shown in Figure B.4.

Constraint Data

N, S	Non-rigid constraints. Add spring stiffness, S, to degree of freedom, N. Repeat NS times.
C(NC)	Array of degrees of freedom, listed from lowest to highest, to be rigidly constrained.

Static Force Data (if IJOB<0)

NF, XFORCE	A force, moment or torque of XFORCE is applied at degree of freedom NF. The sense of XFORCE is according to the global axis system. Repeat |IJOB| times.

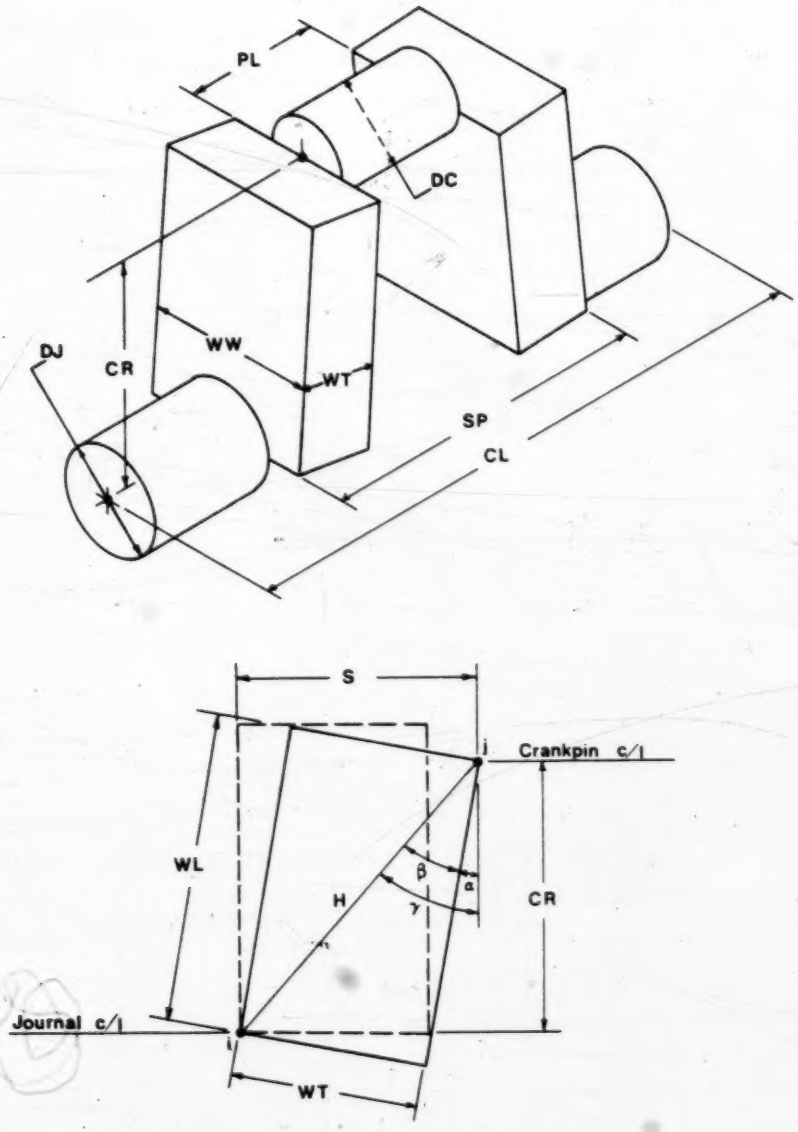

Figure B.1 Geometry for "A" Type Crankthrow

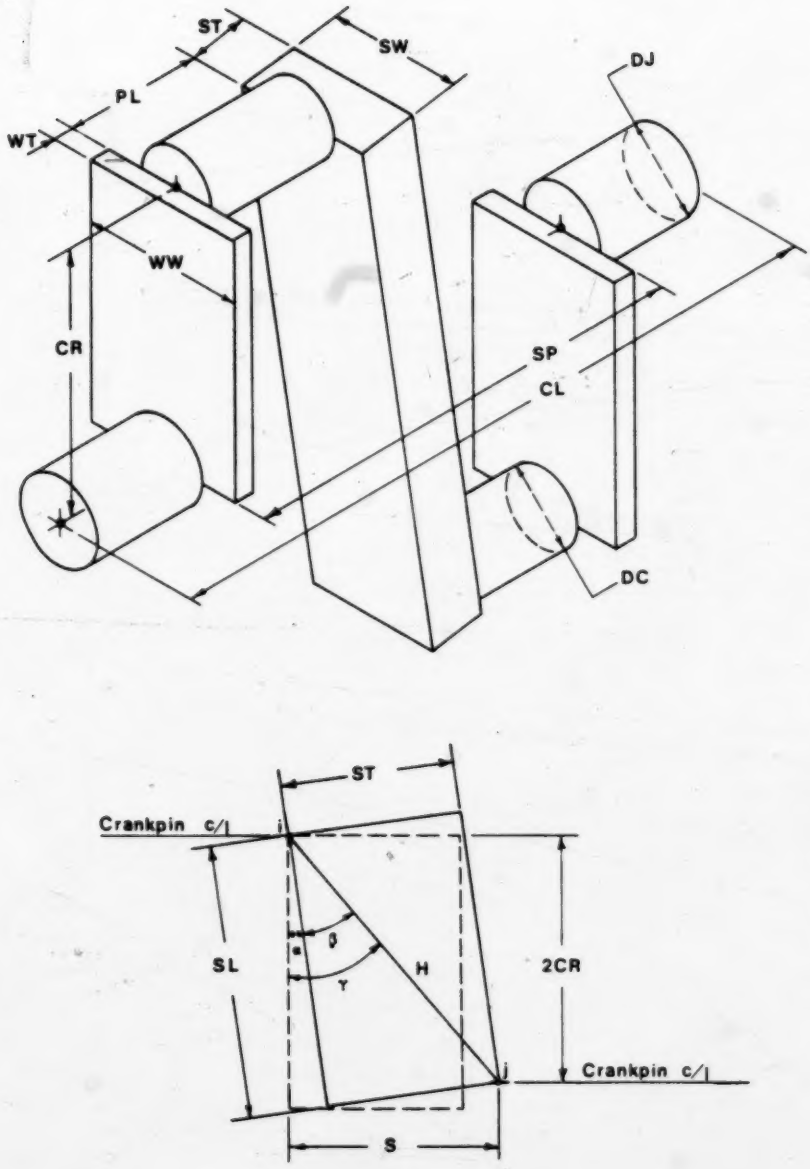

Figure B.2 Geometry for "D" Type Crankthrow

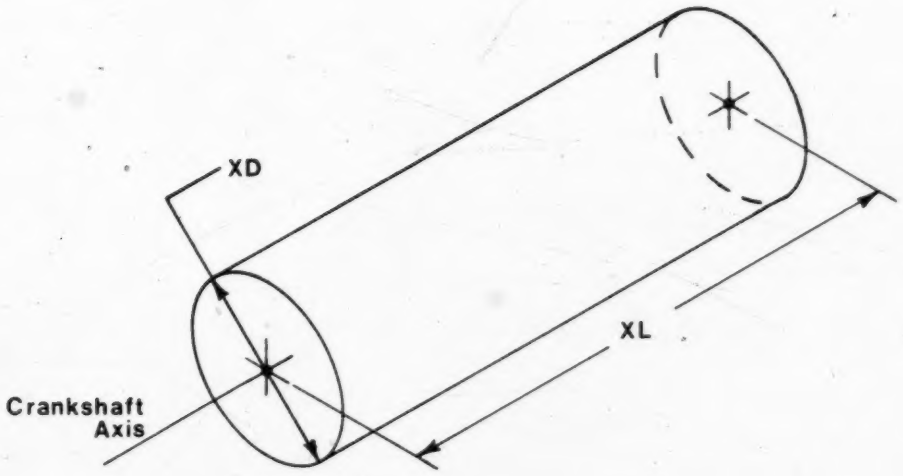

Figure B.3 Geometry for "E" Type Shafting

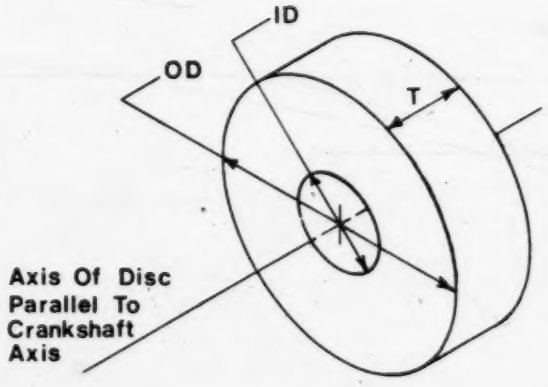

Figure B.4 Geometry for Annular Disc Mass

B2 Program Execution and Plotting

After data is entered into an input file the main structural analysis program may be executed.

```
$RUN *FORTG SCARDS=CRANK+SUBROUTINES SPUNCH=-C
$RUN -C+*IMSLDPLIB 5=DATA 6=OUTPUT 7=PLOTDATA
```

The following variable list is for the plotting routine, P7, and is useful since changes may be made to "PLOTDATA" before the plots are made.

Variable	Description
I	The number of crankshaft modes to be plotted. The following data occurs for each of "I" modes.
II, FREQ	Mode number and natural frequency in Herz.
VP, VT, VR	Viewpoint (see Section B1).
X1, Y1, Z1	Web length modifiers corresponding to C_x, C_y, C_z.
N1, N2	First and last element to be plotted.
NEL, SF	Total number of elements in the model and the scaled maximum deflection in model length units.
NUM(NEL,2)	Nodal numbering array. Each consecutive row corresponds to the first and last node numbers of the elements comprising the finite element model.
XN, YN, ZN	Matrices for the x, y and z coordinates, respectively, of nine points on each element of the system in the undeformed postion.
XE, YE, ZE	Matrices for the x, y and z deflections of the points in XN, YN and ZN. These deflections are relative to the undeformed crankshaft and may be scaled arbitrarily by adjusting "SF" above.

The plotting routine is executed as follows:

```
$RUN *FORTG SCARDS=P7 SPUNCH=-P
$RUN -P+*DISSPLA 5=PLOTDATA 6=-OUT 9=PLOT
```

The plotfile "PLOT" may be used with any compatible plotting facility (eg. ESPP, CALCOMPQ, etc.). The example crankshafts have their output files listed on the following pages. Length units are in inches, "E" is in lb/in^2 and density, RHO, is in $lb \cdot s^2/in^4$.

Output Data for Example Crankshafts

```
       *** CRANK ****** CRANK ****** CRANK ***
 Crankshaft ATX5   Free-Free      October 11, 1985
IJOB=     0 IPLOT=     0
NT=  8 NC=  0 NM=  0 ND= 200 NE= 50
NEL= 24 NG= 150 NR= 150 NN= 11325 NWA= 22800
Web Length Modifiers: CX= 0.0    CY= 0.0    CZ= 0.0
E=  0.30000000E+08 G=  0.11538462E+08
RHO=  0.67930000E-03 PR= 0.3000

-----------------------------------------------------
Throw    1 Type E   Length=  3.1750 Diameter=  1.4000

-----------------------------------------------------
Throw    2 Type E   Length=  0.4680 Diameter=  2.0000

-----------------------------------------------------
Throw    3 Type A   Having Throw Angle Of    0.0
    CL         CR         DC         DJ
  3.66500    1.50000    1.81200    2.00000
    PL         SP         WT         WW
  0.95000    2.70000    0.72000    2.75000

          "Extra - Element" Mass Data
              Inertia About Mass Center
Node      Mass          Ixx          Iyy          Izz
   4  0.3911E-02   0.5400E-02   0.4300E-02   0.1100E-02
   5  0.5430E-03   0.2260E-03   0.1880E-03   0.5300E-04
   6  0.5430E-03   0.2260E-03   0.1880E-03   0.5300E-04
   7  0.1125E-02   0.6310E-03   0.5300E-03   0.1690E-03
   Mass Center Coordinates
     Xg         Yg         Zg
   4   0.3600   -1.1470   -0.0230
   5  -0.2000    0.5000    0.0
   6   0.2000    0.5000    0.0
   7  -0.3000   -0.6000    0.0

Non-dimensional Parameters
   CL/CR      DC/CR      DJ/CR      PL/CR
  2.44333    1.20800    1.33333    0.63333
   SP/CR      WT/CR      WW/CR  Web Angle(deg)
  1.80000    0.48000    1.83333    5.76143

-----------------------------------------------------
Throw    4 Type A   Having Throw Angle Of  180.00
    CL         CR         DC         DJ
  3.66500    1.50000    1.81200    2.00000
    PL         SP         WT         WW
  0.95000    2.70000    0.72000    2.75000
```

"Extra - Element" Mass Data
Inertia About Mass Center

Node	Mass	Ixx	Iyy	Izz
9	0.1125E-02	0.6310E-03	0.5300E-03	0.1690E-03
10	0.5430E-03	0.2260E-03	0.1880E-03	0.5300E-04
11	0.5430E-03	0.2260E-03	0.1880E-03	0.5300E-04
12	0.3720E-02	0.5200E-02	0.4100E-02	0.1200E-02

Mass Center Coordinates

	Xg	Yg	Zg
9	0.3000	0.6000	0.0
10	-0.2000	-0.5000	0.0
11	0.2000	-0.5000	0.0
12	-0.3500	1.1710	-0.0610

Non-dimensional Parameters

CL/CR	DC/CR	DJ/CR	PL/CR
2.44333	1.20800	1.33333	0.63333
SP/CR	WT/CR	WW/CR	Web Angle(deg)
1.80000	0.48000	1.83333	5.76143

Throw 5 Type A Having Throw Angle Of 180.00

CL	CR	DC	DJ
3.66500	1.50000	1.81200	2.00000
PL	SP	WT	WW
0.95000	2.70000	0.72000	2.75000

"Extra - Element" Mass Data
Inertia About Mass Center

Node	Mass	Ixx	Iyy	Izz
14	0.3400E-02	0.4620E-02	0.3400E-02	0.1200E-02
15	0.5430E-03	0.2260E-03	0.1880E-03	0.5300E-04
16	0.5430E-03	0.2260E-03	0.1880E-03	0.5300E-04
17	0.1125E-02	0.6310E-03	0.5300E-03	0.1690E-03

Mass Center Coordinates

	Xg	Yg	Zg
14	0.3500	1.1840	-0.0660
15	-0.2000	-0.5000	0.0
16	0.2000	-0.5000	0.0
17	-0.3000	0.6000	0.0

Non-dimensional Parameters

CL/CR	DC/CR	DJ/CR	PL/CR
2.44333	1.20800	1.33333	0.63333
SP/CR	WT/CR	WW/CR	Web Angle(deg)
1.80000	0.48000	1.83333	5.76143

Throw 6 Type A Having Throw Angle Of 0.0

CL	CR	DC	DJ
3.64500	1.50000	1.81200	2.00000
PL	SP	WT	WW
0.95000	2.70000	0.75000	2.75000

"Extra - Element" Mass Data

Inertia About Mass Center

Node	Mass	Ixx	Iyy	Izz
19	0.1673E-02	0.1049E-02	0.9090E-03	0.3190E-03
20	0.5430E-03	0.2260E-03	0.1880E-03	0.5300E-04
21	0.5430E-03	0.2260E-03	0.1880E-03	0.5300E-04
22	0.3915E-02	0.5500E-02	0.4500E-02	0.9600E-03

Mass Center Coordinates

	Xg	Yg	Zg
19	0.4000	-0.5940	0.0
20	-0.2000	0.5000	0.0
21	0.2000	0.5000	0.0
22	-0.3600	-1.1340	-0.0620

Non-dimensional Parameters

CL/CR	DC/CR	DJ/CR	PL/CR
2.43000	1.20800	1.33333	0.63333
SP/CR	WT/CR	WW/CR	Web Angle(deg)
1.80000	0.50000	1.83333	4.66891

Throw 7 Type E Length= 0.4730 Diameter= 2.0000

Throw 8 Type E Length= 1.0000 Diameter= 2.7800

Non-rigid Constraints

DOF	Stiffness
8	2.00
9	2.00
145	2.00
146	2.00
147	2.00
148	2.00

Natural Frequencies (Hz)

0.65993	0.87757	1.23858	1.23868
1.95464	1.97736	279.76764	315.68150
682.03803	789.73395	809.17059	1149.31745
1347.14028	1466.43650		

```
      *** CRANK ****** CRANK ****** CRANK ***
Crankshaft DT3   Free-Free Case   October 12,1985
IJOB=    0 IPLOT=    0
NT=  5 NC=  0 NM=  0 ND= 200 NE= 50
NEL= 17 NG= 108 NR= 108 NN=  5886 NWA= 11880
Web Length Modifiers: CX= 0.0    CY= 0.0    CZ= 0.0
E=  0.30000000E+08 G=  0.11538462E+08
RHO=  0.73510000E-03 PR= 0.3000

-----------------------------------------------------
Throw    1 Type E   Length= 2.6250 Diameter= 1.5000

-----------------------------------------------------
Throw    2 Type E   Length= 0.8400 Diameter= 1.7450

-----------------------------------------------------
Throw    3 Type D   Having Throw Angle Of    0.0
    CL         CR         DC         DJ         PL
 6.1000     1.5000     1.6200     1.7450     1.1150
    SP         ST         SW         WT         WW
 4.8000     1.2000     2.5500     0.6080     3.4000

          "Extra - Element" Mass Data
              Inertia About Mass Center
Node      Mass          Ixx          Iyy          Izz
   4  0.3460E-02   0.4525E-02   0.3067E-02   0.1687E-02
   5  0.4390E-03   0.1890E-03   0.1490E-03   0.4600E-04
   6  0.3860E-03   0.1500E-03   0.1500E-03   0.1600E-04
   7  0.3860E-03   0.1500E-03   0.1500E-03   0.1600E-04
   8  0.4390E-03   0.1890E-03   0.1490E-03   0.4600E-04
   9  0.3112E-02   0.4458E-02   0.3070E-02   0.1531E-02
   Mass Center Coordinates
      Xg         Yg         Zg
   4   0.3150    -1.1680     0.0
   5  -0.1380     0.5420     0.0
   6   0.2500     0.2500     0.0
   7  -0.2500    -0.2500     0.0
   8   0.1380    -0.5420     0.0
   9  -0.2620     1.1860     0.0

Non-dimensional Parameters
   CL/CR      DC/CR      DJ/CR      SP/CR      WT/CR
   4.0667     1.0800     1.1633     0.7433     3.2000
   ST/CR      SW/CR      WT/CR      WW/CR    Web Ang
   0.8000     1.7000     0.4053     2.2667     2.9091

-----------------------------------------------------
Throw    4 Type D   Having Throw Angle Of  180.00
    CL         CR         DC         DJ         PL
 6.0150     1.5000     1.6200     1.7450     1.1150
    SP         ST         SW         WT         WW
 4.7150     1.2000     2.5500     0.5680     3.3000
```

"Extra - Element" Mass Data

Inertia About Mass Center

Node	Mass	Ixx	Iyy	Izz
11	0.3143E-02	0.4682E-02	0.3278E-02	0.1543E-02
12	0.4390E-03	0.1890E-03	0.1490E-03	0.4600E-04
13	0.3860E-03	0.1500E-03	0.1500E-03	0.1600E-04
14	0.3860E-03	0.1500E-03	0.1500E-03	0.1600E-04
15	0.4390E-03	0.1890E-03	0.1490E-03	0.4600E-04
16	0.3117E-02	0.4205E-02	0.2822E-02	0.1540E-02

Mass Center Coordinates

	Xg	Yg	Zg
11	0.2580	1.1860	0.0
12	-0.1380	-0.5420	0.0
13	0.2500	-0.2500	0.0
14	-0.2500	0.2500	0.0
15	0.1380	0.5420	0.0
16	-0.2750	-1.1860	0.0

Non-dimensional Parameters

CL/CR	DC/CR	DJ/CR	SP/CR	WT/CR
4.0100	1.0800	1.1633	0.7433	3.1433
ST/CR	SW/CR	WT/CR	WW/CR	Web Ang
0.8000	1.7000	0.3787	2.2000	2.8157

Throw 5 Type E Length= 0.6300 Diameter= 1.7450

Non-rigid Constraints

DOF	Stiffness
14	2.00
15	2.00
97	2.00
98	2.00
99	2.00
100	2.00

Natural Frequencies (Hz)

0.70073	0.95172	1.33430	1.33472
1.94445	1.98387	385.54517	449.95529
824.07322	1040.25910	1108.97946	1236.82791
1455.47386	1856.10903		

```
      *** CRANK ****** CRANK ****** CRANK ***
Crankshaft SL2   Free-Free Case    October 12, 1985
IJOB=     0 IPLOT=     0
NT=  2 NC=  0 NM=  0 ND= 200 NE= 50
NEL=  6 NG=  42 NR=  42 NN=   903 NWA=  1848
Web Length Modifiers: CX= 0.0    CY= 0.0    CZ= 0.0
E=  0.30000000E+08 G=  0.11538462E+08
RHO=  0.64160000E-03 PR= 0.3000

-----------------------------------------------------------
Throw    1 Type E   Length= 1.5800 Diameter= 1.3800

-----------------------------------------------------------
Throw    2 Type A  Having Throw Angle Of    0.0
    CL         CR         DC         DJ
  6.54500    1.31000    1.25000    1.38000
    PL         SP         WT         WW
  1.12500    3.05500    0.95000    1.68000

          "Extra - Element" Mass Data
              Inertia About Mass Center
Node      Mass          Ixx          Iyy          Izz
   3  0.2196E-02  0.1512E-02  0.1246E-02  0.5970E-03
   4  0.3590E-03  0.9000E-04  0.1040E-03  0.2400E-04
   5  0.3590E-03  0.9000E-04  0.1040E-03  0.2400E-04
   6  0.2196E-02  0.1512E-02  0.1246E-02  0.5970E-03
   Mass Center Coordinates
     Xg         Yg         Zg
   3   0.4750   -0.8840    0.0
   4  -0.4000    0.2080    0.0
   5   0.4000    0.2080    0.0
   6  -0.4750   -0.8840    0.0

Non-dimensional Parameters
   CL/CR      DC/CR      DJ/CR      PL/CR
 4.99618    0.95420    1.05344    0.85878
   SP/CR      WT/CR      WW/CR  Web Angle(deg)
 2.33206    0.72519    1.28244    0.65333

Non-rigid Constraints
 DOF          Stiffness
   8            2.00
   9            2.00
  37            2.00
  38            2.00
  39            2.00
  40            2.00

Natural Frequencies (Hz)
    1.93242       1.94922       2.68933       2.69229
    4.26730       4.49010    1731.55211    2232.92591
 3028.08364    4398.07640
```

B3 COMPUTER PROGRAMS

CRANK is the main structural analysis routine, subroutines follow and P7 is the mode shape plotting routine.

```
C
C
C     Program CRANK assembles crankshaft by throws.
      REAL*8 KG,MG,KK(20100),MM(20100),P(200,200)
      REAL*8 CT(50,4),S,CX,CY,CZ,PI,WF(200),WKA(40400)
      REAL*8 EL(50),ED(50),EW(50),TA(20),XFORCE(20)
      REAL*8 PX,DABS,DSQRT,DMAX1,E,G,RHO,PR
      REAL*4 VP,VT,VR,SF,TITLE(30)
      INTEGER C(20),NTYP(20),NEL,NR,NG,NN,NWA,NC,NT
      INTEGER IJOB,IPLOT,IEL,ND,N,NE
      INTEGER NS,I1,IER
      INTEGER NM,M(10),NF(20)
      COMMON KG(200,200),MG(200,200)
C     Read In
      READ(5,5050)TITLE
      READ(5,5000)IJOB,IPLOT
      IF (IPLOT.NE.0) READ(5,5005)I1,VP,VT,VR,SF
      READ(5,5000)NT,NC,NS,NM
      READ(5,5020)(NTYP(I),I=1,NT)
      READ(5,5030)(TA(I),I=1,NT)
      READ(5,5095)CX,CY,CZ
      READ(5,5040)E,RHO,PR
C     Calculations
      PI=3.141592654
      ND=200
      NE=50
      NEL=0
      IEL=0
      DO 10 I=1,NT
      IF (NTYP(I).EQ.0) NEL=NEL+1
      IF (NTYP(I).EQ.1) NEL=NEL+5
      IF (NTYP(I).EQ.-2) NEL=NEL+7
   10 CONTINUE
      NG=6*NEL+6
      NR=NG-NC
      NN=NR*(NR+1)/2.0+0.5
      NWA=NR*(NR+2)
      G=E/(2.D0*(1.D0+PR))
C     Echo Check
      WRITE(6,6000)
      WRITE(6,5050)TITLE
      WRITE(6,6010)IJOB,IPLOT
      WRITE(6,6020)NT,NC,NM,ND,NE
      WRITE(6,6030)NEL,NG,NR,NN,NWA
      WRITE(6,6080)CX,CY,CZ
```

```
      WRITE(6,6050)E,G,RHO,PR
C     Zero KG MG EW and CT Arrays
      DO 100 I=1,NG
      DO 100 J=1,I
     KG(I,J)=0.0D0
     MG(I,J)=0.0D0
  100 CONTINUE
      DO 110 I=1,NEL
     EW(I)=0.0D0
     DO 105 J=1,4
       CT(I,J)=0.0D0
  105   CONTINUE
  110 CONTINUE
C     Assembly Of Crankshaft Throws
      DO 1000 N=1,NT
     IF (NTYP(N)) 200,300,400
  200   CALL DTHROW(EL,ED,EW,CT,NE,TA,E,G,RHO,PR,
     #            CX,CY,CZ,IJOB,IEL,N)
      GOTO 500
  300   CALL ETHROW(EL,ED,NE,E,G,RHO,PR,IJOB,IEL,N)
      GOTO 500
  400   CALL ATHROW(EL,ED,EW,CT,NE,TA,E,G,RHO,PR,
     #            CX,CY,CZ,IJOB,IEL,N)
  500   CONTINUE
 1000 CONTINUE
C     Add in Annular Disc Masses and Inertias
      IF (NM.EQ.0) GOTO 1040
     WRITE(6,6060)
     DO 1005 I=1,NM
       READ(5,5075) M(I),(P(I,J),J=1,3)
       WRITE(6,5075) M(I),(P(I,J),J=1,3)
 1005   CONTINUE
     DO 1010 I=1,NM
       WKA(1)=RHO*PI*P(I,1)*(P(I,3)**2-P(I,2)**2)/4.0D0
       WKA(4)=WKA(1)*(P(I,3)**2+P(I,2)**2)/8.0D0
       WKA(2)=WKA(1)
       WKA(3)=WKA(1)
       WKA(5)=WKA(4)/2.0D0
       WKA(6)=WKA(4)/2.0D0
C      If rotational inertias are not to be included,
C      then zero WKA(4)...WKA(6).
C          WKA(4)=0.D0
C          WKA(5)=0.D0
C          WKA(6)=0.D0
         N=6*(M(I)-1)
       DO 1020 J=1,6
         MG(N+J,N+J)=MG(N+J,N+J)+WKA(J)
 1020     CONTINUE
 1010   CONTINUE
 1040 CONTINUE
C     Apply Non-rigid Constraints To System
      IF (NS.EQ.0) GOTO 1050
      WRITE(6,6070)
      DO 1050 I=1,NS
```

```
      READ(5,5070)N,S
      WRITE(6,5070)N,S
      KG(N,N)=KG(N,N)+S
 1050 CONTINUE
C      Apply Rigid Constraints
       IF (NC.EQ.0) GOTO 1600
      READ(5,5020)(C(I),I=1,NC)
      WRITE(6,6040)(C(I),I=1,NC)
      CALL REDM(C,NG,NC)
 1600 CONTINUE
C      Solution
       IF (IJOB) 2000,2500,2500
C      Solve For Deflections Due To Static Loads
 2000   IJOB=-IJOB
      DO 2020 I=1,NG
        WF(I)=0.0D0
 2020   CONTINUE
      DO 2030 I=1,IJOB
        READ(5,5070) NF(I),XFORCE(I)
        WF(NF(I))=XFORCE(I)
 2030   CONTINUE
      IF (NC.EQ.0) GOTO 2040
        CALL REDV(WF,C,NG,NC)
 2040   CONTINUE
      DO 2045 I=1,NR
      DO 2045 J=1,I
        P(I,J)=KG(I,J)
        P(J,I)=KG(I,J)
 2045   CONTINUE
      CALL LEQT1F(P,1,NR,ND,WF,2,WKA,IER)
      IF (NC.EQ.0) GOTO 2050
        CALL EXPV(WF,C,NG,NC)
 2050   CONTINUE
        WRITE(6,6085)
        DO 2055 I=1,IJOB
          WKA(I)=XFORCE(I)/WF(NF(I))
          WRITE(6,6086)NF(I),XFORCE(I),WKA(I)
 2055     CONTINUE
        WRITE(6,6088)
        WRITE(6,7000)(WF(I),I=1,NG)
        IJOB=-IJOB
      IF (IPLOT.NE.0) GOTO 3000
      GOTO 4000
C        Solve For Natural Modes (Eigenvalue Problem)
 2500   N=NR
      IF (N.GT.20) N=20
      IF (IPLOT.NE.0) N=IPLOT
      CALL SSM(KK,MM,NR,NN)
      CALL EIGZS(KK,MM,NR,IJOB,WF,P,ND,WKA,IER)
      DO 2250 I=1,N
        WF(I)=DSQRT(WF(I))/6.2831853D0
 2250   CONTINUE
      WRITE(6,6090)
      WRITE(6,6095)(WF(I),I=1,N)
```

```
      IF (IJOB.EQ.0) GOTO 4000
C        Normalization Of Mode Shape
      DO 2300 J=1,N
        PX=0.0D0
        DO 2320 I=1,NR
          IF (DABS(P(I,J)).GT.DABS(PX)) PX=P(I,J)
 2320       CONTINUE
        DO 2340 I=1,NR
          P(I,J)=P(I,J)/PX
 2340       CONTINUE
 2300     CONTINUE
      IF (IPLOT.EQ.0) GOTO 4000
        IF (NC.EQ.0) GOTO 2600
          CALL EXPMOD(P,C,ND,N,NC,NG)
 2600       CONTINUE
C        PLOT writes data to Unit 7 for plotting routine P7
 3000     CALL PLOTC(TITLE,P,WF,EL,ED,EW,CT,E,PR,CX,CY,CZ,
     #            VP,VT,VR,SF,ND,NE,NEL,NG,I1,IJOB,IPLOT)
 4000 CONTINUE
      STOP
 5000 FORMAT(4I5)
 5005 FORMAT(I5,3F9.2,F9.5)
 5012 FORMAT(12I5)
 5020 FORMAT(20I5)
 5030 FORMAT(10F7.2)
 5040 FORMAT(3D16.8)
 5050 FORMAT(30A4)
 5060 FORMAT(3F10.4)
 5070 FORMAT(I5,F16.2)
 5075 FORMAT(I5,3F12.3)
 5095 FORMAT(3F9.6)
 6000 FORMAT(/' ',10X,3('*** CRANK ***'))
 6010 FORMAT(' IJOB=',I5,' IPLOT=',I5)
 6020 FORMAT(' NT=',I3,' NC=',I3,' NM=',I3,
     #       ' ND=',I4,' NE=',I3)
 6030 FORMAT(' NEL=',I3,' NG=',I4,' NR=',I4,
     #       ' NN=',I6,' NWA=',I6)
 6040 FORMAT(/' Constrained DOF',8I5)
 6050 FORMAT(' E=',D16.8,' G=',D16.8/' RHO=',D16.8,
     #       ' PR=',F7.4)
 6060 FORMAT(' External Mass'/' Node    Width',
     #       8X,'ID',9X,'OD')
 6070 FORMAT(/' Non-rigid Constraints'/
     #       '  DOF          Stiffness')
 6080 FORMAT(' Web Length Modifiers: CX=',F7.4,
     #       ' CY=',F7.4,' CZ=',F7.4)
 6085 FORMAT('  DOF',5X,'Force or Torque',4X,
     #       'Stiffness (Force/Defl''n)')
 6086 FORMAT(I5,2D20.4)
 6088 FORMAT(/' Deflection due to Static Load')
 6090 FORMAT(/' Natural Frequencies (Hz)')
 6095 FORMAT(4F16.5)
 7000 FORMAT(8D12.5)
      END
```

```
      SUBROUTINE CHAIN(KE,ME,NE,N)
      REAL*8 KG,MG,KE(NE,NE),ME(NE,NE)
      INTEGER IE,JE,N,N2,I,J
      COMMON KG(200,200),MG(200,200)
      NX=NE*(N-1)/2.0+0.5
      DO 100 IE=1,NE
     I=IE+NX
     DO 100 JE=1,IE
       J=JE+NX
       KG(I,J)=KG(I,J)+KE(IE,JE)
       MG(I,J)=MG(I,J)+ME(IE,JE)
  100 CONTINUE
      RETURN
      END
C
      SUBROUTINE CIRC(D,A,IY,IZ,JX,RGY,RGZ,SK,PR)
      REAL*8 D,A,IY,IZ,JX,RGY,RGZ,SK,PR,PI
      PI=3.14159265D0
      A=PI*D**2/4.0D0
      IY=PI*D**4/64.0D0
      IZ=IY
      JX=2.0D0*IY
      RGY=D/4.0D0
      RGZ=RGY
      SK=6.D0*(1.D0+PR)/(7.D0+6.D0*PR)
      RETURN
      END
C
      SUBROUTINE CORNTR(A,D)
      REAL*8 A(12,12),D,DH
      DH=D/2.0D0
      A(4,3)=-DH*A(3,3)
      A(4,4)=A(4,4)+A(3,3)*DH**2
      A(5,4)=-DH*A(5,3)
      A(6,1)=DH*A(1,1)
      A(6,6)=A(6,6)+A(1,1)*DH**2
      A(7,6)=DH*A(7,1)
      A(9,4)=-DH*A(9,3)
      A(10,3)=DH*A(9,3)
      A(10,4)=A(10,4)-A(9,3)*DH**2
      A(10,5)=DH*A(9,5)
      A(10,9)=DH*A(9,9)
      A(10,10)=A(10,10)+A(9,9)*DH**2
      A(11,4)=-DH*A(11,3)
      A(11,10)=DH*A(11,9)
      A(12,1)=-DH*A(7,1)
      A(12,6)=A(12,6)-A(7,1)*DH**2
      A(12,7)=-DH*A(7,7)
      A(12,12)=A(12,12)+A(7,7)*DH**2
      RETURN
      END
C
      SUBROUTINE COTRAN(A,C2,C3,C4)
      REAL*8 A(12,12),T(12,12),X(12,12)
```

```
      REAL*8 C2,C3,C4,PD,TH,FI,PS
      PD=3.14159265D0/180.0D0
      TH=PD*C2
      FI=PD*C3
      PS=PD*C4
      DO 100 I=1,12
      DO 100 J=1,12
     T(I,J)=0.0D0
  100 CONTINUE
      T(1,1)=DCOS(FI)*DCOS(PS)
      T(1,2)=DSIN(TH)*DSIN(FI)*DCOS(PS)+DCOS(TH)*DSIN(PS)
      T(1,3)=DSIN(TH)*DSIN(PS)-DCOS(TH)*DSIN(FI)*DCOS(PS)
      T(2,1)=-DCOS(FI)*DSIN(PS)
      T(2,2)=DCOS(TH)*DCOS(PS)-DSIN(TH)*DSIN(FI)*DSIN(PS)
      T(2,3)=DCOS(TH)*DSIN(FI)*DSIN(PS)+DSIN(TH)*DCOS(PS)
      T(3,1)=DSIN(FI)
      T(3,2)=-DSIN(TH)*DCOS(FI)
      T(3,3)=DCOS(TH)*DCOS(FI)
C
      DO 200 K=3,9,3
      DO 200 I=1,3
      DO 200 J=1,3
     T(I+K,J+K)=T(I,J)
  200 CONTINUE
      DO 300 I=1,12
      DO 300 J=1,12
     X(I,J)=0.0D0
     DO 300 K=1,12
       X(I,J)=X(I,J)+T(K,I)*A(K,J)
  300 CONTINUE
      DO 400 I=1,12
      DO 400 J=1,12
     A(I,J)=0.0D0
     DO 400 K=1,12
       A(I,J)=A(I,J)+X(I,K)*T(K,J)
  400 CONTINUE
      RETURN
      END
C
      SUBROUTINE ELKM(KE,ME,L,D,W,E,G,RHO,PR,CTM,IJOB)
      REAL*8 KE(12,12),ME(12,12),L,D,W,E,G,RHO,SK
      REAL*8 A,JX,IY,IZ,P,PY,PZ,FY,FZ,GY,GZ,HY,HZ
      REAL*8 RGY,RGZ,X(20),PR,DSQRT,CTM,JXM,JXS
C
      IF (W) 150,160,170
  150 CALL HOLLOW(D,W,A,IY,IZ,JX,RGY,RGZ,SK,PR)
      GOTO 180
  160 CALL CIRC(D,A,IY,IZ,JX,RGY,RGZ,SK,PR)
      GOTO 180
  170 CALL RECT(D,W,A,IY,IZ,JXM,JXS,RGY,RGZ,SK,PR)
  180 CONTINUE
C
C     Transverse Shear effect may be eliminated by
C     zeroing PY and PZ in the stiffness and mass matrix.
```

```
C     Rotary Inertia effect may be eliminated by
C     zeroing HY and HZ in the mass matrix.
C
      PY=12.0D0*E*IZ/(G*SK*A*L**2)
C     PY=0.D0
      PZ=PY*IY/IZ
      FY=E*IZ/((1.0D0+PY)*L**3)
      FZ=E*IY/((1.0D0+PZ)*L**3)
      GY=RHO*A*L/(1.0D0+PY)**2
      GZ=RHO*A*L/(1.0D0+PZ)**2
      HY=GY*(RGY/L)**2
      HZ=GZ*(RGZ/L)**2
C      HY=0.D0
C      HZ=0.D0
C
      DO 200 I=1,12
      DO 200 J=1,I
     KE(I,J)=0.0D0
     ME(I,J)=0.0D0
  200 CONTINUE
C     Element stiffness matrix
C
      IF (W.GT.0.0D0) JX=JXS
      KE(1,1)=A*E/L
      KE(7,1)=-KE(1,1)
      KE(7,7)=KE(1,1)
      KE(4,4)=G*JX/L
      KE(10,4)=-KE(4,4)
      KE(10,10)=KE(4,4)
      KE(2,2)=FY*12.0D0
      KE(6,2)=FY*6.0D0*L
      KE(6,6)=FY*(4.0D0+PY)*L**2
      KE(8,2)=-KE(2,2)
      KE(8,6)=-KE(6,2)
      KE(8,8)=KE(2,2)
      KE(12,2)=KE(6,2)
      KE(12,6)=FY*(2.0D0-PY)*L**2
      KE(12,8)=-KE(6,2)
      KE(12,12)=KE(6,6)
      KE(3,3)=FZ*12.0D0
      KE(5,3)=-FZ*6.0D0*L
      KE(5,5)=FZ*(4.0D0+PZ)*L**2
      KE(9,3)=-KE(3,3)
      KE(9,5)=-KE(5,3)
      KE(9,9)=KE(3,3)
      KE(11,3)=KE(5,3)
      KE(11,5)=FZ*(2.0D0-PZ)*L**2
      KE(11,9)=-KE(5,3)
      KE(11,11)=KE(5,5)
      IF (IJOB.LT.0) GOTO 375
C
C     Element mass matrix
C
      P=PY
```

```
      DO 300 I=1,2
     X(10*I-9)=13.D0/35.D0+.7D0*P+P**2/3.D0
     X(10*I-8)=(11.D0/210.D0+11.D0*P/120.D0+
     #          P**2/24.D0)*L
     X(10*I-7)=9.D0/70.D0+.3D0*P+P**2/6.D0
     X(10*I-6)=-(13.D0/420.D0+3.D0*P/40.D0+
     #           P**2/24.D0)*L
     X(10*I-5)=(1.D0/105.D0+P/60.D0+P**2/120.D0)*L**2
     X(10*I-4)=-(1.D0/140.D0+P/60.D0+P**2/120.D0)*L**2
     X(10*I-3)=1.2D0
     X(10*I-2)=(.1D0-P/2.D0)*L
     X(10*I-1)=(2.D0/15.D0+P/6.D0+P**2/3.D0)*L**2
     X(10*I)=(-1.D0/30.D0-P/6.D0+P**2/6.D0)*L**2
     P=PZ
300  CONTINUE
      IF (W.GT.0.0D0) JX=JXM
      ME(1,1)=RHO*A*L/3.0D0
      ME(7,1)=0.5D0*ME(1,1)
      ME(7,7)=ME(1,1)
      ME(4,4)=RHO*JX*L/3.0D0
      ME(10,4)=0.5D0*ME(4,4)
      ME(10,10)=ME(4,4)
      ME(2,2)=GY*X(1)+HY*X(7)
      ME(6,2)=GY*X(2)+HY*X(8)
      ME(6,6)=GY*X(5)+HY*X(9)
      ME(8,2)=GY*X(3)-HY*X(7)
      ME(8,6)=-GY*X(4)-HY*X(8)
      ME(8,8)=ME(2,2)
      ME(12,2)=-ME(8,6)
      ME(12,6)=GY*X(6)+HY*X(10)
      ME(12,8)=-ME(6,2)
      ME(12,12)=ME(6,6)
      ME(3,3)=GZ*X(11)+HZ*X(17)
      ME(5,3)=-GZ*X(12)-HZ*X(18)
      ME(5,5)=GZ*X(15)+HZ*X(19)
      ME(9,3)=GZ*X(13)-HZ*X(17)
      ME(9,5)=GZ*X(14)+HZ*X(18)
      ME(9,9)=ME(3,3)
      ME(11,3)=-ME(9,5)
      ME(11,5)=GZ*X(16)+HZ*X(20)
      ME(11,9)=-ME(5,3)
      ME(11,11)=ME(5,5)
375  CONTINUE
      IF (CTM .LT. 2.0D0) GOTO 350
     CALL CORNTR(KE,D)
     IF (IJOB.LT.0) GOTO 350
     CALL CORNTR(ME,D)
350  CONTINUE
      IF (CTM.LE.0.0D0) GOTO 500
      DO 400 I=1,11
     II=I+1
     DO 400 J=II,12
       KE(I,J)=KE(J,I)
       ME(I,J)=ME(J,I)
```

```
  400 CONTINUE
  500 CONTINUE
      RETURN
      END
C
      SUBROUTINE EXPMOD(A,C,ND,NP,NC,NG)
      REAL*8 A(ND,NP),DABS
      INTEGER C(NC),M,L,IR,NG
      M=0
      L=NC
      DO 100 I=1,NG
     IR=NG-I+1
     IF (C(L+M).EQ.IR) GOTO 150
     DO 110 J=1,NP
       IF (DABS(A(IR-L,J)).LT.1.0D-10) A(IR-L,J)=0.0D0
       A(IR,J)=A(IR-L,J)
  110   CONTINUE
      GOTO 100
  150   DO 160 J=1,NP
       A(IR,J)=0.0D0
  160   CONTINUE
     L=L-1
     IF (L.EQ.0) M=1
  100 CONTINUE
      RETURN
      END
C
      SUBROUTINE EXPV(A,C,NG,NC)
      REAL*8 A(NG),DABS
      INTEGER C(NC),L,M,IR
      L=NC
      M=0
      DO 100 I=1,NG
     IR=NG-I+1
     IF (C(L+M).EQ.IR) GOTO 150
     IF (DABS(A(IR-L)).LT.1.0D-10) A(IR-L)=0.0D0
     A(IR)=A(IR-L)
      GOTO 100
  150   A(IR)=0.0D0
     L=L-1
     IF (L.EQ.0) M=1
  100 CONTINUE
      RETURN
      END
C
      SUBROUTINE HOLLOW(DO,DI,A,IY,IZ,JX,RGY,RGZ,SK,PR)
      REAL*8 DO,DI,A,IY,IZ,JX,RGY,RGZ,SK,PR,PI,DSQRT,X
      PI=3.14159265D0
      X=DI/DO
      A=PI*(DO**2-DI**2)/4.0D0
      IY=PI*(DO**4-DI**4)/64.0D0
      IZ=IY
      JX=2.0D0*IY
      RGY=DSQRT(IY/A)
```

```
      RGZ=RGY
      SK=6.D0*(1.D0+PR)*(1.D0+X**2)**2/((7.D0+6.D0*PR)*
     #   (1.D0+X**2)**2+(20.D0+12.D0*PR)*X**2)
      RETURN
      END
C
      SUBROUTINE RECT(D,W,A,IY,IZ,JXM,JXS,RGY,RGZ,SK,PR)
      REAL*8 A,IZ,IY,D,W,B,T,RGY,RGZ,SK,PR,DMAX1,DMIN1
      REAL*8 DSQRT,JXM,JXS
      B=DMAX1(D,W)
      T=DMIN1(D,W)
      A=D*W
      IZ=W*D**3/12.0D0
      IY=D*W**3/12.0D0
C     Formula For 2nd Moment Of Area From STICKLER
      JXS=B*T**3/(3.D0+1.39D0/(B/T)+2.7D0/(B/T)**2)
      JXM=D*W*(D**2+W**2)/12.D0
      RGY=D/DSQRT(12.0D0)
      RGZ=W/DSQRT(12.0D0)
      SK=10.D0*(1.D0+PR)/(12.D0+11.D0*PR)
      RETURN
      END
C
      SUBROUTINE REDM(C,NG,NC)
      REAL*8 KG,MG
      INTEGER C(NC),K,L,M,N
      COMMON KG(200,200),MG(200,200)
      K=1
      M=0
      DO 100 I=1,NG
    IF (C(K-M)-I)10,20,10
 20   K=K+1
    IF (K.GT.NC) M=1
    GO TO 100
 10   L=1
    N=0
    DO 200 J=1,I
      IF (C(L-N)-J)50,60,50
 60     L=L+1
      IF (L.GT.NC) N=1
      GO TO 200
 50     CONTINUE
      KG(I-K+1,J-L+1)=KG(I,J)
      MG(I-K+1,J-L+1)=MG(I,J)
200   CONTINUE
100 CONTINUE
      RETURN
      END
C
      SUBROUTINE REDV(A,C,NG,NC)
      REAL*8 A(NG)
      INTEGER C(NC),L,M
      L=1
      M=0
```

```
      DO 100 I=1,NG
     IF (C(L-M).EQ.I) GOTO 150
     A(I-L+1)=A(I)
      GOTO 100
  150  L=L+1
     IF (L.GT.NC) M=1
  100 CONTINUE
      II=NG-NC+1
      DO 200 I=II,NG
     A(I)=0.0D0
  200 CONTINUE
      RETURN
      END
C
      SUBROUTINE SSM(KK,MM,NR,NN)
      REAL*8 KG,MG,KK(NN),MM(NN)
      INTEGER K,NR
      COMMON KG(200,200),MG(200,200)
      DO 100 I=1,NR
     K=I*(I-1)/2.0+0.5
     DO 100 J=1,I
       KK(J+K)=KG(I,J)
       MM(J+K)=MG(I,J)
  100 CONTINUE
      RETURN
      END
C
      SUBROUTINE WEB(KE,ME,L,D,W,D1,D2,CX,CY,CZ,
     #               E,G,RHO,PR,IJOB)
      REAL*8 KE(12,12),ME(12,12),L,D,W,E,G,RHO,RGY,RGZ
      REAL*8 A,IY,IZ,P,PY,PZ,FY,FZ,GY,GZ,HY,HZ,PR,DSQRT
      REAL*8 D1,D2,CX,CY,CZ,X1,X2,X3,JXM,JXS,X(20),SK
C
      CALL RECT(D,W,A,IY,IZ,JXM,JXS,RGY,RGZ,SK,PR)
C
      X1=L-(D1+D2)*CX
      X2=L-(D1+D2)*CY
      X3=L-(D1+D2)*CZ
C
C     Transverse Shear effect may be eliminated by
C     zeroing PY and PZ in the stiffness and mass
C     matrix. Rotary Inertia effect may be eliminated
C     by zeroing HY and HZ in the mass matrix.
C
      PY=12.0D0*E*IZ/(G*SK*A*X3**2*(1.D0-PR**2))
      PZ=12.0D0*E*IY/(G*SK*A*X2**2)
C     PY=0.D0
C     PZ=0.D0
      FY=E*IZ/((1.D0-PR**2)*(1.0D0+PY)*X3**3)
      FZ=E*IY/((1.0D0+PZ)*X2**3)
C
      DO 200 I=1,12
      DO 200 J=1,I
     KE(I,J)=0.0D0
```

```
      ME(I,J)=0.0D0
  200 CONTINUE
C     Element stiffness matrix
C
      KE(1,1)=A*E/L
      KE(7,1)=-KE(1,1)
      KE(7,7)=KE(1,1)
      KE(4,4)=G*JXS/X1
      KE(10,4)=-KE(4,4)
      KE(10,10)=KE(4,4)
      KE(2,2)=FY*12.0D0
      KE(6,2)=FY*6.0D0*X3
      KE(6,6)=FY*(4.0D0+PY)*X3**2
      KE(8,2)=-KE(2,2)
      KE(8,6)=-KE(6,2)
      KE(8,8)=KE(2,2)
      KE(12,2)=KE(6,2)
      KE(12,6)=FY*(2.0D0-PY)*X3**2
      KE(12,8)=-KE(6,2)
      KE(12,12)=KE(6,6)
      KE(3,3)=FZ*12.0D0
      KE(5,3)=-FZ*6.0D0*X2
      KE(5,5)=FZ*(4.0D0+PZ)*X2**2
      KE(9,3)=-KE(3,3)
      KE(9,5)=-KE(5,3)
      KE(9,9)=KE(3,3)
      KE(11,3)=KE(5,3)
      KE(11,5)=FZ*(2.0D0-PZ)*X2**2
      KE(11,9)=-KE(5,3)
      KE(11,11)=KE(5,5)
      IF (IJOB.LT.0) GOTO 375
C
C     Element mass matrix
C
      PY=12.0D0*E*IZ/(G*SK*A*L**2*(1.D0-PR**2))
      PZ=12.0D0*E*IY/(G*SK*A*L**2)
C     PY=0.D0
C     PZ=0.D0
      GY=RHO*A*L/(1.0D0+PY)**2
      GZ=RHO*A*L/(1.0D0+PZ)**2
      HY=GY*(RGY/L)**2
      HZ=GZ*(RGZ/L)**2
C      HY=0.D0
C      HZ=0.D0
      P=PY
      DO 300 I=1,2
     X(10*I-9)=13.D0/35.D0+.7D0*P+P**2/3.D0
     X(10*I-8)=(11.D0/210.D0+11.D0*P/120.D0+
     #          P**2/24.D0)*L
     X(10*I-7)=9.D0/70.D0+.3D0*P+P**2/6.D0
     X(10*I-6)=-(13.D0/420.D0+3.D0*P/40.D0+
     #           P**2/24.D0)*L
     X(10*I-5)=(1.D0/105.D0+P/60.D0+P**2/120.D0)*L**2
     X(10*I-4)=-(1.D0/140.D0+P/60.D0+P**2/120.D0)*L**2
```

```
      X(10*I-3)=1.2D0
      X(10*I-2)=(.1D0-P/2.D0)*L
      X(10*I-1)=(2.D0/15.D0+P/6.D0+P**2/3.D0)*L**2
      X(10*I)=(-1.D0/30.D0-P/6.D0+P**2/6.D0)*L**2
      P=PZ
  300 CONTINUE
       ME(1,1)=RHO*A*L/3.0D0
       ME(7,1)=0.5D0*ME(1,1)
       ME(7,7)=ME(1,1)
       ME(4,4)=RHO*JXM*L/3.0D0
       ME(10,4)=0.5D0*ME(4,4)
       ME(10,10)=ME(4,4)
       ME(2,2)=GY*X(1)+HY*X(7)
       ME(6,2)=GY*X(2)+HY*X(8)
       ME(6,6)=GY*X(5)+HY*X(9)
       ME(8,2)=GY*X(3)-HY*X(7)
       ME(8,6)=-GY*X(4)-HY*X(8)
       ME(8,8)=ME(2,2)
       ME(12,2)=-ME(8,6)
       ME(12,6)=GY*X(6)+HY*X(10)
       ME(12,8)=-ME(6,2)
       ME(12,12)=ME(6,6)
       ME(3,3)=GZ*X(11)+HZ*X(17)
       ME(5,3)=-GZ*X(12)-HZ*X(18)
       ME(5,5)=GZ*X(15)+HZ*X(19)
       ME(9,3)=GZ*X(13)-HZ*X(17)
       ME(9,5)=GZ*X(14)+HZ*X(18)
       ME(9,9)=ME(3,3)
       ME(11,3)=-ME(9,5)
       ME(11,5)=GZ*X(16)+HZ*X(20)
       ME(11,9)=-ME(5,3)
       ME(11,11)=ME(5,5)
  375 CONTINUE
      CALL CORNTR(KE,D)
       IF (IJOB.LT.0) GOTO 350
      CALL CORNTR(ME,D)
  350 CONTINUE
       DO 400 I=1,11
      II=I+1
      DO 400 J=II,12
        KE(I,J)=KE(J,I)
        ME(I,J)=ME(J,I)
  400 CONTINUE
       RETURN
       END
C
       SUBROUTINE ATHROW(EL,ED,EW,CT,NE,TA,E,G,RHO,PR,
      #                  CX,CY,CZ,IJOB,IEL,N)
       REAL*8 KG,MG,EL(NE),ED(NE),EW(NE),CT(NE,4)
       REAL*8 KE(12,12),ME(12,12),TA(20),E,G,RHO,PR,XJ
       REAL*8 ANG,CL,CR,DC,DJ,PL,SP,WT,WW,A(8),ALF,WL
       REAL*8 CM(4,7),M,IX,IY,IZ,XG,YG,ZG
       REAL*8 CX,CY,CZ,DSQRT,S,BE,GA,H
       INTEGER N,IEL,IJOB
```

```
      COMMON KG(200,200),MG(200,200)
C     Read In
      READ(5,5000)CL,CR,DC,DJ,PL,SP,WT,WW
      READ(5,5020)((CM(I,J),J=1,7),I=1,4)
C     Echo Check
      WRITE(6,6000)
      WRITE(6,6010)N,TA(N)
      WRITE(6,6020)
      WRITE(6,6070)CL,CR,DC,DJ
      WRITE(6,6022)
      WRITE(6,6070)PL,SP,WT,WW
      WRITE(6,6040)
      DO 60 I=1,4
     II=IEL+I+1
     WRITE(6,6045)II,(CM(I,J),J=1,4)
   60 CONTINUE
      WRITE(6,6042)
      DO 65 I=1,4
     II=IEL+I+1
     WRITE(6,6047)II,(CM(I,J),J=5,7)
   65 CONTINUE
C     Calculations
      XJ=0.5D0*(CL-SP)
      S=0.5D0*(SP-PL)
      H=DSQRT(CR**2+S**2)
      GA=DATAN(S/CR)
      BE=DARSIN(WT/H)
      WL=H*DCOS(BE)
      ALF=GA-BE
      IF (WT.GT.S) WT=S
      A(1)=CL/CR
      A(2)=DC/CR
      A(3)=DJ/CR
      A(4)=PL/CR
      A(5)=SP/CR
      A(6)=WT/CR
      A(7)=WW/CR
      A(8)=ALF*180.0D0/3.14159265D0
      WRITE(6,6050)
      WRITE(6,6060)
      WRITE(6,6070)(A(I),I=1,4)
      WRITE(6,6062)
      WRITE(6,6070)(A(I),I=5,8)
C     Form Geometry Arrays For Plotting
      EL(IEL+1)=XJ
      EL(IEL+2)=WL
      EL(IEL+3)=PL
      EL(IEL+4)=WL
      EL(IEL+5)=XJ
      ED(IEL+1)=DJ
      ED(IEL+2)=WT
      ED(IEL+3)=DC
      ED(IEL+4)=WT
      ED(IEL+5)=DJ
```

```
      EW(IEL+2)=WW
      EW(IEL+4)=WW
      CT(IEL+2,1)=2.0D0
      CT(IEL+2,2)=TA(N)
      CT(IEL+2,4)=90.0D0-A(8)
      CT(IEL+4,1)=2.0D0
      CT(IEL+4,2)=TA(N)+180.0D0
      CT(IEL+4,4)=90.0D0-A(8)
C     Assemble Journals
      CALL ELKM(KE,ME,XJ,DJ,0.D0,E,G,RHO,PR,0.D0,IJOB)
      CALL CHAIN(KE,ME,12,IEL+1)
      CALL CHAIN(KE,ME,12,IEL+5)
C     Assemble Crankpins
      CALL ELKM(KE,ME,PL,DC,0.D0,E,G,RHO,PR,0.D0,IJOB)
      CALL CHAIN(KE,ME,12,IEL+3)
C     Assemble Webs
      CALL WEB(KE,ME,WL,WT,WW,DJ,DC,CX,CY,CZ,E,G,RHO,
     #         PR,IJOB)
      ANG=90.0D0-A(8)
      CALL COTRAN(KE,TA(N),0.0D0,ANG)
      CALL COTRAN(ME,TA(N),0.0D0,ANG)
      CALL CHAIN(KE,ME,12,IEL+2)
C     Transform Webs By 180 degrees
      DO 50 I=1,10,3
      DO 50 J=2,11,3
     KE(I,J)=-KE(I,J)
     ME(I,J)=-ME(I,J)
     KE(I,J+1)=-KE(I,J+1)
     ME(I,J+1)=-ME(I,J+1)
     KE(J,I)=-KE(J,I)
     ME(J,I)=-ME(J,I)
     KE(J+1,I)=-KE(J+1,I)
     ME(J+1,I)=-ME(J+1,I)
   50 CONTINUE
      CALL CHAIN(KE,ME,12,IEL+4)
C     Add Mass And Inertia of "Extra-Element" Mass to MG
      DO 100 II=1,4
     I=6*(IEL+II)
     M=CM(II,1)
     IX=CM(II,2)
     IY=CM(II,3)
     IZ=CM(II,4)
     XG=CM(II,5)
     YG=CM(II,6)
     ZG=CM(II,7)
     MG(I+1,I+1)=MG(I+1,I+1)+M
     MG(I+2,I+2)=MG(I+2,I+2)+M
     MG(I+3,I+3)=MG(I+3,I+3)+M
     MG(I+4,I+4)=MG(I+4,I+4)+IX+M*(YG**2+ZG**2)
     MG(I+5,I+5)=MG(I+5,I+5)+IY+M*(XG**2+ZG**2)
     MG(I+6,I+6)=MG(I+6,I+6)+IZ+M*(XG**2+YG**2)
     MG(I+4,I+3)=MG(I+4,I+3)+M*YG
     MG(I+5,I+3)=MG(I+5,I+3)-M*XG
     MG(I+5,I+4)=MG(I+5,I+4)-M*XG*YG
```

```
      MG(I+6,I+1)=MG(I+6,I+1)-M*YG
      MG(I+6,I+2)=MG(I+6,I+2)+M*XG
  100 CONTINUE
      IEL=IEL+5
      RETURN
 5000 FORMAT(8F10.4)
 5010 FORMAT(4F10.4)
 5020 FORMAT(7D12.4)
 6000 FORMAT(/' ',10('------'))
 6010 FORMAT(' Throw',I5,' Type A   Having Throw Angle',
     #       ' of',F8.2)
 6020 FORMAT(' ',4X,'CL',8X,'CR',8X,'DC',8X,'DJ')
 6022 FORMAT(' ',4X,'PL',8X,'SP',8X,'WT',8X,'WW')
 6040 FORMAT(/' ',14X,'"Extra - Element" Mass Data'/
     #       ' ',22X,'Inertia About Mass Center'/
     #       ' Node',5X,'Mass',9X,'Ixx',9X,'Iyy',9X,'Izz')
 6042 FORMAT(' ',6X,'Mass Center Coordinates'/
     #       ' ',8X,'Xg',7X,'Yg',7X,'Zg')
 6045 FORMAT(I5,4D12.4)
 6047 FORMAT(I5,3F9.4)
 6050 FORMAT(/' Non-dimensional Parameters')
 6060 FORMAT('    CL/CR     DC/CR     DJ/CR     PL/CR')
 6062 FORMAT('    SP/CR     WT/CR     WW/CR  Web Angle',
     #       '(deg)')
 6070 FORMAT(4F10.5)
      END
C
      SUBROUTINE DTHROW(EL,ED,EW,CT,NE,TA,E,G,RHO,PR,
     #                  CX,CY,CZ,IJOB,IEL,N)
      REAL*8 KG,MG,EL(NE),ED(NE),EW(NE),CT(NE,4)
      REAL*8 KE(12,12),ME(12,12),TA(20),E,G,RHO,PR,XJ,SL
      REAL*8 CL,CR,DC,DJ,PL,SP,ST,SW,WT,WW,A(10),ANG
      REAL*8 CM(6,7),M,IX,IY,IZ,XG,YG,ZG
      REAL*8 CX,CY,CZ,DSQRT,S,H,BE,GA,ALF
      INTEGER NTYP(20),N,IEL,IJOB
      COMMON KG(200,200),MG(200,200)
C     Read In
      READ(5,5000)CL,CR,DC,DJ,PL
      READ(5,5000)SP,ST,SW,WT,WW
      READ(5,5020)((CM(I,J),J=1,7),I=1,6)
C     Echo Check
      WRITE(6,6000)
      WRITE(6,6010)N,TA(N)
      WRITE(6,6020)
      WRITE(6,5000)CL,CR,DC,DJ,PL
      WRITE(6,6030)
      WRITE(6,5000)SP,ST,SW,WT,WW
      WRITE(6,6040)
      DO 50 I=1,6
      II=IEL+I+1
      WRITE(6,6045)II,(CM(I,J),J=1,4)
   50 CONTINUE
      WRITE(6,6042)
      DO 55 I=1,6
```

```
      II=IEL+I+1
      WRITE(6,6047)II,(CM(I,J),J=5,7)
   55 CONTINUE
C     Calculations
      XJ=0.5D0*(CL-SP)
      S=SP-2.0D0*(PL+WT)
      H=DSQRT(S**2+4.0D0*CR**2)
      GA=DATAN(0.5D0*S/CR)
      BE=DARSIN(ST/H)
      SL=H*DCOS(BE)
      ALF=GA-BE
      IF (ST.GT.S) ST=S
      A(1)=CL/CR
      A(2)=DC/CR
      A(3)=DJ/CR
      A(4)=PL/CR
      A(5)=SP/CR
      A(6)=ST/CR
      A(7)=SW/CR
      A(8)=WT/CR
      A(9)=WW/CR
      A(10)=ALF*180.0D0/3.14159265D0
      WRITE(6,6050)
      WRITE(6,6060)
      WRITE(6,5000)(A(I),I=1,5)
      WRITE(6,6070)
      WRITE(6,5000)(A(I),I=6,10)
C     Form Geometry Arrays For Plotting
      EL(IEL+1)=XJ
      EL(IEL+2)=CR
      EL(IEL+3)=PL
      EL(IEL+4)=SL
      EL(IEL+5)=PL
      EL(IEL+6)=CR
      EL(IEL+7)=XJ
      ED(IEL+1)=DJ
      ED(IEL+2)=WT
      ED(IEL+3)=DC
      ED(IEL+4)=ST
      ED(IEL+5)=DC
      ED(IEL+6)=WT
      ED(IEL+7)=DJ
      EW(IEL+2)=WW
      EW(IEL+4)=SW
      EW(IEL+6)=WW
      CT(IEL+2,1)=2.0D0
      CT(IEL+2,2)=TA(N)
      CT(IEL+2,4)=90.D0
      CT(IEL+4,1)=2.0D0
      CT(IEL+4,2)=TA(N)+180.0D0
      CT(IEL+4,4)=90.0D0-A(10)
      CT(IEL+6,1)=2.D0
      CT(IEL+6,2)=TA(N)
      CT(IEL+6,4)=90.D0
```

```
C     Assemble Journals
      CALL ELKM(KE,ME,XJ,DJ,0.D0,E,G,RHO,PR,0.D0,IJOB)
      CALL CHAIN(KE,ME,12,IEL+1)
      CALL CHAIN(KE,ME,12,IEL+7)
C     Assemble Crankpins
      CALL ELKM(KE,ME,PL,DC,0.D0,E,G,RHO,PR,0.D0,IJOB)
      CALL CHAIN(KE,ME,12,IEL+3)
      CALL CHAIN(KE,ME,12,IEL+5)
C     Assemble Webs
      CALL WEB(KE,ME,CR,WT,WW,DJ,DC,CX,CY,CZ,E,G,RHO,
     #         PR,IJOB)
      CALL COTRAN(KE,TA(N),0.0D0,90.0D0)
      CALL COTRAN(ME,TA(N),0.0D0,90.0D0)
      CALL CHAIN(KE,ME,12,IEL+2)
      CALL CHAIN(KE,ME,12,IEL+6)
      CALL WEB(KE,ME,SL,ST,SW,DC,DC,CX,CY,CZ,E,G,RHO,
     #         PR,IJOB)
      ANG=90.0D0-A(10)
      CALL COTRAN(KE,TA(N)+180.0D0,0.0D0,ANG)
      CALL COTRAN(ME,TA(N)+180.0D0,0.0D0,ANG)
      CALL CHAIN(KE,ME,12,IEL+4)
C     Add Mass And Inertia of "Extra-Element" Mass to MG
      DO 100 II=1,6
     I=6*(IEL+II)
     M=CM(II,1)
     IX=CM(II,2)
     IY=CM(II,3)
     IZ=CM(II,4)
     XG=CM(II,5)
     YG=CM(II,6)
     ZG=CM(II,7)
     MG(I+1,I+1)=MG(I+1,I+1)+M
     MG(I+2,I+2)=MG(I+2,I+2)+M
     MG(I+3,I+3)=MG(I+3,I+3)+M
     MG(I+4,I+4)=MG(I+4,I+4)+IX+M*(YG**2+ZG**2)
     MG(I+5,I+5)=MG(I+5,I+5)+IY+M*(XG**2+ZG**2)
     MG(I+6,I+6)=MG(I+6,I+6)+IZ+M*(XG**2+YG**2)
     MG(I+4,I+3)=MG(I+4,I+3)+M*YG
     MG(I+5,I+3)=MG(I+5,I+3)-M*XG
     MG(I+5,I+4)=MG(I+5,I+4)-M*XG*YG
     MG(I+6,I+1)=MG(I+6,I+1)-M*YG
     MG(I+6,I+2)=MG(I+6,I+2)+M*XG
  100 CONTINUE
      IEL=IEL+7
      RETURN
 5000 FORMAT(5F10.4)
 5010 FORMAT(4F10.4)
 5015 FORMAT(6F10.4)
 5020 FORMAT(7D12.4)
 6000 FORMAT(/' ',10('------'))
 6010 FORMAT(' Throw',I5,' Type D   Having Throw Angle',
     #       ' Of',F8.2)
 6020 FORMAT(' ',4X,'CL',8X,'CR',8X,'DC',8X,'DJ',8X,'PL')
 6030 FORMAT(' ',4X,'SP',8X,'ST',8X,'SW',8X,'WT',8X,'WW')
```

```
 6040 FORMAT(/' ',14X,'"Extra - Element" Mass Data'/
     #       ' ',22X,'Inertia About Mass Center'/
     #       ' Node',5X,'Mass',9X,'Ixx',9X,'Iyy',9X,'Izz')
 6042 FORMAT(' ',6X,'Mass Center Coordinates'/
     #       ' ',8X,'Xg',7X,'Yg',7X,'Zg')
 6045 FORMAT(I5,4D12.4)
 6047 FORMAT(I5,3F9.4)
 6050 FORMAT(/' Non-dimensional Parameters')
 6060 FORMAT('    CL/CR     DC/CR     DJ/CR     SP/CR',
     #       '     WT/CR')
 6070 FORMAT('    ST/CR     SW/CR     WT/CR     WW/CR',
     #       '   Web Ang')
      END
C
      SUBROUTINE ETHROW(EL,ED,NE,E,G,RHO,PR,IJOB,IEL,N)
      REAL*8 KG,MG,EL(NE),ED(NE),E,G,RHO,PR
      REAL*8 KE(12,12),ME(12,12),XL,XD
      INTEGER IJOB,IEL,N
      COMMON KG(200,200),MG(200,200)
      READ(5,5000)XL,XD
      WRITE(6,6000)
      WRITE(6,6010)N,XL,XD
      IEL=IEL+1
      EL(IEL)=XL
      ED(IEL)=XD
      CALL ELKM(KE,ME,XL,XD,0.D0,E,G,RHO,PR,0.D0,IJOB)
      CALL CHAIN(KE,ME,12,IEL)
      RETURN
 5000 FORMAT(2F10.4)
 6000 FORMAT(/' ',10('------'))
 6010 FORMAT(' Throw',I5,' Type E   Length=',F10.4,
     #       ' Diameter=',F10.4)
      END
C
C     PREPARES DATA FOR "P7" FOR 3-D PLOT OF DEFORMATIONS
C     Note that rectangular sections will include
C     plate rigidity.
      SUBROUTINE PLOTC(TITLE,P,WF,EL,ED,EW,CT,E,PR,
     #  CX,CY,CZ,VP,VT,VR,SF,ND,NE,NEL,NG,I1,IJOB,IPLOT)
      REAL*8 EL(NEL),ED(NEL),EW(NEL),E,G,PR,DFLOAT
      REAL*8 CT(NE,4),BY,BZ,HY(4,4),HZ(4,4),H(3,12)
      REAL*8 A,IY,IZ,JX,JXM,JXS,SK,RGY,RGZ,V,D1,XL
      REAL*8 WF(NG),P(ND,IPLOT),CX,CY,CZ,XPLATE,F(4)
      REAL*4 SF,RD,RL,THT,PHI,PSI,VT,VP,VR,CTM,DC(3,3)
      REAL*4 EX(12),EXA(12),T(12,12)
      REAL*4 XN(50,9),YN(50,9),ZN(50,9),B
      REAL*4 XE(50,9),YE(50,9),ZE(50,9),XG(50,9),YG(50,9)
      REAL*4 ZG(50,9),AP(50,3),FREQ
      REAL*4 X1,Y1,Z1,TITLE(30)
      INTEGER NGE(50,12),NUM(50,2),IJOB,II,I1,N1,N2
      II=0
      DO 20 I=1,NEL
     NUM(I,1)=I
     NUM(I,2)=I+1
```

```
   20 CONTINUE
      DO 30 I=1,NEL
     DO 60 J=1,12
       NGE(I,J)=II+J
   60   CONTINUE
     II=II+6
   30 CONTINUE
      DO 5 J=1,3
    5   AP(NUM(1,1),J)=0.0
      DO 10 I=1,12
      DO 10 J=1,12
     T(I,J)=0.0
   10 CONTINUE
      DO 12 I=1,12
     T(I,I)=1.0
   12 CONTINUE
      G=E/(2.D0*(1.D0+PR))
      RL=0.0
      DO 14 I=1,NEL
   14   RL=RL+EL(I)
      RL=RL/FLOAT(NEL)
      SF=SF*RL
      RD=3.141593/180.0
C
      I=IPLOT-I1+1
      WRITE(7,6000)TITLE
      WRITE(7,69) I
      IF (IJOB) 3010,3000,3030
 3010 FREQ=-1.0
      II=1
      DO 3015 I=1,NG
     P(I,1)=WF(I)
 3015 CONTINUE
      GOTO 3020
 3030 DO 3000 II=I1,IPLOT
     FREQ=WF(II)
 3020 CONTINUE
C
      DO 1000 I=1,NEL
     CTM=CT(I,1)
     THT=CT(I,2)*RD
     PHI=CT(I,3)*RD
     PSI=CT(I,4)*RD
     DC(1,1)=COS(PHI)*COS(PSI)
     DC(1,2)=SIN(THT)*SIN(PHI)*COS(PSI)+
     #          COS(THT)*SIN(PSI)
     DC(1,3)=-COS(THT)*SIN(PHI)*COS(PSI)+
     #           SIN(THT)*SIN(PSI)
     DC(2,1)=-COS(PHI)*SIN(PSI)
     DC(2,2)=-SIN(THT)*SIN(PHI)*SIN(PSI)+
     #           COS(THT)*COS(PSI)
     DC(2,3)=COS(THT)*SIN(PHI)*SIN(PSI)+
     #          SIN(THT)*COS(PSI)
     DC(3,1)=SIN(PHI)
```

```
      DC(3,2)=-SIN(THT)*COS(PHI)
      DC(3,3)=COS(THT)*COS(PHI)
      B=0.0
      IF (CTM.EQ.2.0) B=1.0
      XN(I,1)=AP(NUM(I,1),1)-.5*ED(I)*DC(2,1)*B
      YN(I,1)=AP(NUM(I,1),2)-.5*ED(I)*DC(2,2)*B
      ZN(I,1)=AP(NUM(I,1),3)-.5*ED(I)*DC(2,3)*B
      DO 90 J=2,9
        XN(I,J)=.125*FLOAT(J-1)*EL(I)*DC(1,1)+XN(I,1)
        YN(I,J)=.125*FLOAT(J-1)*EL(I)*DC(1,2)+YN(I,1)
        ZN(I,J)=.125*FLOAT(J-1)*EL(I)*DC(1,3)+ZN(I,1)
   90   CONTINUE
      AP(NUM(I,2),1)=XN(I,9)-.5*ED(I)*DC(2,1)*B
      AP(NUM(I,2),2)=YN(I,9)-.5*ED(I)*DC(2,2)*B
      AP(NUM(I,2),3)=ZN(I,9)-.5*ED(I)*DC(2,3)*B
      DO 115 J=1,12
        IF (NGE(I,J).GT.NG)EX(J)=0.0
        IF (NGE(I,J).LE.NG)EX(J)=P(NGE(I,J),II)
  115   CONTINUE
C
      IF (CTM.EQ.0.0) GOTO 120
      DO 142 I2=1,4
      DO 142 J2=1,3
        EXA(3*I2+J2-3)=DC(J2,1)*EX(3*I2-2)+
     #                 DC(J2,2)*EX(3*I2-1)+
     #                 DC(J2,3)*EX(3*I2)
  142   CONTINUE
      IF (CTM.EQ.2.0) GOTO 145
      DO 144 J=1,12
  144     EX(J)=EXA(J)
      GOTO 150
  145   T(1,6)=ED(I)/2.0
      T(3,4)=-T(1,6)
      T(7,12)=-T(1,6)
      T(9,10)=T(1,6)
      DO 146 J=1,12
        EX(J)=0.0
        DO 146 K=1,12
          EX(J)=EX(J)+T(J,K)*EXA(K)
  146     CONTINUE
  150   CONTINUE
  120   CONTINUE
C
      DO 155 J=2,8
        XE(I,J)=0.0
        YE(I,J)=0.0
        ZE(I,J)=0.0
  155   CONTINUE
      DO 160 J=1,2
        XE(I,8*J-7)=EX(6*J-5)
        YE(I,8*J-7)=EX(6*J-4)
        ZE(I,8*J-7)=EX(6*J-3)
  160   CONTINUE
C
```

```
      IF (EW(I)) 162,164,166
  162   CALL HOLLOW(ED(I),EW(I),A,IY,IZ,JX,RGY,RGZ,SK,PR)
      GOTO 168
  164   CALL CIRC(ED(I),A,IY,IZ,JX,RGY,RGZ,SK,PR)
      GOTO 168
  166   CALL RECT(ED(I),EW(I),A,IY,IZ,JXM,JXS,
     #             RGY,RGZ,SK,PR)
  168   CONTINUE
C
      XL=EL(I)
      XPLATE=1.D0
      IF (EW(I).GT.0.0D0) XPLATE=1.D0/(1.D0-PR**2)
      BY=E*XPLATE*IZ/(G*SK*A)
      BZ=E*IY/(G*SK*A)
      D1=XL**4+12.D0*BY*XL**2
      HY(1,1)=1.0D0
      HY(1,2)=0.0D0
      HY(1,3)=0.0D0
      HY(1,4)=0.0D0
      HY(2,1)=-12.D0*BY*XL/D1
      HY(2,2)=(XL**4+6.D0*BY*XL**2)/D1
      HY(2,3)=-HY(2,1)
      HY(2,4)=-6.D0*BY*XL**2/D1
      HY(3,1)=-3.D0*XL**2/D1
      HY(3,2)=-(2.D0*XL**3+6.D0*BY*XL)/D1
      HY(3,3)=-HY(3,1)
      HY(3,4)=(-XL**3+6.D0*BY*XL)/D1
      HY(4,1)=2.D0*XL/D1
      HY(4,2)=XL**2/D1
      HY(4,3)=-HY(4,1)
      HY(4,4)=HY(4,2)
      D1=XL**4+12.D0*BZ*XL**2
      HZ(1,1)=1.0D0
      HZ(1,2)=0.0D0
      HZ(1,3)=0.0D0
      HZ(1,4)=0.0D0
      HZ(2,1)=-12.D0*BZ*XL/D1
      HZ(2,2)=-(XL**4+6.D0*BZ*XL**2)/D1
      HZ(2,3)=-HZ(2,1)
      HZ(2,4)=6.D0*BZ*XL**2/D1
      HZ(3,1)=-3.D0*XL**2/D1
      HZ(3,2)=(2.D0*XL**3+6.D0*BZ*XL)/D1
      HZ(3,3)=-HZ(3,1)
      HZ(3,4)=(XL**3-6.D0*BZ*XL)/D1
      HZ(4,1)=2.D0*XL/D1
      HZ(4,2)=-XL**2/D1
      HZ(4,3)=-HZ(4,1)
      HZ(4,4)=HZ(4,2)
C
      DO 200 J=2,8
        DO 170 I2=1,3
        DO 170 J2=1,12
  170       H(I2,J2)=0.0D0
      V=0.125D0*DFLOAT(J-1)*XL
```

```
      H(1,1)=1.D0-V/XL
      H(1,7)=V/XL
      F(1)=1.0D0
      F(2)=V
      F(3)=V**2
      F(4)=V**3
      DO 175 K=1,4
        H(2,2)=H(2,2)+F(K)*HY(K,1)
        H(2,6)=H(2,6)+F(K)*HY(K,2)
        H(2,8)=H(2,8)+F(K)*HY(K,3)
        H(2,12)=H(2,12)+F(K)*HY(K,4)
        H(3,3)=H(3,3)+F(K)*HZ(K,1)
        H(3,5)=H(3,5)+F(K)*HZ(K,2)
        H(3,9)=H(3,9)+F(K)*HZ(K,3)
        H(3,11)=H(3,11)+F(K)*HZ(K,4)
  175   CONTINUE
      DO 180 J2=1,12
        XE(I,J)=XE(I,J)+H(1,J2)*EX(J2)
        YE(I,J)=YE(I,J)+H(2,J2)*EX(J2)
        ZE(I,J)=ZE(I,J)+H(3,J2)*EX(J2)
  180   CONTINUE
  200 CONTINUE
    DO 250 J=1,9
      XG(I,J)=DC(1,1)*XE(I,J)+DC(2,1)*YE(I,J)+
     #        DC(3,1)*ZE(I,J)
      YG(I,J)=DC(1,2)*XE(I,J)+DC(2,2)*YE(I,J)+
     #        DC(3,2)*ZE(I,J)
      ZG(I,J)=DC(1,3)*XE(I,J)+DC(2,3)*YE(I,J)+
     #        DC(3,3)*ZE(I,J)
  250 CONTINUE
 1000 CONTINUE
      X1=CX
      Y1=CY
      Z1=CZ
      N1=1
      N2=NEL
      WRITE(7,69)II,FREQ
      WRITE(7,51)VP,VT,VR
      WRITE(7,55)X1,Y1,Z1
      WRITE(7,66)N1,N2,NEL,SF
      WRITE(7,59)((NUM(I,J),J=1,2),I=1,NEL)
      WRITE(7,65)((XN(I,J),J=1,9),I=1,NEL)
      WRITE(7,65)((YN(I,J),J=1,9),I=1,NEL)
      WRITE(7,65)((ZN(I,J),J=1,9),I=1,NEL)
      WRITE(7,65)((XG(I,J),J=1,9),I=1,NEL)
      WRITE(7,65)((YG(I,J),J=1,9),I=1,NEL)
      WRITE(7,65)((ZG(I,J),J=1,9),I=1,NEL)
C
 3000 CONTINUE
      RETURN
   51 FORMAT(3F9.2)
   55 FORMAT(3F9.5)
   59 FORMAT(20I5)
   65 FORMAT(8E12.5)
```

```
   66 FORMAT(3I5,F9.5)
   69 FORMAT(I5,F20.2)
 6000 FORMAT(30A4)
      END
```

```
C     Program P7 For Plotting Deformations
      REAL*4 XAX,YAX,ZAX,X3O,Y3O,Z3O,X3M,Y3M,Z3M
      REAL*4 XN(50,9),YN(50,9),ZN(50,9),XE(50,9),YE(50,9)
      REAL*4 ZE(50,9),XP(9),YP(9),ZP(9),SF,FREQ
      REAL*4 X1,Y1,Z1,XD,VP,VT,VR,CNODE(55,6),TITLE(30)
      INTEGER N1,N2,II,NPLOT,NUM(50,2),NEL
C     Read In
      READ(5,5000)TITLE
      READ(5,56) NPLOT
      CALL DSPDEV('PLOTTER ')
      DO 3000 N=1,NPLOT
      READ(5,56)II,FREQ
      READ(5,51)VP,VT,VR
      READ(5,57) X1,Y1,Z1
      READ(5,50)N1,N2,NEL,SF
      READ(5,59)((NUM(I,J),J=1,2),I=1,NEL)
      READ(5,53)((XN(I,J),J=1,9),I=1,NEL)
      READ(5,53)((YN(I,J),J=1,9),I=1,NEL)
      READ(5,53)((ZN(I,J),J=1,9),I=1,NEL)
      READ(5,53)((XE(I,J),J=1,9),I=1,NEL)
      READ(5,53)((YE(I,J),J=1,9),I=1,NEL)
      READ(5,53)((ZE(I,J),J=1,9),I=1,NEL)
C     Scale The Deformations For The Plot
      XD=0.0
      DO 150 I=1,N2
      DO 150 J=1,9
      XD=AMAX1(XD,ABS(XE(I,J)),ABS(YE(I,J)),ABS(ZE(I,J)))
  150 CONTINUE
      DO 160 I=1,N2
      DO 160 J=1,9
     XE(I,J)=XN(I,J)+XE(I,J)*SF/XD
     YE(I,J)=YN(I,J)+YE(I,J)*SF/XD
     ZE(I,J)=ZN(I,J)+ZE(I,J)*SF/XD
  160 CONTINUE
      DO 200 I=1,NEL
     CNODE(NUM(I,2),1)=XN(I,9)
     CNODE(NUM(I,2),2)=YN(I,9)
     CNODE(NUM(I,2),3)=ZN(I,9)
     CNODE(NUM(I,2),4)=XE(I,9)
     CNODE(NUM(I,2),5)=YE(I,9)
     CNODE(NUM(I,2),6)=ZE(I,9)
  200 CONTINUE
C     Determine Plot Size Parameters
      X3O=0.0
      Y3O=0.0
      Z3O=0.0
      X3M=0.0
      Y3M=0.0
      Z3M=0.0
      DO 100 I=N1,N2
      DO 100 J=1,9
     X3O=AMIN1(X3O,XE(I,J),XN(I,J))
     Y3O=AMIN1(Y3O,YE(I,J),YN(I,J))
     Z3O=AMIN1(Z3O,ZE(I,J),ZN(I,J))
```

```
      X3M=AMAX1(X3M,XE(I,J),XN(I,J))
      Y3M=AMAX1(Y3M,YE(I,J),YN(I,J))
      Z3M=AMAX1(Z3M,ZE(I,J),ZN(I,J))
  100 CONTINUE
      XAX=ABS(X3M-X3O)
      YAX=ABS(Y3M-Y3O)
      ZAX=ABS(Z3M-Z3O)
      IF (XAX.LT.0.01*SF) X3M=X3M+SF
      IF (XAX.LT.0.01*SF) XAX=SF
      IF (YAX.LT.0.01*SF) Y3M=Y3M+SF
      IF (YAX.LT.0.01*SF) YAX=SF
      IF (ZAX.LT.0.01*SF) Z3M=Z3M+SF
      IF (ZAX.LT.0.01*SF) ZAX=SF
C     Set Up The Plot
      CALL GRACE(2.0)
      CALL NOBRDR
      CALL PAGE(8.5,11.)
      CALL PHYSOR(1.5,1.5)
      CALL AREA2D(6.,8.)
      CALL FRAME
      CALL VOLM3D(XAX,YAX,ZAX)
      CALL VUANGL(VP,VT,VR)
      CALL GRAF3D(X3O,1.,X3M,Y3O,1.,Y3M,Z3O,1.,Z3M)
      CALL MARKER(16)
      CALL BASALF('L/CSTD')
      CALL MIXALF('STANDARD')
      CALL MESSAG(TITLE,100,0.5,-0.5)
      IF (FREQ) 2010,2030,2020
 2010   CALL MESSAG('(S)TATIC (D)EFLECTION AND (L)OAD$',
     #            100,.3,8.15)
      GOTO 2030
 2020   CALL MESSAG('(M)ODE$',100,0.3,8.27)
     CALL INTNO(II,'ABUT','ABUT')
     CALL MESSAG('(N)ATURAL (F)REQUENCY$',100,.3,8.08)
     CALL REALNO(FREQ,2,'ABUT','ABUT')
     CALL MESSAG('(H)Z$',100,'ABUT','ABUT')
 2030   CONTINUE
      CALL HEIGHT(.1)
      CALL MESSAG('(CX) = $',100,4.5,8.35)
      CALL REALNO(X1,5,'ABUT','ABUT')
      CALL MESSAG('(CY) = $',100,4.5,8.2)
      CALL REALNO(Y1,5,'ABUT','ABUT')
      CALL MESSAG('(CZ) = $',100,4.5,8.05)
      CALL REALNO(Z1,5,'ABUT','ABUT')
      CALL RESET('HEIGHT')
C     Begin Loop For Plotting Each Element
      DO 2000 I=N1,N2
     DO 510 J=1,9
       XP(J)=XN(I,J)
       YP(J)=YN(I,J)
       ZP(J)=ZN(I,J)
  510   CONTINUE
     CALL LINEAR
     CALL DASH
```

```
      CALL CURV3D(XP,YP,ZP,9,0)
      CALL RESET('DASH')
      DO 520 J=1,9
        XP(J)=XE(I,J)
        YP(J)=YE(I,J)
        ZP(J)=ZE(I,J)
  520   CONTINUE
      CALL POLY3
      CALL CURV3D(XP,YP,ZP,9,8)
       IF (I.EQ.1) GOTO 400
      X1=CNODE(NUM(I,1),1)
      Y1=CNODE(NUM(I,1),2)
      Z1=CNODE(NUM(I,1),3)
      CALL DASH
      CALL RLVEC3(X1,Y1,Z1,XN(I,1),YN(I,1),ZN(I,1),0)
      CALL RESET('DASH')
      X1=CNODE(NUM(I,1),4)
      Y1=CNODE(NUM(I,1),5)
      Z1=CNODE(NUM(I,1),6)
      CALL RLVEC3(X1,Y1,Z1,XE(I,1),YE(I,1),ZE(I,1),0)
  400 CONTINUE
 2000 CONTINUE
      CALL BLREC(0.,8.,6.,0.5,2)
      CALL ENDPL(II)
 3000 CONTINUE
      CALL DONEPL
      STOP
   50 FORMAT(3I5,F9.5)
   51 FORMAT(3F9.2)
   53 FORMAT(8E12.5)
   56 FORMAT(I5,F20.2)
   57 FORMAT(3F9.5)
   59 FORMAT(20I5)
 5000 FORMAT(30A4)
      END
```